Simulating organized convection and precipitation in Northwestern South America at convection-permitting resolution

Kevin Santiago Hernández Uribe

Tesis de maestría presentada para optar al título de Magíster en Ingeniería Ambiental

Directora

Angela María Rendón Pérez, Doctora (PhD) en Ingeniería Ambiental

Codirector

Juan José Henao Castañeda, Doctor (PhD) en Ingeniería Ambiental

Universidad de Antioquia

Facultad de Ingeniería, Escuela Ambiental

Maestría en Ingeniería Ambiental

Medellín, Antioquia, Colombia

2023

Maestría en Ingeniería Ambiental, Cohorte XXVI.

Grupo de Investigación GeoLimna.

Centro de Investigación Ambientales y de Ingeniería (CIA).

Línea de investigación en modelación atmosférica y cambio ambiental

Centro de Documentación Ingeniería (CENDOI)

Repositorio Institucional: http://bibliotecadigital.udea.edu.co

Universidad de Antioquia - www.udea.edu.co

A mí madre, quién pasó por un proceso complejo durante el desarrollo de esta maestría.

¿Por qué la Tierra es mi casa? ¿Por qué la noche es oscura?
¿Por qué la luna es blancura que engorda como adelgaza?
¿Por qué una estrella se enlaza con otra, como un dibujo?
¿Y por qué el escaramujo es de la rosa y del mar?
Yo vivo de preguntar, saber no puede ser lujo

El agua hirviente en puchero suelta un ánima que sube
A disolverse en la nube que luego será aguacero
Niño, soy tan preguntero, tan comilón del acervo
Que marchito si le pierdo una contesta a mi pecho
Si saber no es un derecho, seguro será un izquierdo

Escaramujo, Silvio Rodríguez

Agradecimientos

Quiero agradecer a la profe Ángela por haber creído en mí desde el pregrado, alentarme a investigar, y darme la oportunidad de llevar a cabo esta maestría. Al profe Juan José, además de ser mí guía en el camino de la investigación, le agradezco por sus enseñanzas y su apoyo permanente durante todo el proceso.

También agradezco a Sebastián Gómez, Vanessa Robledo y Álvaro Villegas, con quienes tuve la fortuna de coincidir en este proyecto de investigación y de quienes aprendí desde el primer hasta el último día del proyecto. En particular, le agradezco a Sebastián por su apoyo y sus aportes durante toda la investigación. Asimismo, le agradezco al profe John Mejía por sus comentarios al trabajo.

Agradezco a mi familia por su apoyo incondicional, especialmente a mis padres Maricela y Diego, quienes se esforzaron por verme aquí. A mis abuelas, quienes también fueron un pilar fundamental en toda esta historia, y a mis tíos y tías, especialmente Diana por su apoyo permanente.

A Mariana, a quién conocí durante este proceso, le agradezco por todo el amor, la paciencia y el apoyo durante el desarrollo de este trabajo, y además, por sufrir conmigo durante la escritura de este documento. Asimismo, quiero agradecer a mis amigos y amigas de la universidad, de SIATA, y del barrio, quienes siempre fueron pacientes conmigo y me animaron a continuar, aún en los momentos más difíciles. En especial, quiero agradecer a Paola, Evans y Yesit por su amistad incondicional durante todos estos años.

Debo agradecerle también al Alma Mater por ser fuente inagotable de conocimiento, por encenderme la mente y por permitirme conocer a personas maravillosas a lo largo de 8 años. Además, me gustaría dar las gracias a los profesores de la Escuela Ambiental, especialmente a la profe Paola Arias, el profe Alejandro Martínez, y el profe Juan Fernando Salazar, con quienes descubrí mi pasión por las ciencias atmosféricas y quiénes son una constante fuente de inspiración académica y personal.

Finalmente, agradezco a los profesores Daniel Hernández y Manuel Zuluaga por tomarse el tiempo de revisar este trabajo con detalle y brindar apreciaciones para su mejora.

Simulating organized convection and precipitation in Northwestern South America at convection-permitting resolution

Kevin Santiago Hernández Uribe

A thesis submitted in partial fulfillment of the requirements for the degree of:
M.Sc in Environmental Engineering

Advisor: Angela M. Rendón (Ph.D)
Co advisor: Juan J. Henao (Ph.D)

Research field: Atmospheric modeling and environmental change
Research group: Geolimna

University of Antioquia
Engineering Faculty, Environmental School
Medellín, Colombia
2023

Abstract

Organized deep convection can trigger severe weather phenomena, compromising human life and impacting agriculture, infrastructure, and aviation. Convection-permitting (CP) models have emerged as useful tools to investigate the environments and mechanisms causing deep convection and precipitation. However, in Northwestern South America (NWSA), where organized convection is widespread and frequent, modeling studies at CP resolution are still limited. This research analyzes the representation of organized convection and precipitation in NWSA using CP simulations. A set of 4-km resolution simulations with the Weather Research and Forecasting (WRF) model covering the continental region of the NWSA are used to: study processes that cause high sensitivity to the selection of microphysics (MP) and boundary layer (PBL) schemes; assess the spatio-temporal representation of Mesoscale Convective Systems (MCSs) through an object-based approach; and identify mechanisms behind the diurnal cycle of rainfall and the organization of convection. The main results of this investigation strengthen the findings of earlier research and show advances in the modeling and understanding of convection in NWSA. In general, MP and PBL schemes strongly impact the simulation of rainfall, revealing key processes to improve the representation of rainfall in the region. On the other hand, CP simulations exhibit a good capacity to represent the main features of MCSs, including seasonality and diurnal frequency. Finally, the model unveils mechanisms that contribute to explaining the diurnal rainfall cycle and the organization of convection in different regions of NWSA. This research not only represents the first implementation of CP simulations to study convection in continental NWSA, but also highlights their potential to advance the study of convection in the region.

Keywords: Convection-permitting simulations, Northwestern South America, Mesoscale convective systems, WRF model, Sensitivity analysis, Object-based evaluation.

Contents

List of Figures

List of Tables

Chapter 1. Introduction

Deep convection is essential for rainfall occurrence and, therefore, for water security. However, convection can also trigger severe weather phenomena like extreme rainfall events, flash floods, hailstorms, and severe winds. Consequently, convective events compromise human life and impact agriculture, infrastructure, and aviation. In this sense, it is necessary to advance the understanding of the physical mechanisms that trigger and maintain severe convection in different regions.

Atmospheric models are widely used for the study and forecast of deep convection. As physically-based tools, models allow the understanding of mechanisms triggering convection in a given region (e.g., Yang et al., 2017; Karki et al., 2018; Hoyos et al., 2019). They allow projecting changes in the distribution, frequency, and intensity of convective rainfall under a future climate (Feng et al., 2016; Prein et al., 2017b; Rasmussen et al., 2020; Arias et al., 2021), permitting the design of mitigation and adaptation strategies. The occurrence of extreme precipitation events can also be anticipated using atmospheric models (e.g., Hoyos et al., 2019; Rogelis and Werner, 2018), which helps inform decision-making processes.

Compared to global models, high-resolution regional models promote the understanding of the complex interactions that determine convection in particular regions (Prein et al., 2013; Mohan et al., 2018; Posada-Marín et al., 2019; Gutowski et al., 2020). Particularly, simulations at convection-permitting (CP) resolution (less or equal to 4 km) have shown good performance to represent organized convective systems (Prein et al., 2013; Feng et al., 2018; Prein et al., 2020; Rasmussen et al., 2020; Gutowski et al., 2020), allowing the study of the mechanisms leading to convective organization on scales larger than an individual storm. Despite the usefulness of CP modeling, these simulations have to be implemented in specific regions and evaluated in detail, in order to know their limitations and provide useful information for decision-making.

In Northwestern South America (NWSA), where organized deep convection is frequent (Houze et al., 2015; Zuluaga and Houze, 2015; Jaramillo et al., 2017), previous studies have simulated convective events in specific regions (Martinez et al., 2021; Gomez-Rios et al., 2023) showing that regional CP simulations have the capacity to represent these systems and their associated mechanisms. Progress has been made in forecasting convective or precipitation events (e.g., Ceballos B et al., 2017; Rogelis and Werner, 2018; Hoyos et al., 2019), highlighting the usefulness of these strategies for forecasting this type of events. Likewise, evaluations have been performed with different parameterization schemes (e.g., Martínez-Castro et al., 2019; Yepes et al., 2020; Junquas et al., 2022; Martinez et al., 2022; Gomez-Rios et al., 2023), evidencing a great sensitivity to the microphysics and boundary layer schemes. However, these studies have been developed on specific regions, and some do not reach CP resolutions, resulting in the absence of research that implements, evaluates, and analyzes the performance of CP simulations on a subcontinental scale in NWSA.

This research analyzes the representation of organized convection and precipitation in north-western South America (NWSA) using CP-scale simulations. For this purpose, a set of state-of-the-art questions in atmospheric modeling are raised: what processes cause high sensitivity to the selection of microphysics and boundary layer schemes in the region? How is the spatio-temporal representation of convective systems in NWSA using an object-based approach? What mechanisms are behind the diurnal cycle of rainfall and the organization of convection in different regions of NWSA? To achieve these goals, different CP simulations were performed using the Weather Research and Forecasting (WRF) model covering continental NWSA. According to an exhaustive literature review, this is a pioneering work in the region, which implements subcontinental CP simulations to study convection in NWSA. The chapters have an article-like structure and each one addresses the previously exposed research questions. Chapter 2 studies the sensitivity of microphysics and boundary layer parameterization schemes. Chapter 3 evaluates the performance of the WRF model for the representation of convective systems. Chapter 4 identifies convection-related mechanisms in different regions. Finally, Chapter 5 presents the main findings and proposes future research.

Chapter 2. Precipitation sensitivity to Microphysics and Boundary Layer parameterization schemes: studying key processes

Abstract

Numerical models are an essential tool to advance our understanding of rainfall occurrence. However, parameterization schemes remain one of the greatest uncertainties in atmospheric modeling, determining the rainfall intensity, occurrence, duration, and propagation. Here we study the role of three microphysics (MP: WSM6, Thompson, Morrison) and two planetary boundary layer (PBL: YSU, MYNN) parameterization schemes in the rainfall representation over Northwestern South America (NWSA). Simulations were performed using the Weather Research and Forecasting (WRF) model at convection-permitting resolution (4km), and results were evaluated against satellite data. The simulations represented the spatio-temporal features of precipitation, with better results for the WSM6 MP and the YSU PBL schemes. MP and PBL schemes exerted a high sensitivity to simulated rainfall in the Colombian Amazon and Pacific zones, revealing some key processes behind the representation of rainfall in the regions of interest. We observed that PBL schemes not only influenced low-level dynamics and heat fluxes but also vertical cloud distribution. On the other hand, MP schemes influenced cloud development through latent heat release caused by solid-phase hydrometeor formation. This study provides insights into the assessment of physical parameterizations in numerical models.

Keywords: WRF, Sensitivity, Microphysics, Planetary boundary layer, Processes

2.1 Introduction

Precipitation is essential for water security, determining the maintenance of life and being crucial for many activities. Numerical models offer a tool to understand non-linear and highly complex processes, mechanisms, and environments associated with rainfall occurrence. One of the advantages of numerical models is the ability to represent atmospheric phenomena at a broad range of scales. However, certain processes such as microphysics, radiation, land-surface interactions, boundary layer fluxes, cumulus formation, among others, cannot be completely represented by the models as these processes usually occur at a sub-grid scale, and then need to be parameterized, which gives uncertainty to model results (Stensrud, 2009). Specifically, for simulations developed with a grid size equal to or less than 4 km, cumulus parameterizations can be turned off and convection can be explicitly solved, this is called convection-permitting simulations and usually gives better results than using cumulus parameterizations (Woodhams et al., 2018; Gutowski et al., 2020). In addition to cumulus schemes, previous studies have highlighted the enormous impact of microphysics and boundary layer processes in the rainfall representation (e.g., Karki et al., 2018; Srinivas et al., 2018).

Microphysics parameterizations (MP) account for small-scale processes that determine the formation and growth of hydrometeor species. As microphysics governs the cloud particle populations, these processes are highly relevant for precipitation development (Morrison et al., 2020). Besides, phase changes of water vapor, also represented by microphysics, affect latent and sensible heat fluxes (Morrison et al., 2020), which in turn influence dynamics (Efstathiou et al., 2013) and induce convective patterns. Several studies have evidenced a high sensitivity to MP schemes on rainfall representation (Feng et al., 2018; Martínez-Castro et al., 2019; Das et al., 2021). When simulating a severe rain event in India, Thomas et al. (2021) showed high sensitivity to MP schemes, which impacts thermodynamic profiles and convection. After evaluating the simulated precipitation over Asia Liu et al. (2018) found that MP schemes impacted rainfall amounts, stratiform rainfall production, and cloud properties. Huang et al. (2020) observed differences in the distribution and intensity of an extreme rainfall event in China using three MP schemes. Sensitivities were mainly associated with the latent heat produced, as well as the cooling generated by the evaporation of rainwater in the implemented MP schemes.

Planetary boundary layer (PBL) processes determine the exchange of momentum, energy, and moisture between the earth's surface and the free atmosphere, which plays a crucial role in rainfall development. PBL processes are turbulent and highly non-linear owing to the heterogeneity of the terrain and the surface differential heating (Lehner and Rotach, 2018). Several studies have exhibited significant sensitivities among PBL schemes in determining the timing, intensity, and spatial distribution of rainfall (Klein et al., 2015; Qian et al., 2016; Chawla et al., 2018; Srinivas et al., 2018). Specifically in tropical regions, Qian et al. (2016) showed that the selection of the PBL scheme had a great impact in simulating moisture fluxes, convective initiation, and precipitation. Srinivas et al. (2018) simulated an extreme rainfall event in India using various boundary layer schemes. Their results showed that upper atmosphere circulation, energy transport, moisture convergence, and convection intensity are

influenced by the selection of the PBL scheme. Taraphdar and Pauluis (2021) also observed higher sensitivity to PBL than to MP schemes in rainfall representation, with variations in precipitation of up to 40% between the PBL schemes. Altogether, these studies highlight the relevance of PBL schemes for the simulation of convection and rainfall occurrence.

Some sensitivity studies have been previously performed in Northwestern South America (NWSA). In the central Andes of Perú, Moya-Alvarez et al. (2018) and Martínez-Castro et al. (2019) developed sensitivity studies with different MP schemes for precipitation forecast and representation of a convective event, respectively. Furthermore, Moya-Álvarez et al. (2020) studied the influence of PBL schemes for rainfall forecasting in the same region and exhibited large differences in convection between schemes, conditioning rainfall amounts. Junquas et al. (2022) performed sensitivity analyses to different MP parameterizations in the Ecuadorian Andes and highlighted a marked influence in the diurnal behavior of rain. In western Colombia, the selection of MP schemes affected rainfall propagation off-shore of the Colombian Pacific coast (Yepes et al., 2020). Martinez et al. (2022) studied the moisture transport by the Orinoco low-level jet with three PBL schemes, the selection of PBL parameterization not only induced differences in horizontal moisture flux but also in downwind precipitation. In the inter-Andean Magdalena Valley, Gomez-Rios et al. (2023) exhibited spatiotemporal differences in rainfall patterns when conducting a sensitivity analysis between three MP schemes.

Nevertheless, many sensitivity studies in the region only provide a shallow description of processes influencing rainfall representation. As physical parameterizations are constantly being improved, studies that evaluate their performance and explore mechanisms that generate rainfall sensitivity can help to focus improvements on relevant processes for rainfall representation.

In this chapter, rainfall-related processes influenced by the selection of MP and PBL schemes are studied. First, convection-permitting (4 km) simulations performed with the WRF model are assessed against satellite data, which is useful both for model evaluation and to elucidate regions where sensitivity is higher. Then, the sensitivity of different processes to the selection of MP and PBL schemes is analyzed, focusing on regions of interest. The rest of the chapter is structured as follows. Section 2.2 presents the description of the study area, the period of interest, modeling details, and the metrics used for the evaluation. Section 2.3 contains the assessment of the parameterizations, the analysis of processes that control the sensitivity, and discusses. Section 2.4 concludes.

2.2 Data and methods

2.2.1 Study area and period of interest

NWSA is a tropical region located in the northernmost part of South America (see Figure 2.1). The hydro-climatology in NWSA is highly driven by the meridional shift of the Intertropical Convergence Zone (ITCZ) and by the seasonal variations of three low-level-jets (LLJ) known as the Caribbean, Orinoco, and Choco (Poveda et al., 2006; Torrealba and Amador, 2010; Poveda et al., 2014). Furthermore, the region is crossed by the Andes mountain range, divided into three branches in Colombia, and forming inter-Andean valleys that favor atmospheric environments for convection development and rainfall.

According to previous studies (Urrea et al., 2019; Hernandez-Deckers, 2022), some regions in NWSA are prone to rainfall occurrence. The Colombian Pacific coast, which is known as one of the rainiest sites on earth and where the Choco LLJ takes place; the Magdalena valley, with strong localized convection due to intra-valley processes; the Colombian Caribbean
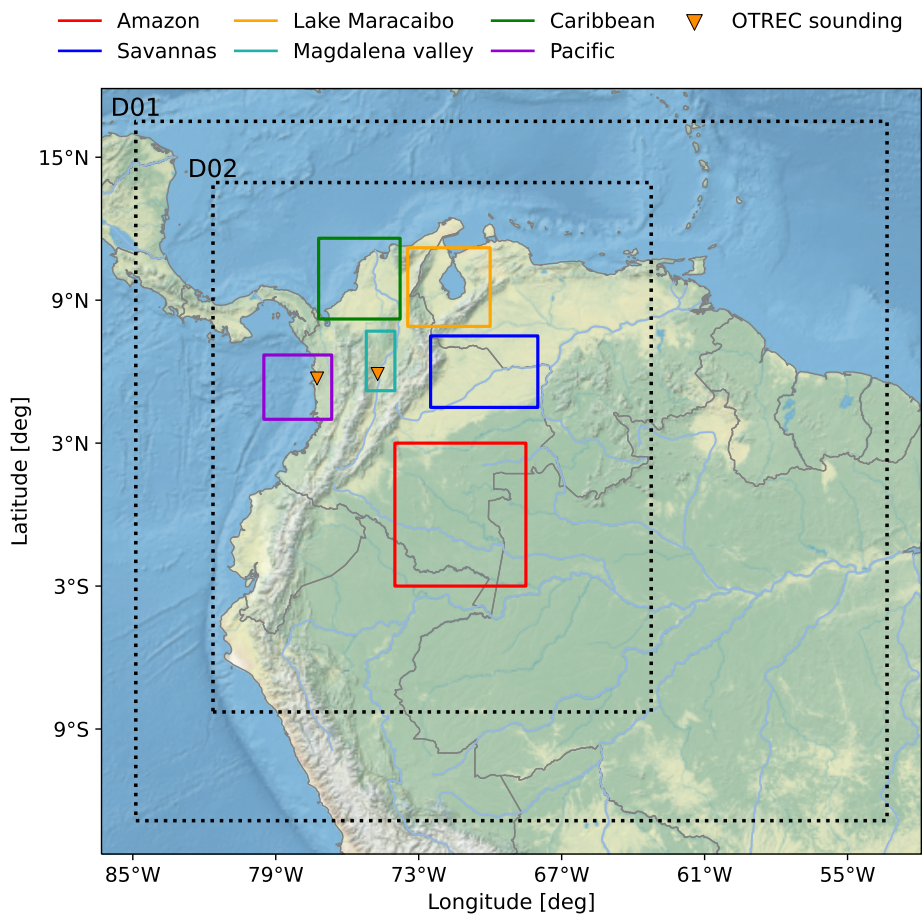
Figure 2.1: Study region and domains of the WRF simulations. Colored squares show the regions of interest and orange triangles the location of OTREC soundings launched during the study period.

coast, a lightning hotspot where sea-land breezes interact with topography causing moist convection; the gulf of Maracaibo in Venezuela, another well-known lightning hotspot; and the Amazon-Orinoco basin, two relatively flat regions with LLJ influence and high precipitation rates. Some extreme precipitation events have been reported in NWSA with important implications on infrastructure and the loss of human lives such as the Salgar event in 2015 (Hoyos et al., 2019) and the Mocoa event in 2017 (Martinez et al., 2021). The relevance of convection and rainfall occurrence in these regions justifies the implementation and evaluation of numerical models for representing precipitation, providing a tool to improve the understanding of physics causing rainfall in tropical mountainous sites. Figure 2.1 shows the six regions in which we focused our assessment.

Seven days in September 2019 were selected to perform the sensitivity analysis. The selected period is between September 18 00UTC and 25 00UTC and obeys two main reasons. First, data from the OTREC field campaign were available for this period (OTREC project; Fuchs-Stone et al., 2020), with soundings data from Nuquí (Colombian Pacific coast) and Puerto Triunfo (Magdalena valley; see Figure 2.1), which are two regions with high convective activity but scarce observations. Second, the well-reported high convective activity during September in different regions of the country (see e.g., Hernandez-Deckers, 2022). As an example, Figure S.1 shows some convective events that occurred during the study period.

2.2.2   Modeling experiment

The Weather Research and Forecasting (WRF) model, which is developed and supported by NCAR (National Center for Atmospheric Research), is used in this study (Skamarock et al., 2019). The WRF v4.2 was configured following a two-domain (one-way nested) strategy with a resolution of 12 km in the external domain (parameterized convection) and 4 km in the inner domain (convection-permitting). Simulations were initialized with ERA reanalysis data from the European Centre for Medium-Range Forecast with a spatial resolution of 0.25° and boundary conditions were updated every 3 hours.

The spatial configuration of the domains is shown in Figure 2.1. The outer domain covers the eastern region of Colombia, attempting to capture large-scale winds at low and medium levels, Atlantic flows, and moisture from terrestrial evapotranspiration, which have been identified as important humidity sources in the region (Hoyos et al., 2018; Sakamoto et al., 2011; Ruiz-Vásquez et al., 2020; Escobar et al., 2022). This domain also contains the regions where the three previously described LLJs occur. The inner domain covers the whole country and the regions of interest (Section 2.2.1), where all the analysis will be focused. In this domain, a convection-permitting configuration is used to solve the convection explicitly. A total of 65 vertical levels were used and the time step was set to 48 seconds in the external domain. Additional details of the model configuration can be found in Table 2.1.

Three MP and two PBL parameterization schemes were used to assess the simulated rainfall's sensitivity, representing a total of six WRF simulations. For MP, the implemented schemes are the WSM6 scheme (WRF Single-Moment 6-class; Hong and Lim, 2006) which considers six different types of hydrometeors and only simulates the mixing ratio of these

species; the Thompson scheme (Thompson et al., 2008) that predicts the mixing ratio for 6-class hydrometeors and number concentrations (double-moment) for ice and rain, and the Morrison double-moment scheme (Morrison et al., 2009) which predicts the mixing ratio of 6-class hydrometeors, and number concentrations for ice, snow, rain, and graupel. On the other hand, for PBL the Yonsei University (YSU; Hong et al., 2006) and the Mellor-Yamada Nakanishi Niino (MYNN; Nakanishi and Niino, 2006) were the two schemes implemented. YSU is a non-local first-order closure PBL scheme while MYNN is a local scheme with 1.5-order turbulence closure. Despite having differences in the level of complexity, these schemes are well known for providing good results in previous studies worldwide (Tian et al., 2017; Gbode et al., 2019; Mohan et al., 2018; Yáñez-Morroni et al., 2018; Martínez-Castro et al., 2019).

The rest of the setup includes the New Tiedtke cumulus scheme (only in Domain 1; Zhang and Wang, 2017), the revised MM5 surface layer scheme (Jiménez et al., 2012), the Noah-MP land-surface model (Niu et al., 2011), Dudhia (Dudhia, 1989) to represent shortwave radiation, and the Rapid Radiative Transfer Model (RRTM; Mlawer et al., 1997) for longwave radiation.

2.2.3   Model evaluation

Model evaluation is based on satellite information to cover the whole country at high temporal resolution. Precipitation data from the Global Precipitation Measurement (GPM) satellite network was used to evaluate the simulated rainfall. The "IMERG Final Run"

Table 2.1: Summary of the WRF configuration for the performed simulations.

Model parameter	Domain 1	Domain 2
Domain size	292 x 275	511 x 622
Grid size	12 km	4 km
Vertical levels	65	65
Initial conditions	ERA5	ERA5
Boundary conditions	ERA5	Domain 1
Physical parameterizations		
Microphysics	WSM6 Thompson Morrison	WSM6 Thompson Morrison
Planetary Boundary Layer	YSU MYNN level 2.5	YSU MYNN level 2.5
Cumulus	New Tiedtke	Off
Surface layer	Revised MM5	Revised MM5
Land surface	Noah-MP	Noah-MP
Shortwave radiation	Dudhia	Dudhia
Longwave radiation	RRTM	RRTM

product was used due to its high spatial (0.1°) and temporal (30 minutes) resolutions (Huff-man et al., 2019). Also, for completeness, we included precipitation measurements from the Institute of Hydrology, Meteorology and Environmental Studies (IDEAM) and Corantioquia (Piragua network) rain gauges. However, the evaluation was not focused on this information due to its limited spatial coverage (the network is focused on populated areas) and the type of evaluation metrics implemented (described below). Furthermore, given the relationship between vertical cloud development and low brightness temperature (BT) values, we assess the model's ability to simulate deep convective clouds using the brightness temperature product MERGIR (Janowiak et al., 2017) with spatial and temporal resolutions of 4 km and 30 minutes, respectively.

Soundings from the OTREC project were also used from 19th September 00UTC to 24th September 00UTC. These soundings contain valuable information about atmospheric dynamics and thermodynamics, which is helpful to the model assessment. The OTREC project soundings were launched from two locations: Nuquí, located on the Pacific coast (5.71 °N, 77.27 °W), and Puerto Triunfo in the Magdalena Valley (5.9 °N, 74.72 °W). The soundings were launched two times each day at 00 and 12 UTC, and four times (00, 06, 12, and 18 UTC) in days with NCAR research flights. Additional information about the OTREC field campaign is described by Fuchs-Stone et al. (2020) and Mejía and Poveda (2020).

Different metrics were used in order to evaluate the performance of the model simulations. Both, WRF and satellite fields were linearly interpolated seeking a common grid with a spatial resolution of 12 x 12 km. First, classic verification metrics based on 2 x 2 contingency tables were applied to the precipitation fields. In these methods, a table is created using the number of times that the model captures whether or not rainfall will overcome a certain percentile (which is called an event). Several skill metrics can be computed using this strategy, including the probability of detection (POD), the false alarm ratio (FAR), and the critical success index (CSI), check (Wilks, 2011) for more details about these metrics. Remarkably, the CSI (also known as Threat Score) accounts for the model's ability to represent observed events relative to the times the event was both simulated and observed. It allows not only account for the number of successes but also those successes relative to the errors. The CSI method for a given pixel and the whole study period is calculated following equation 2.1, where Hits represent that the model was able to capture the event, False Alarms are events simulated but not observed, and Misses are observed events that were not simulated. This method accounts for the model simulations' ability to capture spatially and temporally the occurrence of precipitation events that exceed a certain threshold.

$$CSI = \frac{Hits}{Hits - FalseAlarms - Misses} \tag{2.1}$$

Additionally, the Fractions Skill Score (FSS, Roberts and Lean, 2008) was used for the spatial evaluation of the model. The FSS compares the ratio of pixels that exceed a threshold between the model and observations in a spatial rolling window for a given time step. In

doing so, a neighborhood has to be defined by means of a tunable window. As the FSS considers a fraction of pixels in a window instead of a pixel-to-pixel comparison, it avoids double penalties because of little spatial biases in the model which is a common issue in traditional skill metrics.

Particularly, a variation of the original skill metric called Localized FSS (LFSS, Woodhams et al., 2018) was used here. This metric is similar to the original but allows quantifying the spatial performance of the model, which is useful for evaluating differences in performance by region. Equation 2.2 details the procedure to calculate the LFSS. The metric is computed for a neighborhood centered in the pixel i, j and averaged over k time steps. The numerator on the right-hand of Equation 2.2 is the Mean Squared Error (MSE) of the number of pixels exceeding the threshold in observation $Fo_{i,j,k}$ and simulations $Fs_{i,j,k}$, while the denominator represents a low-skill MSE which is used as a reference.

$$LFSS_{i,j} = 1 - \frac{\sum_{k=1}^{n}(Fo_{i,j,k} - Fs_{i,j,k})^2}{\sum_{k=1}^{n}(Fo_{i,j,k}^2 + Fs_{i,j,k}^2)} \qquad (2.2)$$

2.3 Results and discussion

2.3.1 Model evaluation

In this section the evaluation of the different MP and PBL simulations is presented. Figure 2.2 shows the mean spatial distribution of rainfall during the study period for both observations and simulations. In general terms, the WRF simulations adequately represented the spatial distribution of rainfall in the different regions of the country, with higher precipitation rates to the west of Colombia (Pacific region) and towards the north of the domain (in the Lake Maracaibo), and less and more scattered rain over other regions in the study domain. Regarding satellite information, the model overestimated the magnitude of precipitation, especially towards the north and west of the country (see also Figure S.2).

MP and PBL parameterization schemes exhibited important differences in the simulated rainfall fields. The simulations performed with YSU showed more precipitation in the Savannas and Amazon regions, as well as in the north of Perú. On the other hand, Morrison
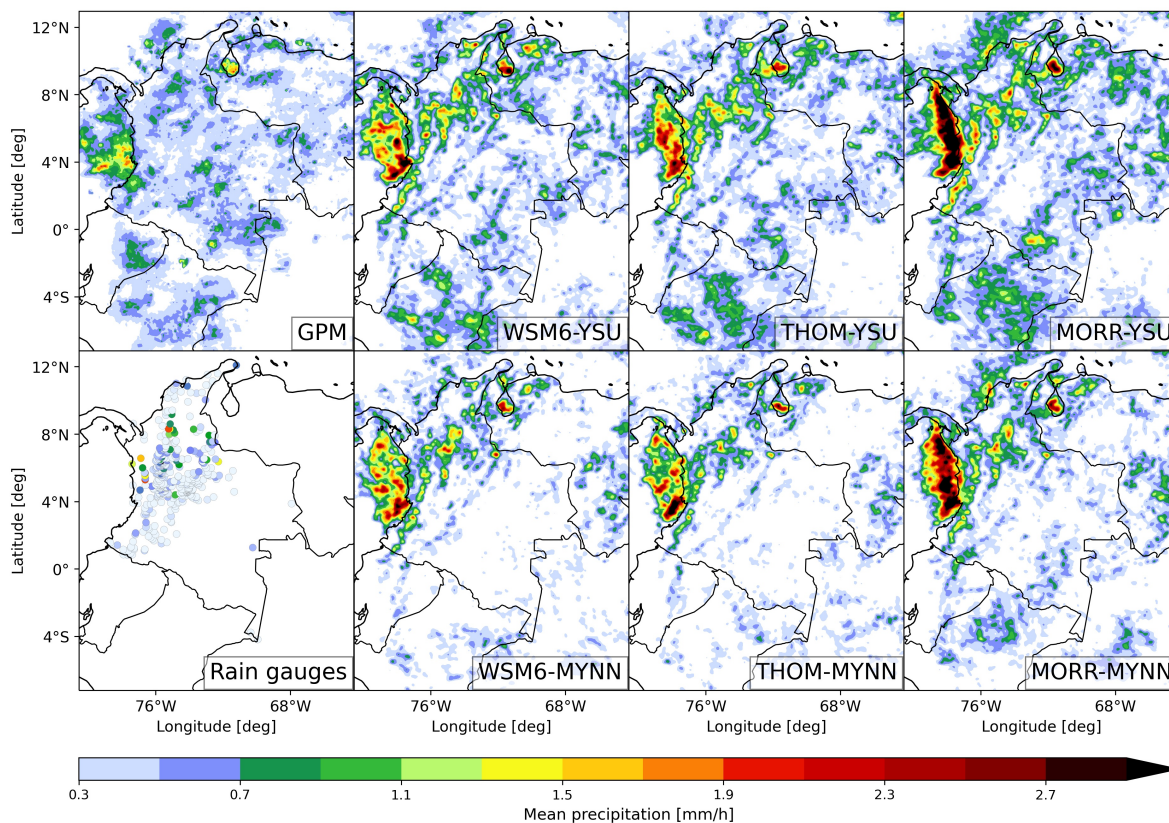
Figure 2.2: Spatial distribution of mean precipitation during the study period for the whole region. Satellite information (GPM) and rain gauges (IDEAM and Piragua) are depicted on the leftmost side of the figure, followed by the results of the WRF simulations. Parameterization schemes were plotted as a function of their complexity. Differences in the spatial distribution of precipitation between WRF simulations and GPM are plotted in Figure S.2.

produced higher precipitation rates in the Pacific and near the shoreline, while rainfall distribution with WSM6 and THOM shows a better agreement with observations. Particularly, WSM6 transported the rain patch further from the coastline than THOM and MORR. This is indicative of the offshore propagation of convective systems in the region (e.g., Mejía et al., 2021).

Time series of cumulative rainfall are presented in Figure 2.3 for the different regions of interest. Satellite-derived precipitation shows a similar variability to that from rain gauges, having comparable magnitudes in all regions. Of note is that the number of stations and the area coverage of rain gauges is limited, and time series derived from gauges is not directly comparable to model or satellite-derived data and is just used as a reference. WRF simulations were able to capture the occurrence of most rainfall events during the study periods, with differences in intensity. In general, the model overestimated precipitation in Maracaibo, Magdalena Valley, Caribbean, and Pacific regions, which are close to mountainous areas, whereas, in the Savannas-Amazon region, where orography is relatively flat, cumulative rainfall was underestimated. Simulations performed with the MYNN local PBL scheme (discontinuous lines) produced less rain in all the regions of interest, with a higher difference in the Amazon-Savannas regions. Similarly, MP schemes influenced the amount of rainfall in these regions, with MORR producing more rainfall in the six regions of interest, but especially in the Pacific and Caribbean.

Figure 2.4 shows the Critical Success Index (CSI) computed for different thresholds and for the performed simulations. Results show that there is no generalized behavior in the performance of the simulations, as in some regions certain schemes demonstrated better performance, but other schemes performed better in other regions. The results in Amazonas, Savannas, and the Caribbean show that the simulations with YSU generally had a better performance. In the case of Lake Maracaibo and the Pacific, the runs with the WSM6 scheme showed a better performance. In the Caribbean region, THOM (MP) with YSU (PBL) showed the best performance, although the performance decreases for high percentiles (over the 90th percentile).

The spatial and temporal representation of cloudiness is also important to determine multiple processes in the atmosphere. Following this, Figure 2.5 presents the LFSS for brightness temperature (BT) in the whole country. Simulations with MORR had issues reproducing the spatial distribution of BT through the model domain. WSM6 and THOM showed similar performance with better results in Maracaibo, Pacific, and the Caribbean, while the performance was poorest in the Savannas and Amazon. THOM outperformed WSM6 in the Caribbean, while WSM6 had better performance in the inter-Andean Magdalena valley. Besides, as consistent with the results for precipitation, simulations with MYNN presented less performance for brightness temperature in the Amazon and Savannas regions in comparison with YSU.

Other studies have evidenced better results for less computationally expensive MP and PBL parameterization schemes. Despite being a single-moment MP scheme, WSM6 has shown good results to simulate rainfall events in different studies (Tian et al., 2017; Yáñez-Morroni

et al., 2018; Liu et al., 2020b; Huang et al., 2020). Likewise, THOM has shown better results compared to more complex schemes such as MORR (Mohan et al., 2018; Karki et al., 2018). On the other hand, the non-local scheme YSU has shown better results compared to local schemes like MYNN (Efstathiou et al., 2013; Tian et al., 2017; Comin et al., 2021; Zhu et al., 2022), which is computationally more expensive. The results presented in this chapter are consistent with the findings of these studies. Additionally, the importance of these results lies in the fact that WSM6 and YSU are computationally less expensive schemes, and they provide a more realistic rainfall representation, which is essential for forecasting tasks.

In order to check the capacity to represent the vertical behavior of dynamic and thermodynamic variables, an analysis with the OTREC soundings was performed. Figure 2.6 displays the average zonal and meridional wind profiles, relative humidity, and equivalent potential temperature during the study period for the two OTREC soundings (see Figure 2.1). Also, in order to assess both vertical and temporal variables, Figure S.3 shows Taylor diagrams for the variables measured with the soundings. In general, the simulations were able to capture variations in height of these variables, even though some differences between the schemes are observed. In Nuquí (upper panels), zonal winds were overestimated by the sim-
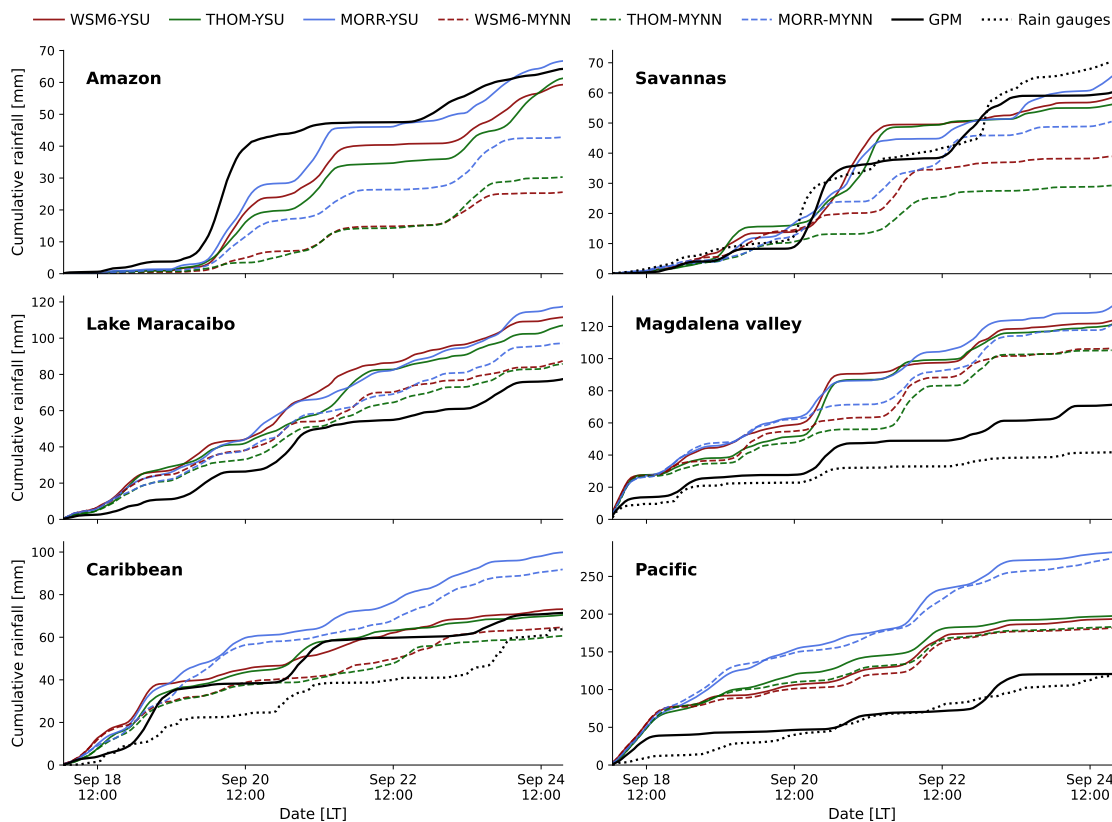
Figure 2.3: Cumulative rainfall during the study period averaged for each of the six different regions of interest shown in Figure 2.1. Continuous black lines show satellite-based rainfall (GPM), discontinuous black lines represent gauge-based rainfall, and colored lines are the simulated rainfall using different schemes.

ulations, especially by WSM6-YSU, although this scheme was able to capture the winds at medium and high levels. The simulations with MORR showed good results at low levels, however, westerly winds were observed at medium levels instead of easterlies as well as an underestimation of easterly winds at high levels. As for southerly winds, the simulations were systematically biased at low levels, although speeds above 800 hPa were adequately captured. The relative humidity is high from the surface to 400 hPa, with a sharper decrease at high levels, this behavior was captured by the simulations, although simulations with WSM6 and the performed with THOM-MYNN presented underestimations of humidity at upper levels, while MORR overestimated between 600 and 400 hPa. In addition, the equivalent potential temperature in Nuquí showed lower values at low levels, especially for the simulations carried out with WSM6, which is consistent with lower humidity at these levels. On the other hand, at high levels, a higher temperature was observed for MORR, which may be related to deeper convection, and consequently, a greater latent heat release at high levels for this scheme.

In Puerto Triunfo, low-level winds were overestimated by the model, with a marked overestimation of the up-valley component in all WRF simulations. However, THOM-YSU exhibited a greater similarity with the observations. At medium levels, low sensitivity between parameterizations was observed, while at high levels, the simulations with WSM6 had a better performance. In addition, the relative humidity and the equivalent potential temperature
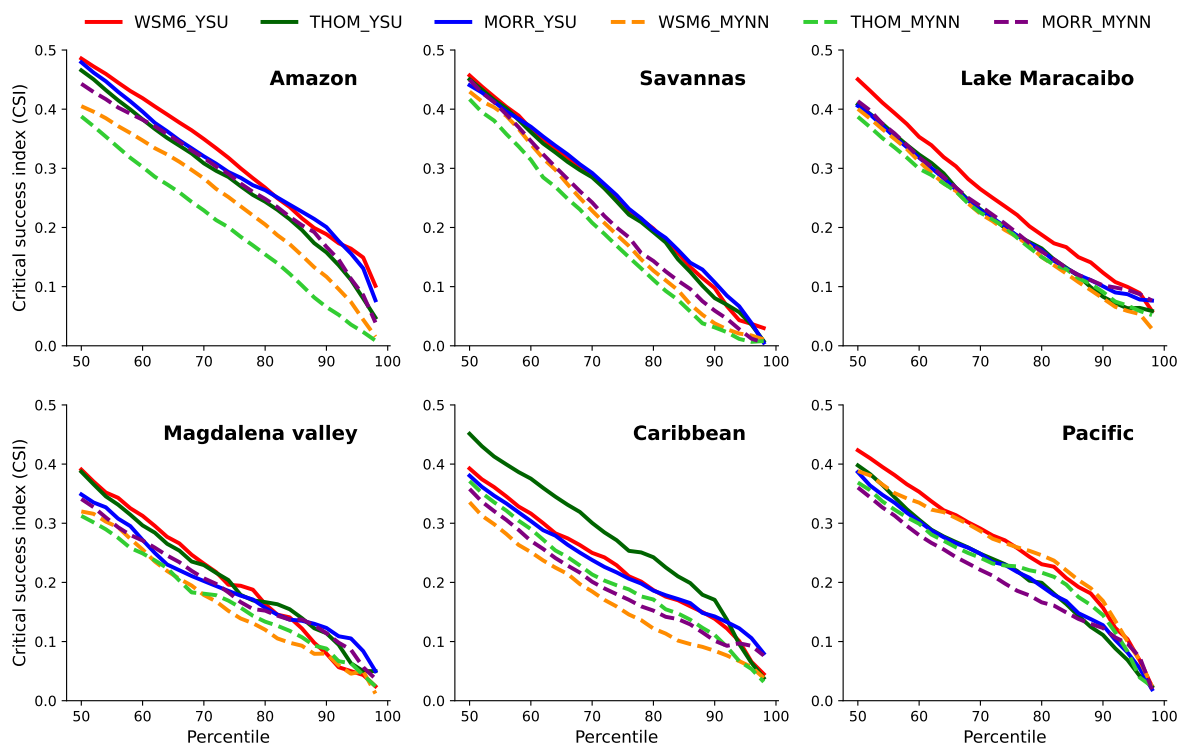
Figure 2.4: Critical success index (CSI), also called threat score, computed as a function of a rainfall percentile. Values were calculated for each of the six regions of interest (panels) and parameterization schemes (colored lines). Higher values indicate better performance.

presented a behavior similar to that described in the Nuquí radiosondes. Overestimations observed in the zonal winds (Nuquí soundings) and in the up-valley winds (Puerto Triunfo soundings) are likely related to the rainfall overestimation in the Pacific and the Magdalena Valley, respectively.
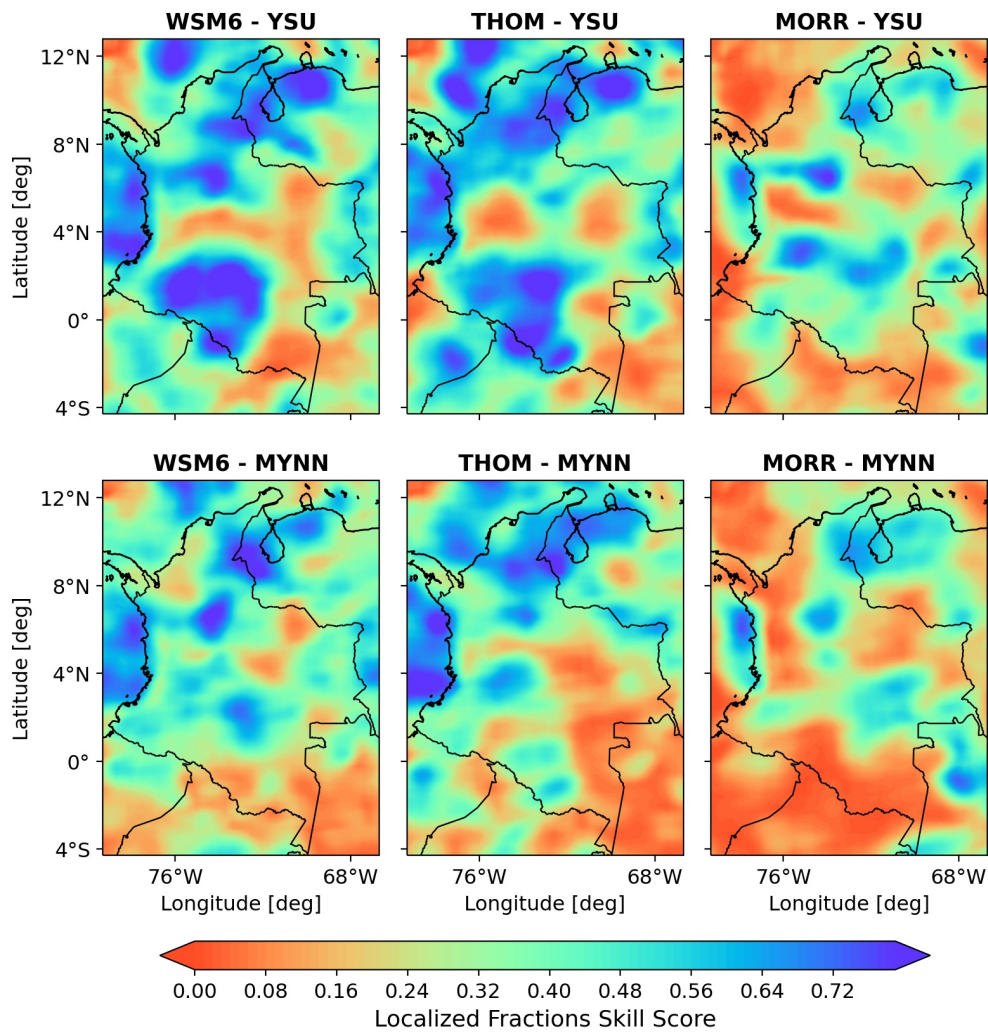
Figure 2.5: Localized Fractions Skill Score (LFSS) computed for brightness temperature during the whole study period using the implemented parameterization schemes. Metrics were calculated using a 40-pixels window and the 10th percentile was used as a threshold.
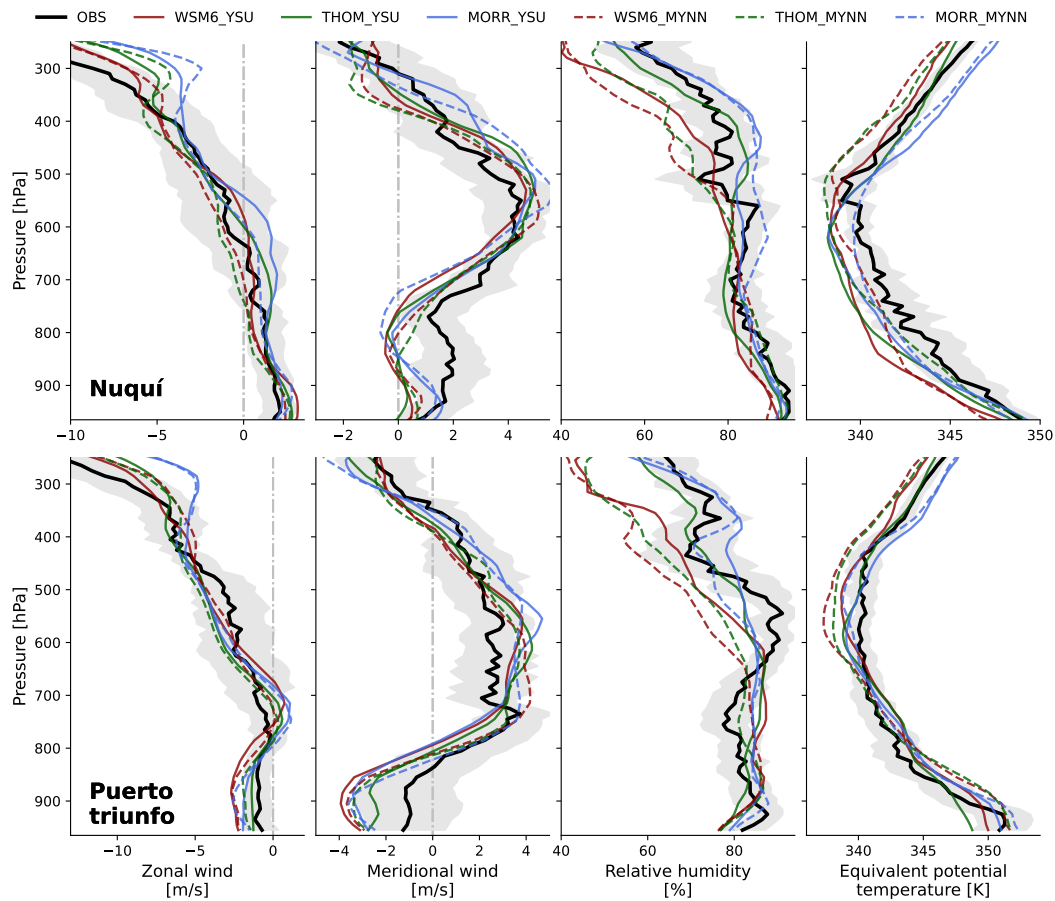
Figure 2.6: Profiles of dynamic and thermodynamic variables for the radiosondes released in Nuquí (upper panels) and Puerto Triunfo (lower panels). The black line denotes the values measured by the radiosondes with the standard deviation shaded in gray, and the colored lines show the values simulated by each of the experiments. From right to left are the zonal wind, meridional wind, relative humidity, and equivalent potential temperature. The launch locations for the soundings are specified in Figure 2.1.

2.3.2 Model sensitivity

This section analyses different processes that explain the sensitivity of MP and PBL parameterizations to precipitation during the period of interest. Identifying the processes that have greater uncertainty could help to elucidate the atmospheric mechanisms playing a fundamental role in the occurrence, magnitude, and intensity of rainfall in a certain region. Due to the substantial differences among the six regions of interest, to simplify the analysis, emphasis was placed on the regions in which the greatest differences were observed in the representation of rainfall, that is greater sensitivity to the choice of parameterizations. The study of these processes is crucial to improve physical parameterizations in atmospheric models, as this exposes which features must be carefully and precisely simulated by models.

Figures S.4 and S.5 show differences in mean precipitation fields by PBL and MP schemes, respectively. In general, it is shown that more marked differences between PBL schemes can be seen in the Colombian flatlands. On the other hand, maximum differences among MP schemes are allocated on the Pacific coast, with differences up to 1 mm/h. Due to these differences, the Amazon region was selected for the analysis of processes that trigger sensitivity among PBL schemes, and the Pacific for MP processes. In order to study only the sensitivity associated with PBL schemes, the simulations were averaged for different MP schemes. The same procedure was carried out to study the sensitivity to MP schemes.

2.3.2.1 Sensitivity to Planetary Boundary Layer

In this section, an analysis of possible processes causing sensitivity to PBL schemes is carried out. The PBL schemes exhibited a larger sensitivity to rainfall representation in the Colombian flatlands (see Figure S.4). As the Colombian Amazon is a region of high climatological, ecological, and hydrological importance, processes causing sensitivity between PBL schemes are studied in detail. Previously, low-level processes have been identified as drivers of convection and precipitation in the Colombian flatlands (Martinez et al., 2022). In this sense, Figure 2.7 shows the lower tropospheric integrated moisture flux, its convergence, and 700 hPa vertical moisture flux averaged for the two PBL schemes. Simulations performed with YSU, which previously showed higher precipitation, exhibited increased moisture flux from the southeast (left-hand panels), which flows from the Amazon rainforest into the Colombian Amazon. In addition, a notable decrease in low-level moisture flux (orange to red colors) for YSU coincides with greater convergence of moisture (colored contours in the right figures) over the Colombian Amazon. Besides, MYNN showed a greater moisture flux towards the north, outside the region of interest, which coincides with less convergence over the Colombian Amazon. Moisture convergence patterns resulted in stronger wet convection for YSU compared to MYNN (gray contours in right panels) over the entire region of interest, favoring deep cloud formation and precipitation occurrence.

Energy and moisture fluxes from the earth's surface are key factors in determining wet convection and rainfall occurrence. PBL parameterization schemes exert a great influence on sensible and latent heat fluxes. Figure 2.8 presents the mean daytime simulated sensible and

latent heat fluxes, as well as the incoming shortwave radiation. In general, greater sensible
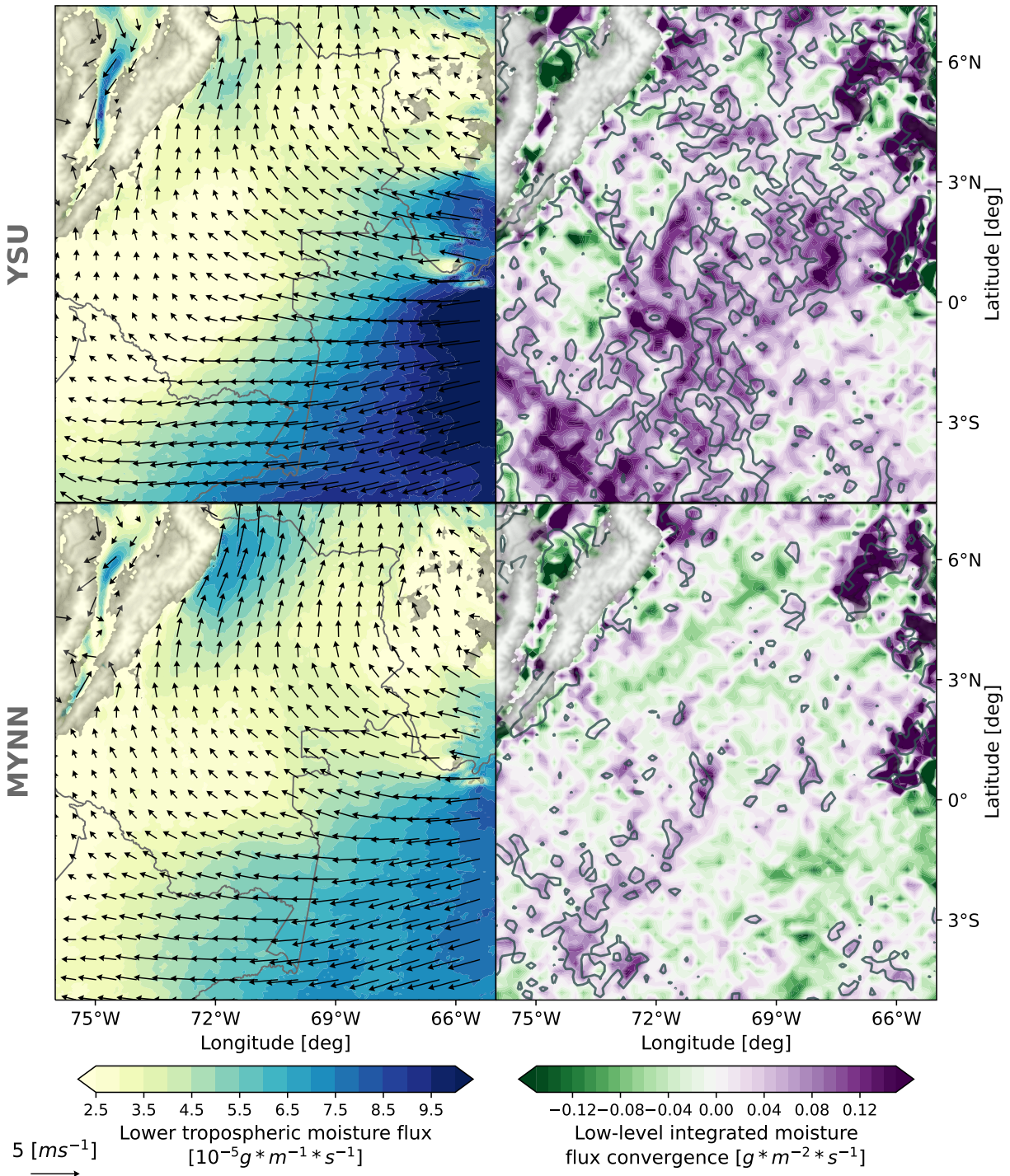
Figure 2.7: Left panels: magnitude of mean lower tropospheric (1000 to 800 hPa) moisture flux (colored contours) and horizontal winds at 850 hPa (arrows). Right panels: mean lower tropospheric moisture flux convergence (colored contours) and 0.05 $g*kg^{-1}*m*s^{-1}$ vertical moisture flux at 700 hPa (gray contours)

and latent heat fluxes can be seen in the simulations with YSU compared to MYNN, with differences of 30% for sensible heat and 20% for latent heat in the Colombian Amazon. This implies that the YSU-simulated atmosphere has more energy to trigger deep convection and more moisture for condensation. Differences in heat fluxes are consistent with enhanced horizontal and vertical moisture transport in YSU. Additionally, the incident shortwave radiation was also higher in the YSU than in MYNN simulations, with a difference of more than 100 Wm^{-2}. Thus, differences in heat fluxes are highly related to the entrance of solar radiation to the surface, which is also conditioned by the PBL schemes.

In order to explain the differences observed in the incident radiation, and in the sensible and latent heat fluxes, Figure 2.9 shows the daytime distributions of the cloudiness fraction aver-
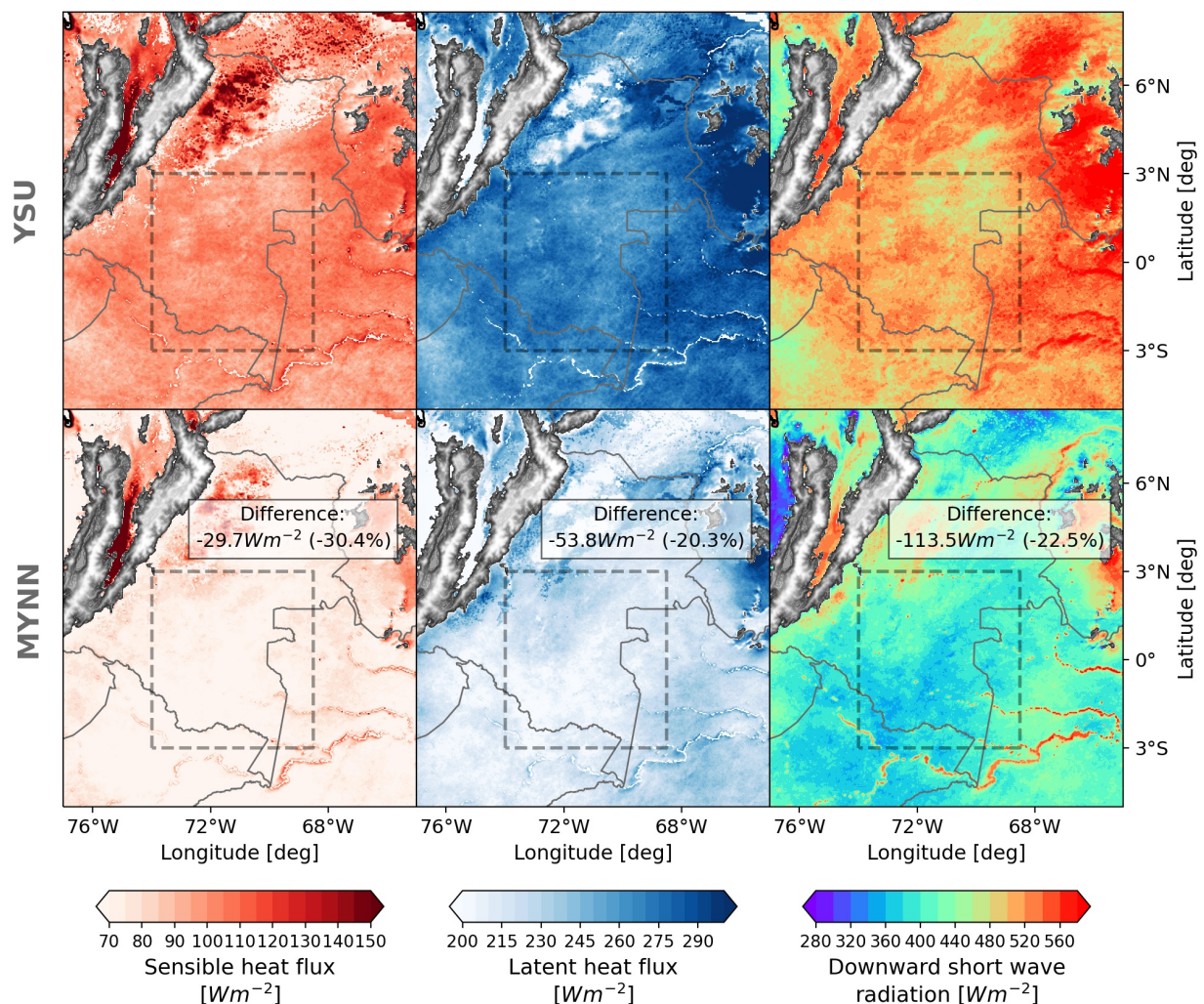
Figure 2.8: Mean daytime (07 to 17 LT) sensible heat (left), latent heat (center), and downward shortwave radiation (right) as simulated by YSU (upper panels) and MYNN (lower panels) simulations. Annotations in lower panels show the absolute and percentage differences between schemes (MYNN minus YSU) in the Colombian Amazon (delimited region).

aged for different levels in the atmosphere. MYNN produced a higher cloudiness fraction at low levels (between 900 and 600 hPa) compared to YSU. Low-level clouds (especially stratus and stratocumulus) are widely known to have high optical depth, so these have a high albedo and produce a net cooling effect in the surface (Hartmann et al., 1992; Chen et al., 2000; Mace et al., 2006). In this sense, a greater amount of low clouds in MYNN could decrease sensible and latent heat fluxes. Furthermore, in MYNN a possible positive feedback can be inferred, where the presence of low clouds decreases the sensible and latent heat fluxes, causing shallower convection than YSU which produces more amount of lower clouds and reduces heat fluxes. Otherwise, YSU exhibited a higher mid-level cloudiness fraction, which can be associated with deeper convection and the occurrence of precipitation. At high levels, no marked differences were identified between the PBL schemes.

Previously, sensitivity analyses in different regions have highlighted that non-local PBL schemes (such as YSU) generate greater mixing and produce more precipitation than local schemes (such as MYNN). For example, Efstathiou et al. (2013) performed a sensitivity study to represent a heavy rainfall event with the non-local YSU and the local Mellor–Yamada–Janjic (MYJ) PBL schemes. The authors showed that the vertical mixing produced by MYJ was lower, diminishing the water vapor transport to higher levels, and thus causing lower precipitation rates than YSU. In the Asian summer monsoon region, Que et al. (2016) exhibited a strong overestimation of precipitation intensity with the non-local YSU in comparison with the local MYJ. In Northeast Brazil, an extreme rainfall event was simulated using YSU and MYNN, with higher accumulated rainfall for YSU and better results (Comin et al., 2021). Recently, Zhu et al. (2022) studied the impacts of YSU and MYNN to forecast the heavy rainfall generated by the passage of a tropical cyclone. The authors observed that less vertical mixing was generated by MYNN, and therefore, compared to YSU, a decrease in upward fluxes of moisture and temperature was evidenced. Consequently, less precipitation was generated at MYNN compared to YSU. These studies are in agreement with the results presented in this chapter and highlight the importance of the selection of the PBL scheme
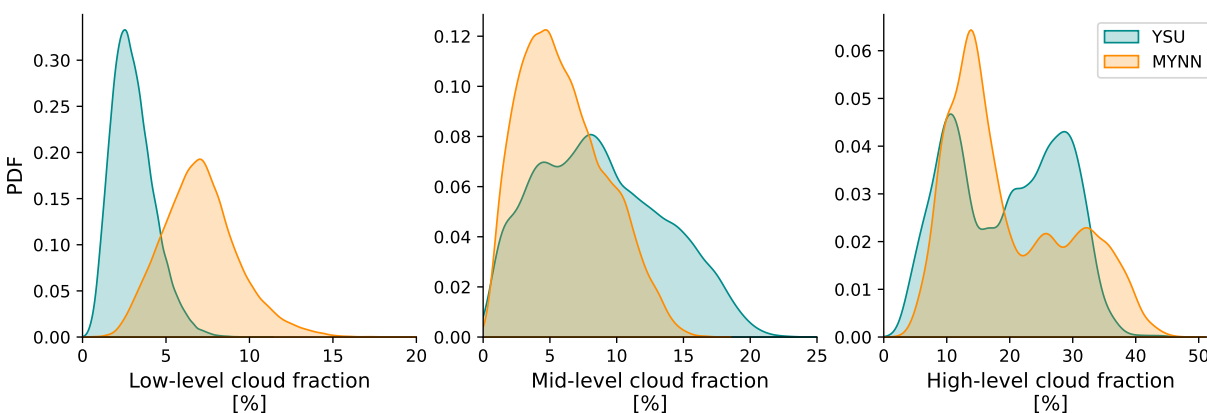
Figure 2.9: Distributions of low-level (900 to 600 hPa), mid-level (600 to 400 hPa), and high-level (400 to 200 hPa) mean daytime cloud fraction. Blue (orange) distributions show the results with YSU (MYNN).

in regions such as the Colombian Amazon.

2.3.2.2   Sensitivity to Microphysics

As previously described and highlighted in Figure S.5, rainfall sensitivity to MP schemes is larger in western Colombia, along and off-shore the Pacific coast. Here an analysis of processes causing this sensitivity is carried out. Previous studies have shown the importance of low-level moisture fluxes for the development of moist convection in the Pacific (Mejía et al., 2021). Figure 2.10 presents the lower tropospheric integrated humidity flux and the vertical humidity flux along the day. Surprisingly, remarkable differences in moisture transport are observed among MP schemes. First, WSM6 and THOM showed similar low-level moisture flux patterns (left panels) with enhanced transport toward the continent between 14 and 20 LT, which then produce moist convection in the western foothills of the Andes (around 76.5°W; right panels). Afterward, convection develops in the ocean during the early night and the morning. By contrast, MORR showed a more intense and longitudinally deeper low-level moisture flux throughout the day. Also, the convection in MORR was more intense and long-lasting than that of WSM6 and THOM. These results show that in the Pacific, the selection of MP schemes impacts low-level and vertical moisture fluxes, which are relevant factors for rainfall development in the region.

In order to elucidate how MP schemes modify vertical fluxes, Figure 2.11 shows the longitude-height section of vertical and horizontal winds, as well as diabatic heating. It can be seen that the microphysical schemes had a marked impact on convection in the Pacific. WSM6 and THOM showed similar patterns, with convection near the shoreline from 900 to 600 hPa and a broader convective region aloft, although WSM6 presented a more intense and further offshore convective structure that is consistent with a greater spread of rain towards the ocean. Contrarily, MORR exposed a broader convective region with stronger convection. Also, the more intense convection patterns for MORR were consistent with a greater amount of rain generated by this scheme along and further from the shoreline (between 77.5°W and 78.5°W). This shows that the MP parameterization schemes significantly affect the intensity and location of the convection in the Pacific region, which also can influence low-level humidity fluxes and convergence by mass continuity. Moreover, sources and sinks of heat are represented by diabatic heating in Figure 2.11. Large amounts of heat are released at medium to high levels (500 to 300 hPa), with the simulations carried out with MORR producing a more intense top-heavy diabatic heating profile compared to WSM6 and THOM. The implications of these heating differences are further discussed below.

Figure 2.12 shows the longitude-height section of the mixing ratio for different hydrometeor species. Notable differences were observed in the solid phase hydrometeors. WMS6 featured graupel around 500 hPa and ice aloft, with both extending and reaching a maximum in the oceanic region. THOM produced a large amount of snow between 500 and 300 hPa, which extends into the ocean, although not as far as WSM6. MORR showed the presence of the three solid-phase hydrometeors (ice, graupel, and snow), with graupel and snow much closer to the shoreline than WSM6 and THOM, and between 500 and 300 hPa. Ice was produced above 300 hPa with a much higher mixing ratio than WSM6, and extended into the oceanic

region as well. In addition, MORR produced a higher condensate mixing ratio (Q cloud) between 600 and 500 hPa. In the simulations performed with MORR, ice-nucleation could be favored by the presence of water below the freezing point (supercooled water) above 600
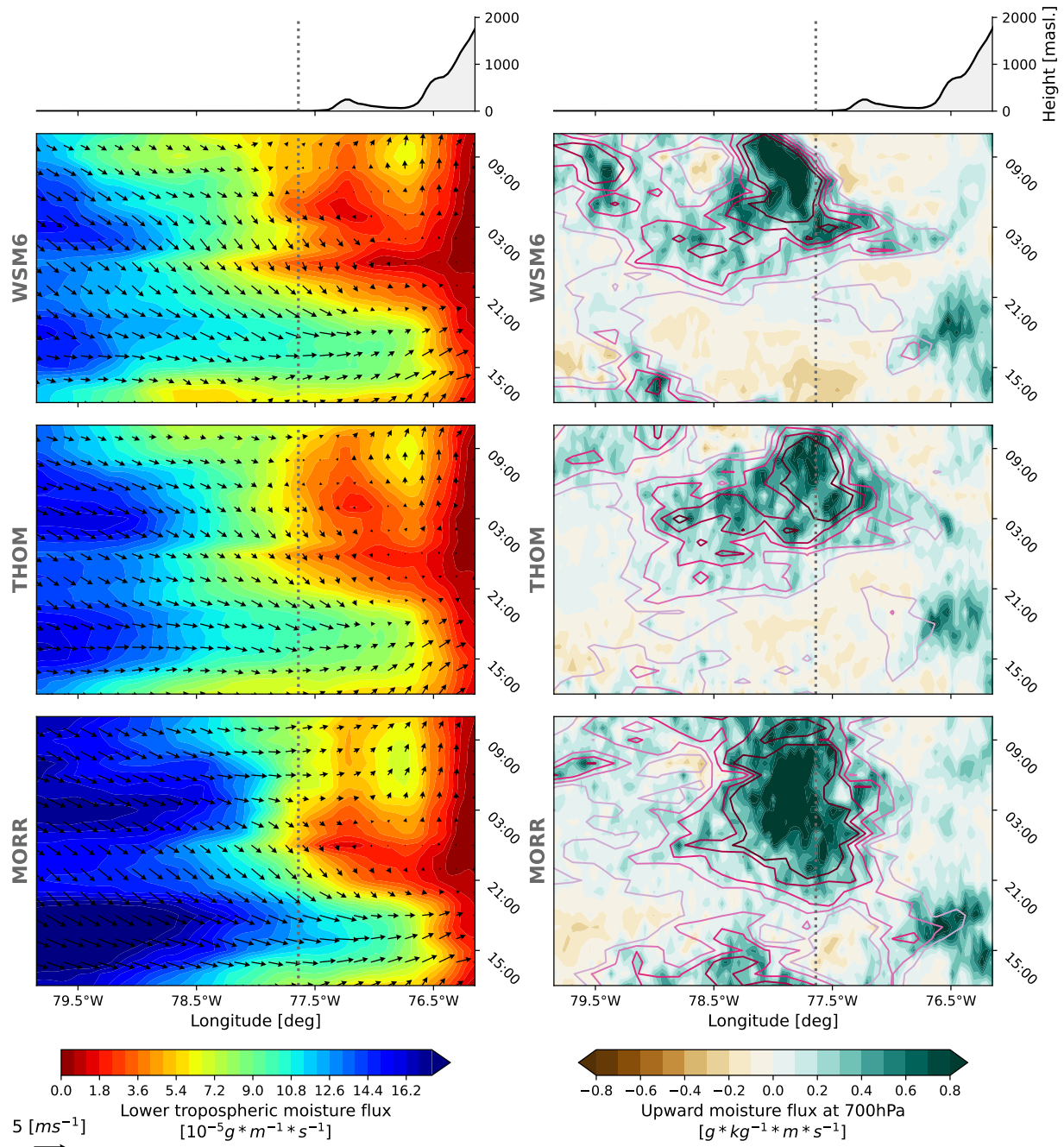
Figure 2.10: Mean diurnal and longitudinal behavior of lower tropospheric moisture flux integrated from 1000 to 800 hPa (left panels) and vertical moisture flux at 700 hPa (right panels). The convergence of lower tropospheric moisture flux is represented as purple contours in the right-side panels and arrows in the right panels show 850 hPa horizontal winds. Mean topography is indicated at the top of the figure.
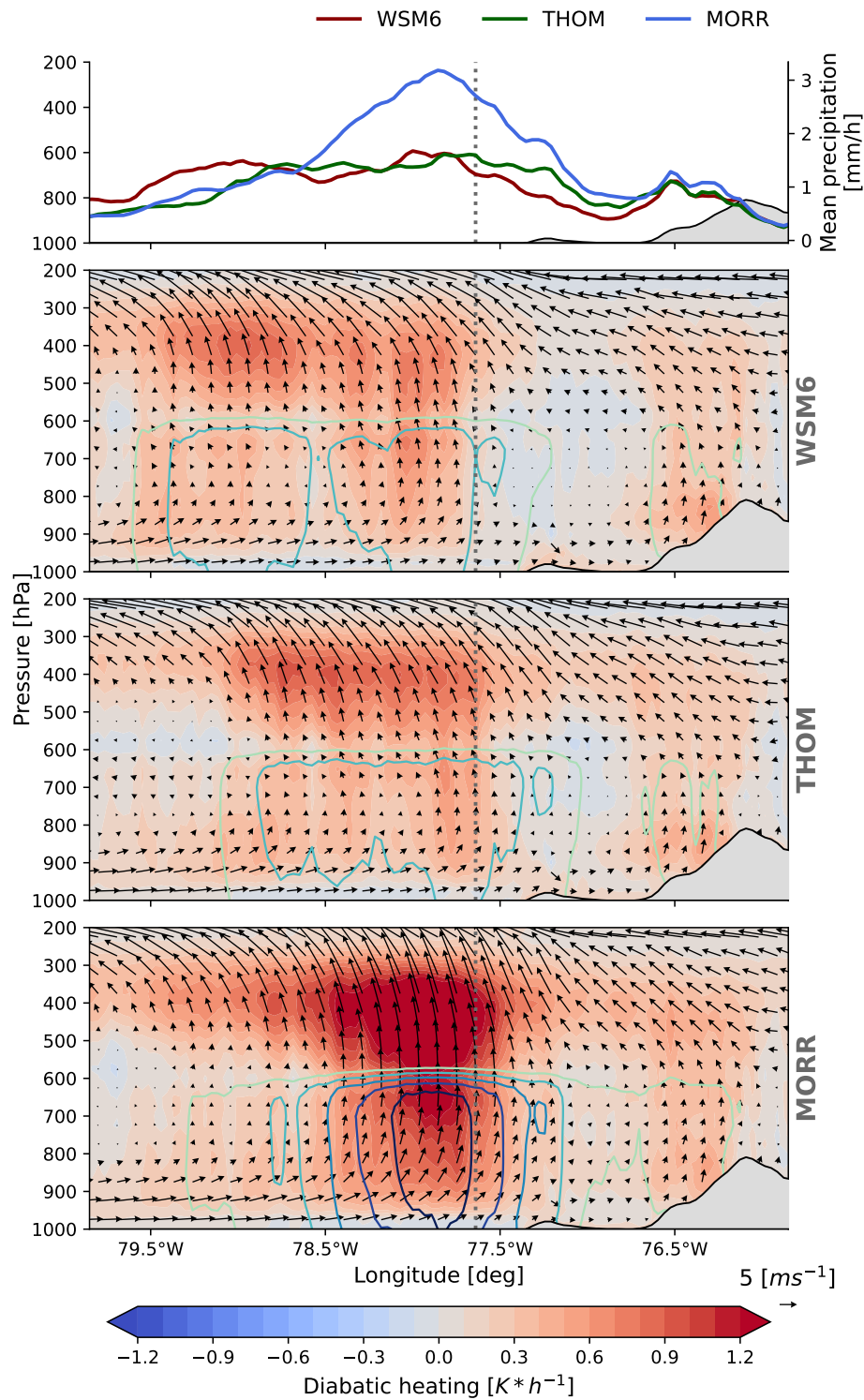
Figure 2.11: Longitude-height section of mean vertical and zonal winds (arrows) and diabatic heating (colored contours). Yellow to blue contours represent the rain mixing ratio. Note that vertical winds were multiplied by 100 in order to improve representation.

hPa. Furthermore, graupel production by riming could be favored in the mixed-phase region allocated between 600 and 400 hPa. These processes imply phase changes from liquid to solid and vapor to solid, and a subsequent release of latent heat, which could explain the greater diabatic heating observed in MORR. The possible implications of these results are discussed below.
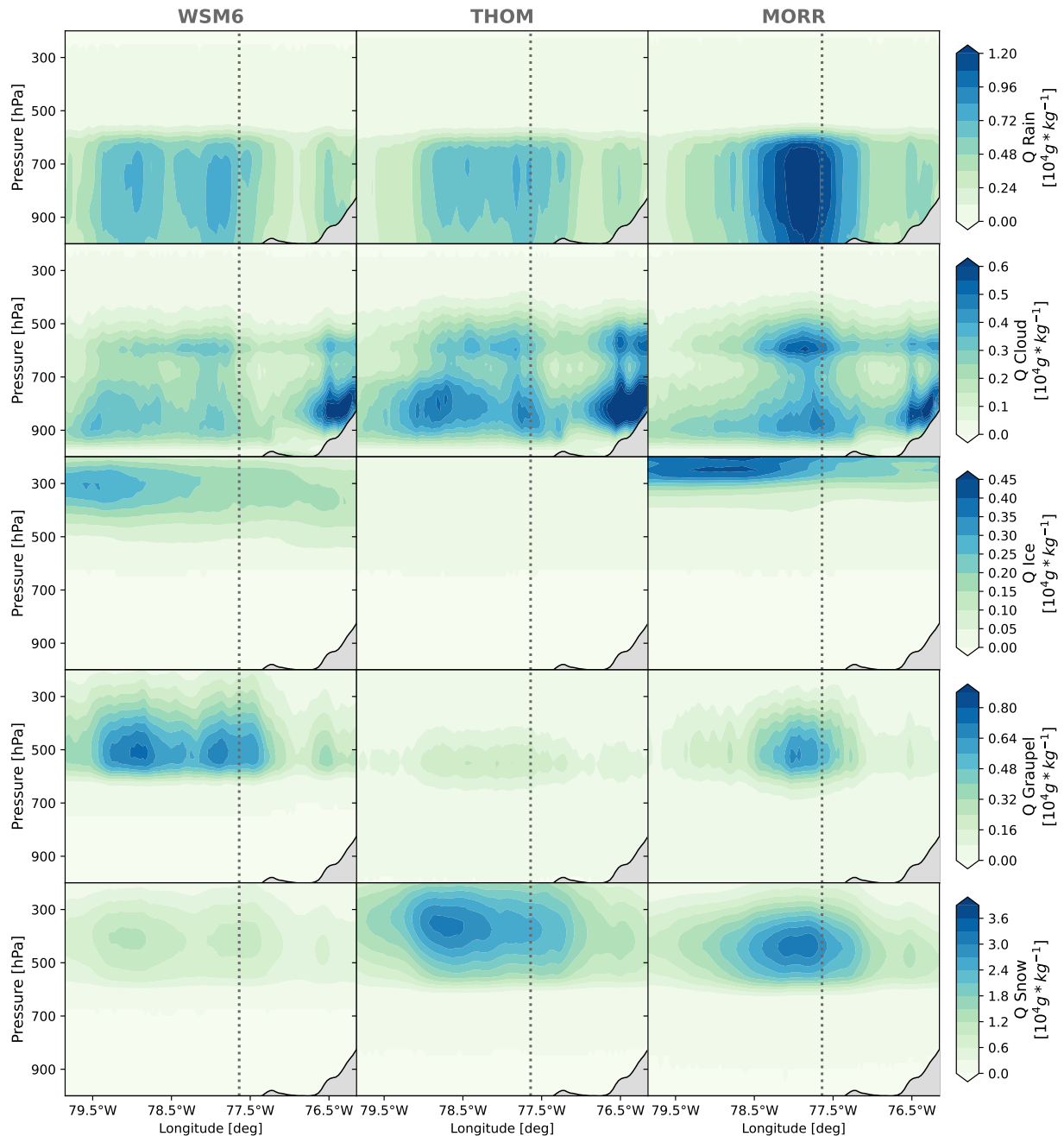
Figure 2.12: Longitude-height section of averaged mixing ratio for different species of hydrometeors. From left to right: WSM6, THOM, MORR. From top to bottom: mixing ratio for rain, cloud, ice, graupel, and snow species.

Different studies have shown the importance of latent heat release in the development and maintenance of convection. Halder et al. (2015) modified the ice-nucleation formulation in MP Morrison's scheme. The modified version generated a greater release of latent heat in the upper atmosphere due to deposition, causing changes in the vertical wind speed. Huang et al. (2020) studied the sensitivity of three MP schemes to representing an extreme rainfall event. The authors attributed the sensitivity to condensation-associated heating and evaporative cooling, influencing storm development and convection propagation. Studying Mesoscale Convective Systems (MCSs) in the United States, Yang et al. (2017) and Feng et al. (2018) demonstrate the role of diabatic heating in producing feedbacks that influence circulation fields and contribute to forming more long-lived MCSs. Furthermore, the impact of latent heat release on dynamics could be greater in tropical regions (Fan et al., 2015; Das et al., 2021). Altogether, the results of these studies are consistent with that presented in this subsection and suggest that the release of latent heat, caused by the formation of ice-phase hydrometeors, may be essential for the development of rainfall and convection in the Pacific.

2.4   Conclusions

In this chapter, the sensitivity of MP and PBL schemes to the representation of precipitation in Northwestern South America was analyzed. 7-day simulations with the WRF model were performed using three MP schemes (WSM6, THOM, MORR) and two PBL schemes (YSU and MYNN). The simulations were evaluated using satellite information and soundings from the OTREC campaign as reference.

In general, the performed simulations were able to capture the spatiotemporal characteristics of precipitation during the study period, with some differences between the parameterization schemes. Simulations with MORR showed higher precipitation rates, especially in the Pacific and near the coastline. In terms of PBL, higher rainfall rates were observed with YSU, especially in the Colombian flatlands. Although the performance was highly dependent on the study region, WSM6 and THOM provided the best results among the MP schemes, while the PBL YSU scheme showed a better performance compared to MYNN. These results were consistent with other previous studies and imply that less computationally expensive schemes exhibited better performance, which is convenient for forecasting tasks. In addition, the different simulations were able to capture the vertical profiles of different dynamic and thermodynamic variables.

Since PBL parameterizations determined precipitation rates in the flatlands of the study region, processes related to these differences were studied in the Colombian Amazon. PBL schemes exerted a marked influence on the moisture transport at low levels, where YSU presented higher fluxes, a more marked convergence, as well as higher humid convection compared to MYNN. When analyzing the sensible and latent heat fluxes, YSU showed higher values with differences that exceeded 20%. In addition, it was observed that the PBL schemes impact the incident solar radiation through variations in the vertical distribution of cloudiness. Specifically, MYNN produced a greater amount of low-level clouds, blocking the incident solar radiation. These results suggest that the differences between PBL schemes may be associated with positive feedback between cloud partitions and heat fluxes for MYNN.

In the Pacific, where the MP schemes had less agreement, microphysics modified the intensity and spatial structure of low-level moisture flux. Particularly, MORR showed a higher moisture flux that extended longitudinally deeper than for THOM and WSM6. Likewise, MORR showed a greater low-level flux convergence and a more marked upward moisture transport. The enhanced convection in MORR is mainly related to diabatic heating at medium to high levels, which also coincides with the area of greatest rainfall. Particularly, it was observed that higher latent heat release in MORR was associated with the production of solid-phase hydrometeors in the mixed-phase zone, which in turn can influence the vertical velocity. According to these results, MP schemes can influence low-level moisture fluxes due to mass continuity. Future modeling studies in the Pacific should carefully consider the selection of the MP scheme due to its sensitivity in representing precipitation.

Finally, it is important to point out that this study was carried out during a study period of

7 days, so it is necessary to perform longer simulations in order to obtain more robust conclusions. Additionally, a more detailed assessment could be done using information available from weather radars and surface stations. Future studies could be oriented in this sense. Studies like this provide a framework that can contribute to the continuous improvement of parameterization schemes, which is fundamental to reducing the uncertainty of numerical models.

Chapter 3. Assessing the spatio-temporal representation of Mesoscale Convective Systems in Northwestern South America

Abstract

Organized thunderstorms can compromise human life and impact agriculture, infrastructure, and aviation. Convection-permitting models have emerged as useful tools to investigate the environments and mechanisms causing deep convection. However, in northwestern South America (NWSA), where deep convection is widespread and frequent, modeling studies at convection-permitting resolution are limited. In this context, we perform subcontinental scale convection-permitting simulations to represent Mesoscale Convective Systems (MCSs) in NWSA using the Weather Research and Forecasting model. The model was assessed following an object-based approach, using an algorithm to identify and track MCSs. Simulated features of MCSs such as frequency, intensity, size, evolution, and propagation were compared with satellite-derived MCSs characteristics. Results showed that the model adequately represented the seasonal occurrence of MCSs in NWSA, which is consistent with the latitudinal migration of the ITCZ. WRF also represented the diurnal cycle of MCSs and precipitation in different regions of the country, with nocturnal convection in northwestern Colombia, a notable oceanic hotspot during the morning in the Colombian Pacific, and a diurnal maximum in the Savannas-Amazon flatlands. WRF underestimated the area and overestimated the intensity of MCSs, although simulations captured the evolution of MCSs from initiation to dissipation. Also, the model correctly captured the MCSs' initiation hour, especially for systems lasting less than 10 hours. Consistent with observations, simulated MCSs propagated westward and presented higher speeds on the Amazon-Savannas flatlands, whereas lower velocities were observed over and to the west of the Andes. In general, convective patterns were associated with the seasonality of low-level winds and moisture, which are highly modulated by the Choco and Orinoco low-level jets. This study provides insights into the strengths and weaknesses in the simulation of MCSs in NWSA at convection-permitting resolution. As far as know, this is the first effort to assess the representation of MCSs in the region using convection-permitting simulations.

Keywords: WRF, Mesoscale convective systems, Northwestern South America, Object-based evaluation, Seasonal, Diurnal

3.1   Introduction

Deep convection can trigger severe weather phenomena like extreme rainfall events, flash floods, hailstorms, and severe winds. As a consequence, convective events compromise human life and impact agriculture, infrastructure, and aviation. The relevance of convective systems for society translates into the growing scientific interest in studying and forecasting their formation and evolution.

Convection varies enormously over a wide range of spatial and temporal scales (Houze et al., 2015) due to the confluence of multiple atmospheric mechanisms, including high amounts of water vapor, features causing air to rise (e.g., orographic barriers or low-level convergence), and atmospheric instability (Schumacher and Rasmussen, 2020). Consequently, mechanisms causing deep convection are strongly dependent on the study region. Regional models are valuable tools for studying convection in certain regions because they can represent atmospheric physics and dynamics at high resolutions, improving the representation of land-atmosphere interactions and localized convection (Prein et al., 2013; Posada-Marín et al., 2019; Gutowski et al., 2020). These models have been used, for instance, to: understand physical processes that trigger deep convection in different regions (Mohan et al., 2018; Karki et al., 2018; Flores Rojas et al., 2019); forecast the occurrence of convective events (Rogelis and Werner, 2018; Hoyos et al., 2019); and project long-term changes in the frequency and intensity of MCSs (Prein et al., 2017a; Klein et al., 2021; Arias et al., 2021). Thus, regional modeling is essential for risk management and mitigation-adaptation strategies.

Regional convection-permitting (CP) simulations have acquired great relevance for the study of MCSs (Prein et al., 2013; Feng et al., 2018; Rasmussen et al., 2020; Prein et al., 2020; Gutowski et al., 2020). In CP simulations, convection is explicitly solved by the model, providing an opportunity to understand the physical mechanisms related to the occurrence and development of deep convection. Previous studies have evaluated the ability of CP simulations to represent deep convection. Yang et al. (2017) studied the environments of long-lived MCSs over great plains using the WRF model. In general, the model captured the main features of MCSs, including lifetime and the associated precipitation. Likewise, Feng et al. (2018) showed good performance when simulating the characteristics of MCSs in the United States. In West Africa, Crook et al. (2019) assessed the representation of convective systems using simulations with and without permitted convection and found that CP simulations showed a better representation of diurnal cycles and lifetimes of convective events. Furthermore, Prein et al. (2020) carried out a simulation of 13 years in North America using the WRF model at CP scale and the results showed that the model represented the main characteristics of the MCSs, including size, precipitation, speed of propagation, and lifetime. Recently, Feng et al. (2023) performed CP global simulations, highlighting that despite models overestimated convective rainfall, these captured fundamental characteristics of deep convection such as the diurnal cycle, the area, and the speed of movement. These studies point to the need to advance in the evaluation and understanding of CP models.

There is a lack of investigations using convection-permitting simulations to assess and study

deep convection in tropical regions. Particularly, in northwestern South America (NWSA) where deep convective events are frequent (Zuluaga and Houze, 2015; Jaramillo et al., 2017), a few case studies have been carried out on specific regions. In the central Andes of Peru, Martínez-Castro et al. (2019) evaluated different microphysical schemes of the WRF model for the forecast of two convective precipitation events. Yepes et al. (2020), studied mechanisms behind the diurnal cycle of precipitation in the Colombian Pacific during November 2016. Gomez-Rios et al. (2023) used two-week simulations to study the mechanisms associated with the formation of convective events in the inter-Andean Magdalena Valley. Nonetheless, these studies have focused on specific regions, used short simulation periods, and did not employ an object-based analysis. No previous studies evaluating the performance of CP model simulations to represent MCSs in NWSA at subcontinental scales and for different seasons were found in an extensive literature review. Advances in evaluating this type of model would be helpful to study processes triggering convection in this region.

In this chapter, the spatio-temporal representation of Mesoscale Convective Systems in NWSA is assessed. Four convection-permitting simulations are performed to represent distinct hydroclimatological conditions in the region. A tracking algorithm and satellite data are used to evaluate model results, and different characteristics of the MCSs, such as the area, intensity, and direction of propagation, are assessed. The remainder of the chapter is organized as follows: Section 3.2 provides context about convection and precipitation in the study area, gives some details of the simulation and study periods, and offers an explanation of the algorithm; Section 3.3 presents the spatio-temporal assessment of the simulations and discusses with previous observational and modeling studies in the region; Section 3.4 presents the main findings of this chapter.

3.2 Data and methods

3.2.1 Context

The region of interest is northwestern South America (NWSA). As described in Chapter 2, NWSA has multiple zones prone to deep convective events and extreme rainfall occurrence. The interannual variability of precipitation in the region is modulated by the latitudinal movement of the intertropical convergence zone (ITCZ), and the activity of low-level jets and their interactions with the Andes mountain range (Poveda et al., 2006, 2014; Urrea et al., 2019). Deep convection in NWSA is characterized by a high occurrence from December to February in the Colombian Amazon flatlands and from June to August in the Colombian Pacific and Caribbean regions (Hernandez-Deckers, 2022). Concerning the diurnal cycle, deep convection (and precipitation) in NWSA is maximum in the afternoon over land, but nocturnal rainfall predominates in particular regions, such as Lake Maracaibo and some inter-Andean valleys (Mapes et al., 2003; Poveda et al., 2005; Hernandez-Deckers, 2022). Further, a marked nocturnal-early morning maximum has been described offshore of the Colombian Pacific coast (Mapes et al., 2003; Zuluaga and Houze, 2015; Jaramillo et al., 2017), considered one of the rainiest places on Earth and a Mesoscale Convective System hotspot (Mejía et al., 2021). Despite the necessity to further understand deep convection in the NWSA, previous studies have mainly concentrated on observational approaches. The implementation and evaluation of numerical models to study convection in NWSA still need to be improved. Any study aiming to close the gap between observational and model-based studies could provide valuable information to inform decision-making.

3.2.2 Experiments

As in the previous chapter, the Weather Research and Forecasting (WRF; Skamarock et al., 2019) model version 4.2 was used to simulate MCSs in NWSA. The WRF model is widely used for research and operational forecast, with satisfactory results for simulating MCSs (e.g., Feng et al., 2018; Prein et al., 2020). The setup of the model is based on the results obtained in Chapter 2, where three microphysics (WSM6, Thompson, and Morrison) and two boundary layer (YSU and MYNN) schemes were tested. Simulations were carried out with the WSM6 and YSU parameterizations, which showed the best performance in Chapter 2 and keep a moderate computational cost. Similarly to the previous chapter, two one-way nested domains were configured (see Figure 3.1), with the first domain (D1) covering the north of South America at a resolution of 12 km and the inner domain (D2) covering northwestern South America at 4 km (convection-permitting resolution). The ERA5 reanalysis data were used as boundary and initial conditions, including weak spectral nudging above the planetary boundary layer to preserve the synoptic-scale variability while allowing the model to simulate low-level processes. The entire model configuration is detailed in Chapter 2.

Four simulations were performed in different months of 2019, each for one month. Table 3.1 details the model integration periods of each simulation as well as how we will refer to each simulation (acronym) henceforth. The selected periods aim to represent distinct hydro-

climatological conditions in NWSA, and considered periods with high convective activity, as well as differences in the spatial occurrence of convection, according to previous studies (e.g., Hernandez-Deckers, 2022). The number of convective events observed during the study period is plotted in Figure 3.1. Further details of the detection of events are described in the next Section.

3.2.3 Object-based evaluation

3.2.3.1 Observations

Model evaluation is focused on spatio-temporal convective features and rainfall patterns. Particularly, an object-based approach is proposed to assess the model performance. These approaches have gained great relevance as they permit the evaluation of features of deep convective events such as area, intensity, shape, and trajectory (Davis et al., 2009; Prein et al., 2020). In this study, the Algorithm for TRACKing Convective Systems (ATRACKCS; Ramírez-Cardona et al., 2022) was used to track deep convective clouds using Brightness Temperature (BT) and precipitation data from satellite images. For BT, the used data is a merge of infrared data from geostationary satellites (MERGIR; Janowiak et al., 2017), with a spatial resolution of 4 km. For precipitation, the used data is the final precipitation product (level 3) of the integrated multi-satellite retrievals for the global precipitation measurement (GPM) mission (IMERG; Huffman et al., 2020) with a spatial resolution of 0.1°. Both data sources have a 30-minute temporal resolution but were resampled to 1 hour to reduce the computational demand while keeping the ability to track the convective features. Several studies have also used 1-hour temporal resolution using the same data (Feng et al., 2018; Prein et al., 2020).

ATRACKCS detects cold cloud tops following similar criteria from previous studies (Nesbitt et al., 2000; Vizy and Cook, 2018; Li et al., 2021; Feng et al., 2021) in terms of BT threshold, area, intensity, and duration. First, ATRACKCS identifies contiguous regions of $\leq 225K$ BT in a satellite image (time i) and defines an object through the convex hull. Objects with an area > 2000 km^2 and at least 5 pixels with precipitation greater than $2mmh^{-1}$ are kept in the analysis, while objects that do not meet these criteria are discarded. The same procedure is applied to the next image (time i+1). Then, identified objects in time i are matched with the ones identified in time i+1 based on maximum overlapping criteria (objects with a higher overlap fraction are matched), establishing a track. The track ends if the last identified object does not overlap any other object. ATRACKCS computes and

Table 3.1: Periods selected for the four one-month WRF simulations.

Start time	End time	Acronym
January 1, 2019 - 00 UTC	February 2, 2019 - 00 UTC	JF
March 22, 2019 - 00 UTC	April 22, 2019 - 00 UTC	MA
July 12, 2019 - 00 UTC	August 12, 2019 - 00 UTC	JA
September 18, 2019 - 00 UTC	October 18, 2019 - 00 UTC	SO

retrieves different features of the identified objects such as the centroid, area, mean BT, mean and maximum precipitation, total distance traveled, total duration, and propagation direction and velocity. Mean and maximum rainfall is computed among the pixels with $>$ $2mmh^{-1}$ rain rates. The algorithm was run for each one-month period and the results are considered as the reference for the model assessment.

In this study, tracks with more than six objects (i.e., lasting 6 hours or more) are referred to as Mesoscale Convective Systems (MCSs) and are considered for the evaluation of the model. Due to their duration, these events are considered organized storms. Other studies have used more restrictive thresholds in order to study robust MCSs. However, since the study period is relatively short (a few months), more restrictive criteria result in a sharp decrease in the population of events, compromising the robustness of the analyses. It is highlighted that the selected events are highly relevant for many sectors such as aviation and agriculture. Moreover, this approach allows the comparison and discussion with other studies that have detailed general characteristics of organized deep convection in the region.

3.2.3.2 Simulations

In order to ensure consistency in the comparison, ATRACKCS was also implemented using WRF fields. For this purpose, WRF outputs in the innermost domain were adapted to satisfy the ATRACKCS requirements. BT and precipitation fields were retrieved at every hour and formatted in the netCDF format required by the algorithm. A 3 x 3 kernel (12 km) was used to smooth modeled BT fields, which is a common procedure in tracking studies based on model simulations due to their noisy fields (Feng et al., 2018; Prein et al., 2020). A preliminary sensitivity test showed that larger window sizes cause the overlap of objects that do not belong to the same MCS, resulting in a reduction in the number of systems and altering features such as areas and lifetimes (not shown).
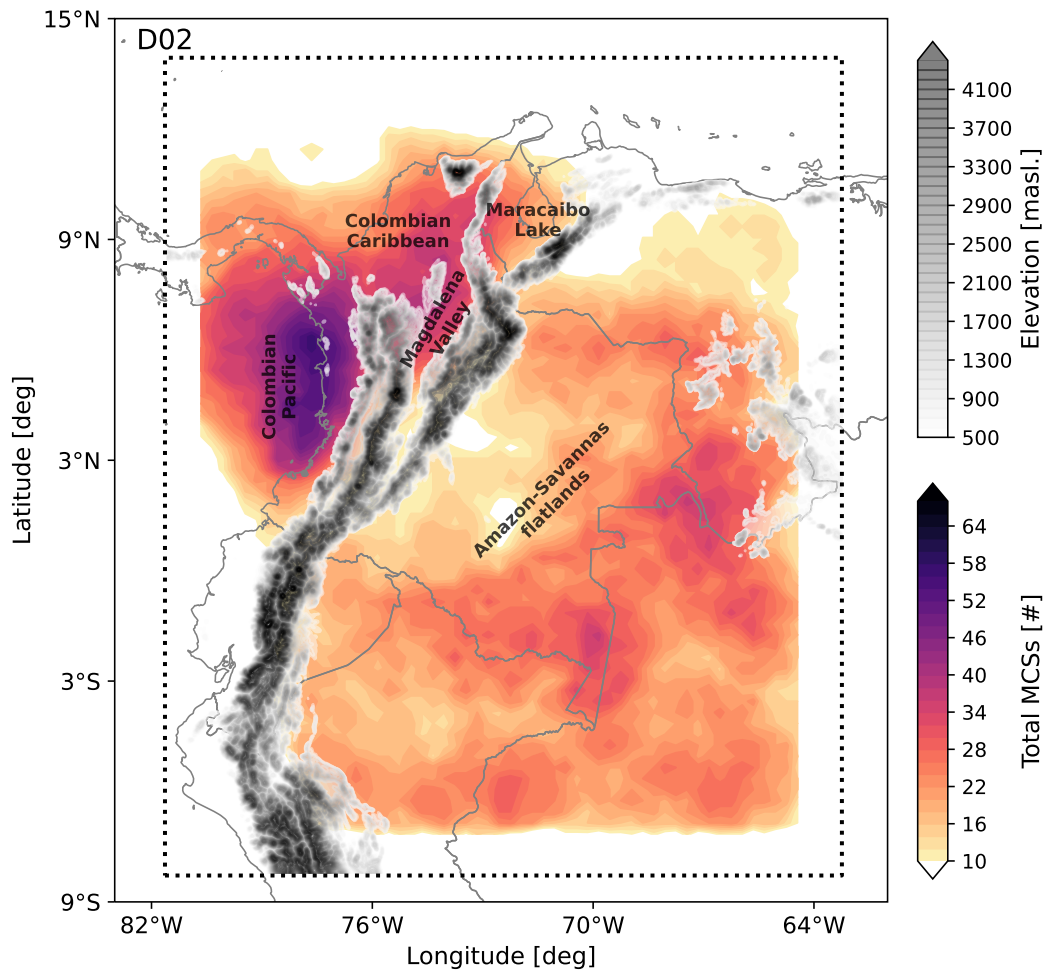
Figure 3.1: Study area. Colored contours show the occurrence of MCSs, and black and white contours depict the height of the terrain. The spatial coverage of domain 2 is delimited by the discontinuous square.

3.3 Results and discussion

The number of MCSs, the objects identified, and the differences for the four periods are shown in Table 3.2. Overall, 748 MCSs were observed while the model simulated 624 storms. The underestimation in the amount of MCSs persisted in all simulations, with differences ranging from 10 to 20 %. The model agrees with the observed interannual variability, resulting in the highest (lowest) occurrence of MCSs in SO (JF), and a similar amount during MA and JA. The temporal evolution of daily rainfall and MCSs during the four simulated periods is presented in Figure 3.2. Simulations reproduced the temporal variations of convective activity during the four periods. Specifically in JF, JA, and SO, the model adequately represented the day-to-day rainfall variability. However, a lower performance was observed during MA, especially at the end of the period. WRF captured the synoptic behavior, as well as the seasonality of rainfall and MCSs. This is of great importance as this study seeks to analyze a representative population of MCSs at different times of the year.

In order to evaluate the performance of the model to represent the seasonality of MCSs, Figure 3.3 shows the spatial distribution of the relative frequency of MCSs for the analyzed periods. The model represented the spatial distribution of the systems throughout the year. During JF, WRF adequately showed a higher frequency of MCSs in the south of the domain (in the northwest of the Amazon basin), and a lower activity in the Pacific. In MA convection propagates toward the north and extends over most of the domain, with a relatively higher occurrence in northwestern Colombia. The model represented this northward displacement of convection relative to JF, but overestimated the frequency of systems in the Colombian Amazon and underestimated the frequency in the north of the region. In JA, deep convection predominates towards the northwest of the domain, with maxima on the Colombian Pacific and Caribbean coasts, a minor hotspot near the Colombia-Venezuela border, and a lower occurrence in the south of the domain. For this period, WRF exhibited a higher (lower) occurrence of MCSs in the Colombian Pacific (Caribbean) regions. Finally, showing good agreement with observations, the spatial frequency of the systems in SO was spread over the whole domain, similar to MA, but with higher frequencies of MCSs in the north of Colombia and in the Pacific. These results indicate that the model can capture the main patterns of convection in NWSA, adequately representing the areas of maximum MCS frequency and their interannual variability. Also, Figure S.6 shows that the variability of rainfall in the different periods is also well represented by the model.

The described interannual variability of convection is consistent with the latitudinal mi-

Table 3.2: Total observed and simulated MCSs and ≤225K objects in Domain 2. Absolute and percentage differences for MCSs estimates are also included.

Experiment	JF	MA	JA	SO
Observed MCSs (objects)	129 (1018)	198 (1542)	167 (1326)	254 (1979)
Simulated MCSs (objects)	109 (835)	158 (1185)	136 (1081)	221 (1665)
Differences (percentage)	-20 (15.5%)	-40 (-20.2%)	-31 (-18.6%)	-33 (-13.0%)
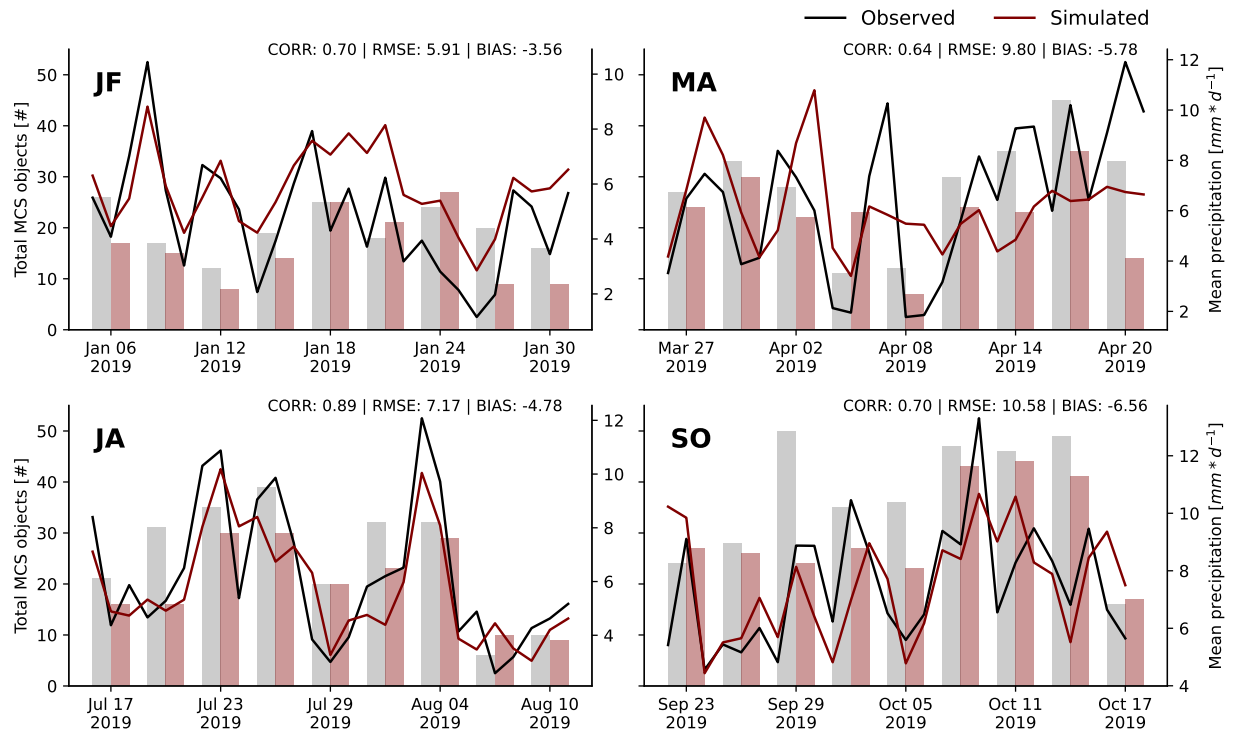
Figure 3.2: Temporal variability of observed (black lines) and simulated (red lines) domain-averaged daily precipitation for the four simulations (panels). Bars represent observed (gray) and simulated (red) 3-day active MCSs in the whole model domain. Annotations in each panel show error metrics for the active MCSs.

gration of the ITCZ, as also suggested in previous studies (see e.g., Jaramillo et al., 2017; Hernandez-Deckers, 2022), reaching its southernmost (northernmost) location during the austral -DJF- (boreal -JJA-) summer (Poveda et al., 2006; Urrea et al., 2019).

MCSs and precipitation are strongly modulated by the diurnal variability of different atmospheric mechanisms. Due to the importance of diurnal variations, we analyzed the ability of the WRF model to reproduce the occurrence of MCSs throughout the day. Figure 3.4 shows the frequency of observed and modeled MCSs in Colombia during different hours of the day. According to satellite information (upper panels), during the afternoon and early night (15 to 21 LT) MCSs occur mainly along the flatlands of the Orinoco and Amazon regions, and in northwestern Colombia. Around midnight, the frequency of MCSs increases in NWSA, especially in northwestern Colombia and the Colombian Amazon, where MCSs have also occurred earlier. A marked hotspot is observed along the Pacific during the morning hours (03-09 LT), where MCSs occur in the ocean. The Colombian Caribbean region and the border with Venezuela are also relevant locations for convection, with a relatively high frequency of MCSs. Of note is that during the late morning and early afternoon, MCSs are scarce in continental areas, but show a high occurrence in the Pacific Ocean, probably in their dissipation stage.

The simulated occurrence of MCSs throughout the day is depicted in the middle panels of
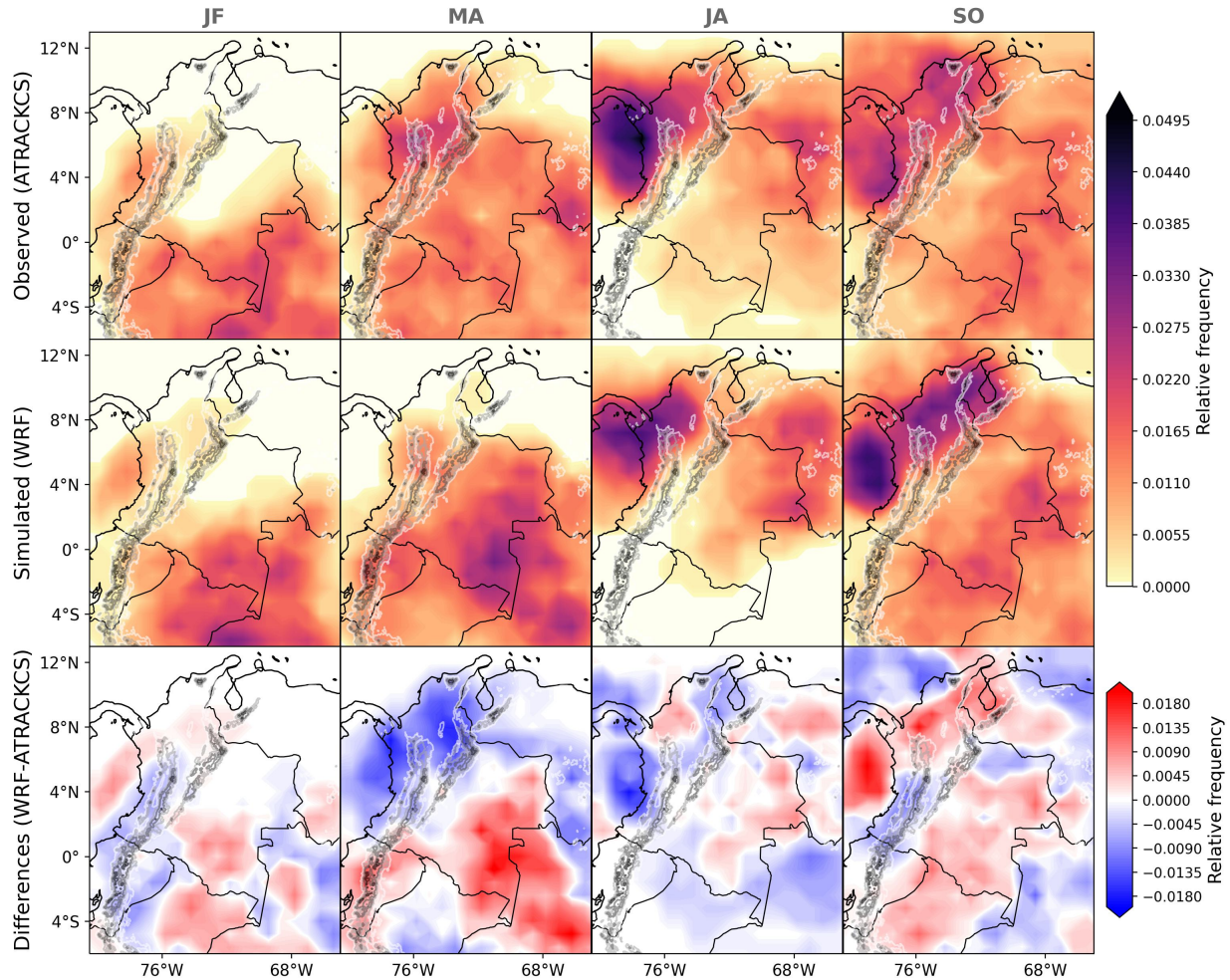
Figure 3.3: Relative frequency of occurrence of observed (upper panels) and simulated (mid panels) MCSs identified by the tracking algorithm in the different seasons. Lower panels show differences (WRF minus observations). A MCS occurs in a certain pixel if the ≤225K area in any object of the MCS intersects that pixel. The frequency was calculated against the total observed and simulated MCSs in each case. Topography is depicted as gray contours.

Figure 3.4. In general, the model had a good ability to represent the time and location of the systems, with some differences regarding satellite-derived results. First, WRF overestimated the frequency of MCSs in the flatlands, especially during the early morning and noon. Also, between 03 and 09 LT, the model underestimated the frequency of systems along the Pacific coast and overestimated convection in the north of Colombia. At last, around noon (09-15 LT) MCSs occurring in the southwest had a spatial bias towards Colombia. Despite these differences, the model has a remarkable performance, capturing the preference zones and hours of MCSs occurrence. Furthermore, of special interest is the model's ability to propagate systems off the shoreline in the Pacific, which is a feature assessed previously (Yepes et al., 2020).

The diurnal variation of precipitation and MCSs in different regions of NWSA is depicted in
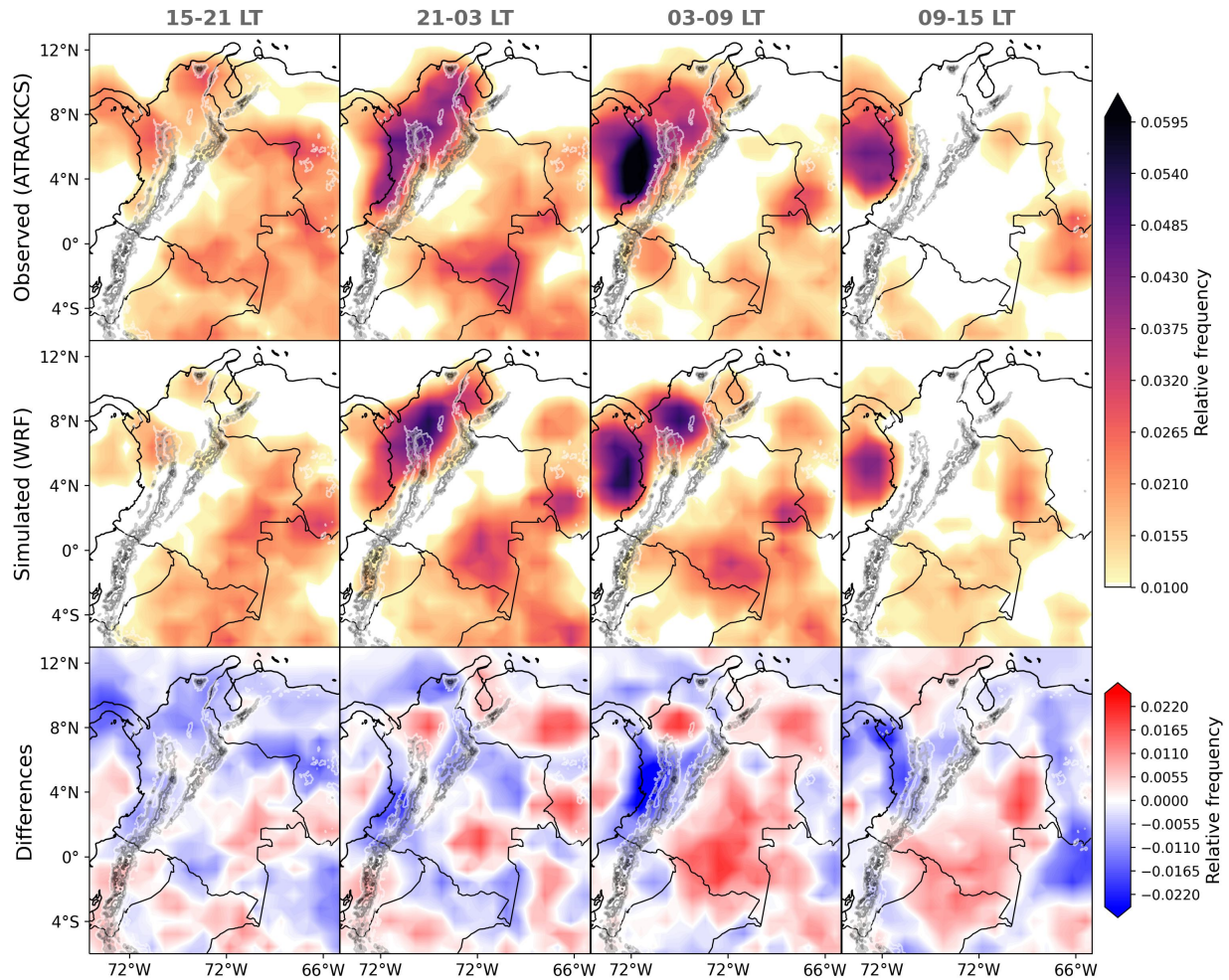
Figure 3.4: Relative frequency of occurrence of observed (upper panels) and simulated (mid panels) MCSs identified by the tracking algorithm throughout the day. Lower panels show differences (WRF minus observations). Values were aggregated for the four simulations. Topography is depicted as gray contours.

Figure 3.5. Consistent with previous results, the model adequately represented the amplitude and diurnal cycle of precipitation and MCSs over the regions of interest. In the Colombian Pacific, the model captured the maximum rainfall around 06-07 LT, which coincides with greater convective activity during the morning hours. Similarly, WRF captured the diurnal cycle of rainfall and convective activity in the inter-Andean valley of the Magdalena River, with a marked peak around midnight. In the Colombian Caribbean, the model simulated the after-midnight maximum rainfall, even though nocturnal convection was underestimated (18-23 LT). In Lake Maracaibo, simulated precipitation peaked 3 hours earlier (at about 4:00 p.m.), although the model maintained rainfall until the early morning, as shown by observations. In the Amazon, simulated rainfall increased in the afternoon, in agreement with observations, but rainfall intensity and the amount of MCSs were overestimated. Further, the model underestimated rainfall and convective activity between 18:00 and 23:00, which remain high in the observations. Finally, in the Savannas, the model adequately captured
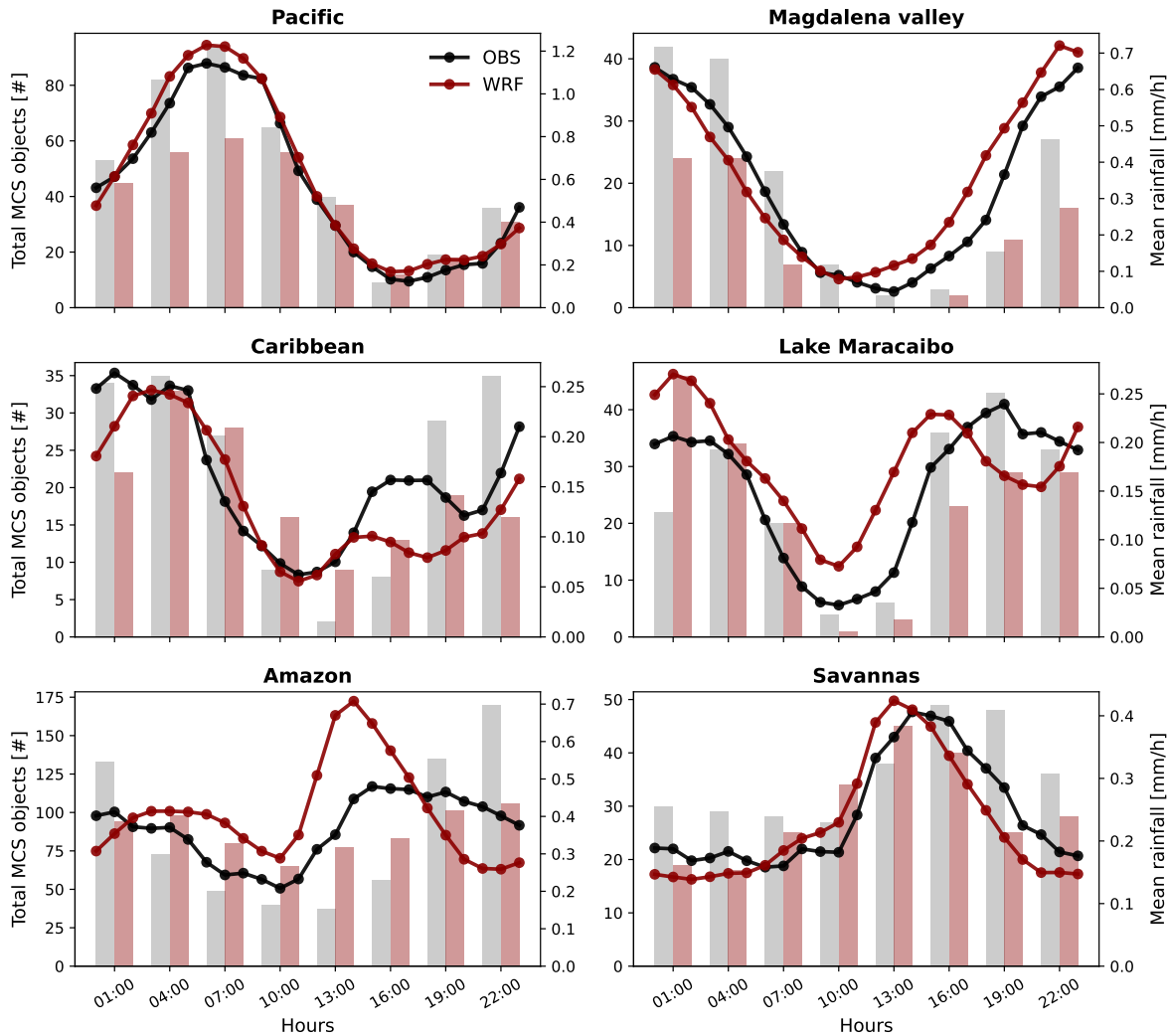
Figure 3.5: Diurnal cycle of 3-hour MCSs objects (bars) and mean rainfall (lines) for the six regions of Chapter 2 (see Figure 2.1). Results for the model are depicted in red, while observations are represented by gray and black colors. Note differences in scale.

the diurnal variability of rainfall and MCSs, with a one-hour lag relative to observations. Overall, the model performs well in representing the diurnal cycle of rainfall and convection in different regions of NWSA, which is also illustrated in Figure S.7.

The diurnal cycles in these regions are consistent with previous research in NWSA. In the Pacific, MCSs are widely known to develop during the early morning and morning hours (Mapes et al., 2003; Jaramillo et al., 2017; Mejía et al., 2021). In the inter-Andean Magdalena Valley, intense moist convection arises around midnight (Hernandez-Deckers, 2022; Gomez-Rios et al., 2023). In the Caribbean and Lake Maracaibo, two hotspots of lightning activity worldwide (Holle and Murphy, 2017; Liu et al., 2020a), nocturnal convective activity has been highlighted (Mapes et al., 2003; Holle and Murphy, 2017). Finally, in the Amazon and the Savannas, where further research about deep convection is needed,

Hernandez-Deckers (2022) highlighted a greater number of convective events in the afternoon.

In comparison to traditional approaches, object-based evaluations allow the assessment of different MCS features such as size, lifetime, shape, and velocity, among others (Davis et al., 2009; Prein et al., 2020). Figure 3.6 shows the distribution of different MCS features derived from satellite observations and simulated by the model. WRF produced smaller systems relative to observations, with a mean underestimation of about 5000 km^2. Additionally, the model significantly overestimated the mean MCS-associated rainfall, producing about twice the observed values. On the other hand, MCSs had shorter lifetimes in the model than in observations, although the traveled distances were generally similar. WRF also adequately reproduced the zonal and meridional displacement of the systems. This underestimation of the MCSs' areas occurs mainly in northwestern Colombia S.8, where observed MCS are largest, while the model showed similar areas in the remainder of the domain. Despite biases in MCSs duration and rainfall, the model correctly represented higher precipitation and longer duration in the Pacific, as seen in the mid and right panels of Figure S.8. Hernandez-Deckers (2022) also found more prolonged convective events in the Pacific.

In order to assess the spatial structure of rainfall, Figure 3.7 presents rainfall composites around observed and simulated MCSs. Consistent with the results of Figure 3.6, the model

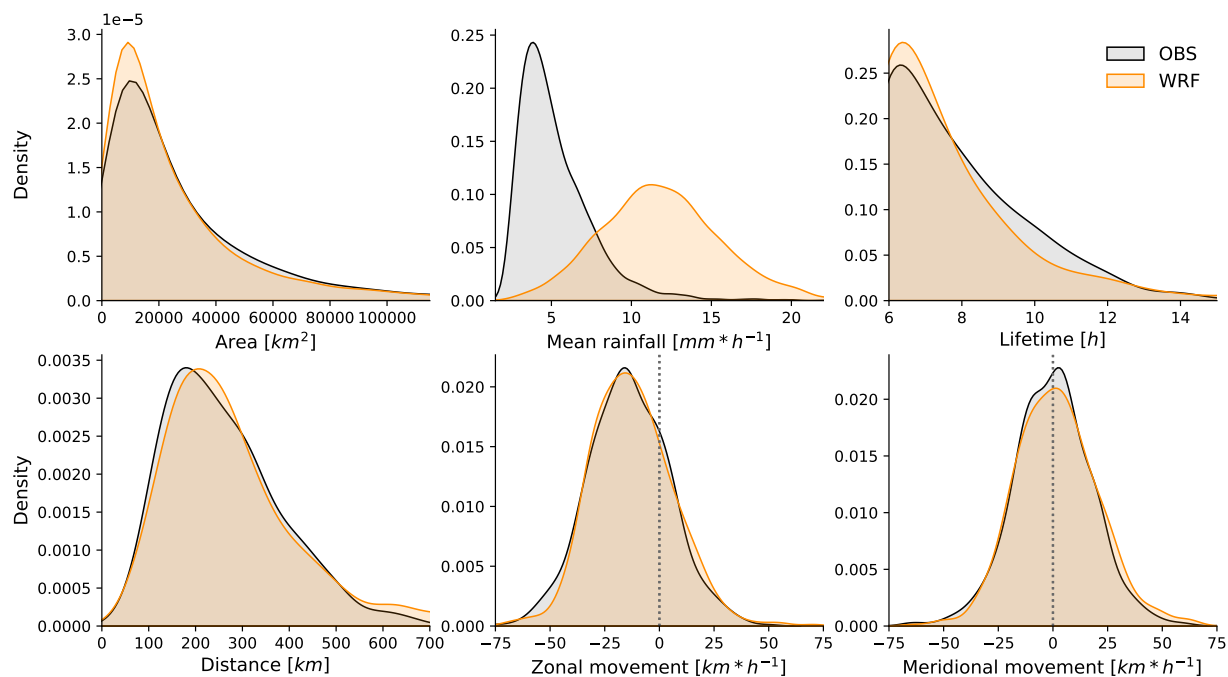**Figure 3.6:** Distribution of observed (gray) and simulated (orange) MCS features identified by the algorithm. Distributions were constructed taking the four WRF simulations. The area represents the region of BT ≤225K. The mean rainfall represents the average of the >2 mm^{-1} pixels. Lifetime and distance are retrieved for each MCS. Zonal and meridional movement are retrieved for each step of the MCSs.
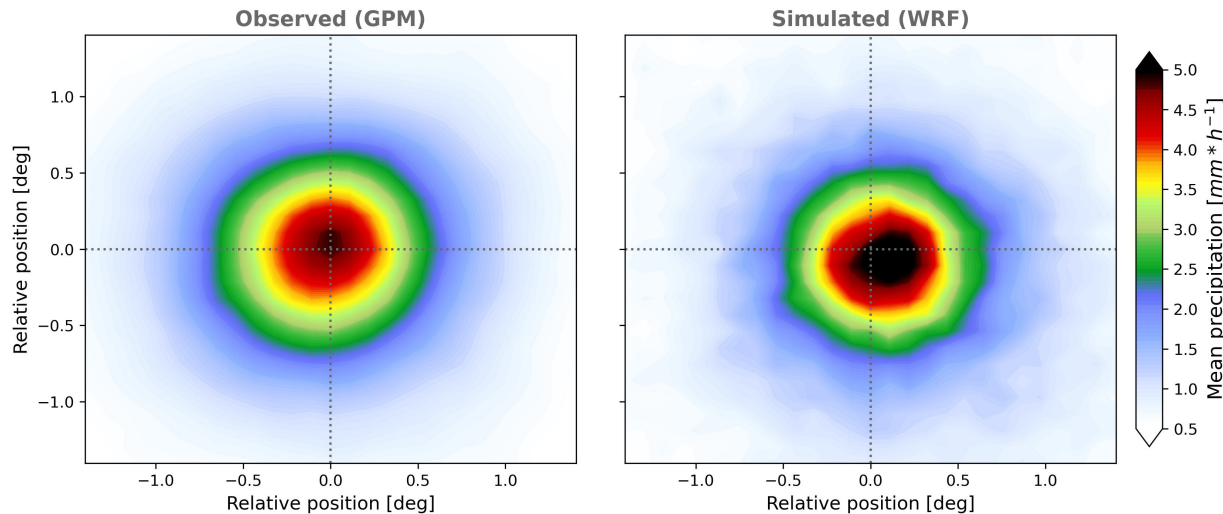
Figure 3.7: Composites of mean precipitation relative to the centroids of each MCS object. Values were averaged over all the observed (left) and simulated (right) MCSs.

overestimated the precipitation associated with MCSs, especially in the system's core, with values exceeding 5 mmh^{-1} over a considerable area. These results agree with Feng et al. (2023), which also evidenced an overestimation in the intensity of precipitation associated with tropical MCSs using global convection-permitting simulations. Despite the overestimation, the magnitude of the rain outside the core is similar, and the model was able to simulate the size and shape of the convective rainfall. Remarkably, the observed precipitation core is aligned in the center of the composite, whereas a slight southeasterly bias was evidenced in the model. This difference can be associated with the fact that IMERG uses GOES brightness temperature data to estimate precipitation fields (Huffman et al., 2020), causing a high relationship between the location of the cold cloud top and generated rainfall, whereas as a physically-based model, WRF's convective core could continue moving while the rainfall is deposited on the surface.

Figure 3.8 shows the evolution (initiation to dissipation) of the MCS area and maximum rainfall. Rainfall is standardized for better comparability (due to the significant bias) and to focus on temporal variability. The model reproduced the initiation, development, and dissipation of MCSs, with increases in the area up to 60-70% of the event duration when MCSs start decreasing in size until the end of the track. In addition, WRF represented the evolution of MCSs' maximum rainfall, with lower values during the beginning and end of the track, and maximum values around 40-50% of the system's duration. Previous studies in the great plains of the United States have also shown that the model captures the evolution of MCSs (Feng et al., 2018; Prein et al., 2020). This analysis not only highlights the capacity of the model to represent the evolution of MCSs but also shows that ATRACKCS adequately identifies and tracks observed and simulated MCSs, capturing their initiation and dissipation.

Figure 3.9 shows the main times of initiation of short- and long-lived MCSs. MCSs with a duration of fewer than 10 hours (here referred to as short-lived) generally initiate during the

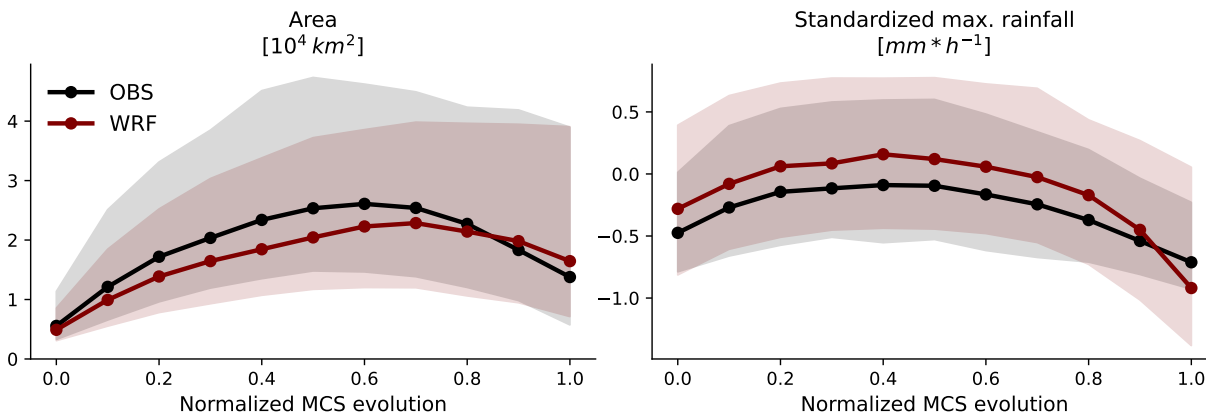**Figure 3.8:** Evolution of observed (black) and simulated (red) MCS area and standardized rainfall. The lifetime of the MCSs was normalized from 0 (initiation) to 1 (dissipation) trying to capture the evolution of systems with different duration and following Feng et al. (2018). The shaded region represents the interquartile range.

afternoon and evening (12 to 23 LT) in NWSA. In contrast, more than 60% of MCSs with longer duration (more than 10 hours) initiate mainly during the evening and night (18 to 02). WRF adequately represented the diurnal cycle of the initiation of MCSs, especially the short-lived ones, while some discrepancies occur for long-lived systems, which is probably related to an insufficient number of samples.

The averaged propagation and speed of MCSs in NWSA is depicted in Figure 3.10. Here, propagation refers to the displacement between the first and last MCS's objects, while velocity refers to the displacement between each consecutive object of the track. The propagation of the systems in the domain exhibited a marked westward direction. Northward of 2°N, observed MCSs propagate mainly to the northwest, while southwest propagation occurs in the south of the domain. The highest speeds of the MCSs are found to the east of the Andes, in the Amazon-Savannas flatlands, where the effect of the topography is less. Likewise, objects also reach relatively high speeds in the northwest of Colombia, while speed propagation in the Andes is considerably reduced. In the Pacific, where MCSs were most frequent, MCSs also move northwestward with slower velocities than in northwestern Colombia and the flatlands. In general, the model was able to represent the mean propagation and the velocity of MCSs in the domain, with higher speeds in the flatlands and minor speeds crossing the Andes and toward the west. The largest differences in propagation were observed to the northwest of Brazil, with a more pronounced southern propagation and an overestimation of the speed. Regarding other studies, the reported propagation speed (Feng et al., 2018) and velocity of the objects (Prein et al., 2020) are comparable.

Altogether, the results of this chapter show that the model can represent the main features of MCSs in NWSA, which provides confidence to analyze the physical processes that explain the simulated convection patterns. For example, as shown in Figures 3.11 and 3.12, the four performed simulations exhibit significant differences in the flow and moisture fields:
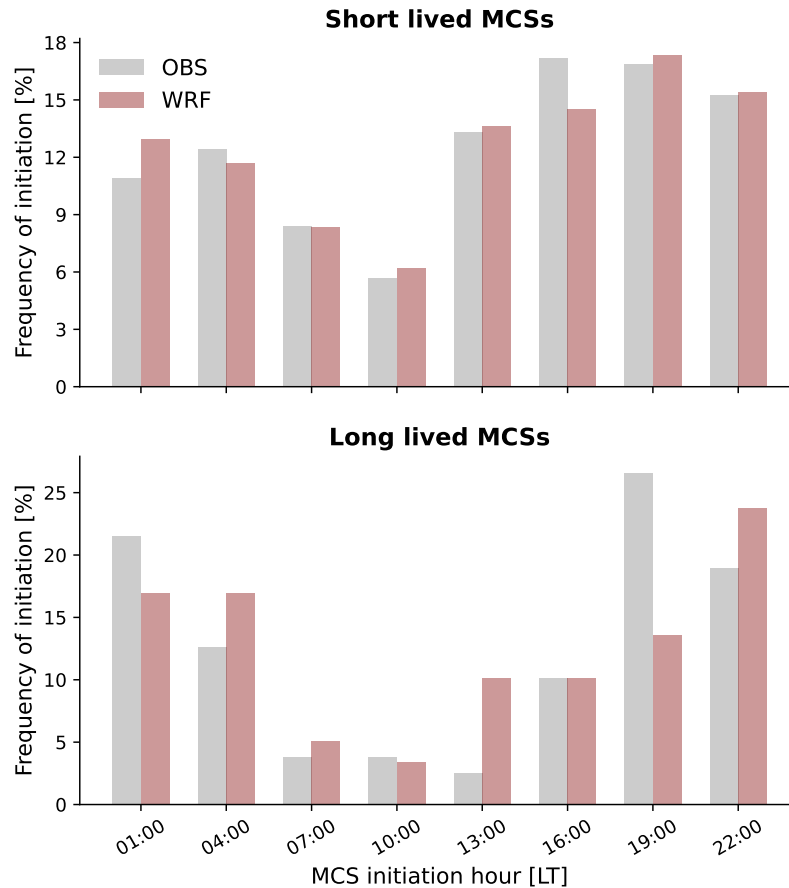
Figure 3.9: Diurnal cycle of initiation of short-lived (lifetime less than or equal to 10 hours, upper panel) and long-lived (lifetime of more than 10 hours, lower panel) MCSs. Simulations (observations) are plotted in red (black) lines.

- In JF, when MCSs are more frequent in the south, specific humidity is higher, and the sea level pressure of around 1011 hPa is lower compared to the higher pressure of 1015 hPa to the northeast of the domain (Figure 3.11). Pressure patterns seem to be in agreement with the direction of the flow, with winds blowing through the Venezuelan and Colombian plains, where the Orinoco low-level jet takes place (Jiménez-Sánchez et al., 2019; Builes-Jaramillo et al., 2022). At 500 hPa (Figure 3.12) humidity is higher to the south consistent with the distribution of deep convection in JF.

- In MA, when the convective activity is spread throughout the domain, more uniform pressure patterns are observed (Figure 3.11) with higher moisture over Colombia as compared to JF, and weaker mid-level winds. Furthermore, there is a reduction in the intensity of the northeasterly flow across the plains, which is consistent with a weaker Orinoco low-level jet (Jiménez-Sánchez et al., 2019).

- In JA, moist convection occurs mainly in the northwest of Colombia and over Venezuela's savannas, and patterns exhibit important differences. Contrarily to JF and MA, winds flow mainly from the Amazon rainforest towards the northwest. Builes-Jaramillo et al.
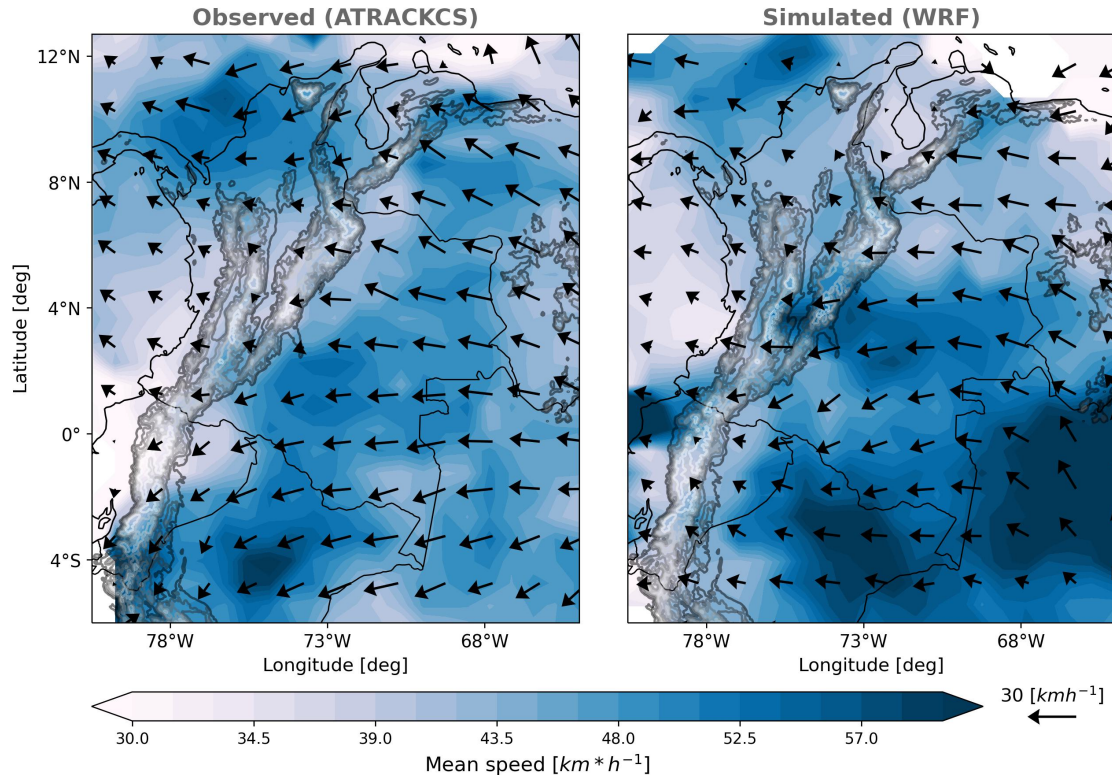
Figure 3.10: Observed (left) and simulated (right) mean MCSs' propagation (arrows) and mean velocity of MCSs (colored contours). Propagation refers to the displacement between the first and last MCS's objects, while colored contours refer to the displacement between each consecutive object of the track.

(2022) described the importance of this southern cross-equatorial flow for the rainfall in the Orinoco basin. Furthermore, lower pressure values and higher moisture are positioned in the Colombian Pacific and the Caribbean. Also, easterlies are stronger than in the other simulations, with a low in the middle of Colombia (around 4°N) and higher humidity levels between 0°N and 8°N.

- Similarly to MA, MCSs in SO occur over the whole domain but especially in the Pacific and northern Colombia. At 850 hPa, moisture is distributed along the domain and, in contrast with JF and JA, marked pressure gradients are not observed. Mid-level winds in SO have a marked eastward component, with a lower magnitude than in JA and high humidity values in the domain. Moreover, greater activity of the Choco-jet is seen in Figure 3.11 during SO, which enhances the deep convection in the Colombian Pacific (Yepes et al., 2019; Mejía et al., 2021).

Although this is an analysis of average patterns in the whole domain, this description is useful to highlight the coherence between the simulated convective patterns and the large-scale environment that may favor the occurrence of MCSs in different months and zones of NWSA. Besides, despite the fact that some of these patterns have been previously described, further efforts are required to connect large-scale environments with the occurrence of deep

convective events. An analysis of the physical mechanisms related to the diurnal occurrence
of MCSs in particular regions is developed in the following chapter.
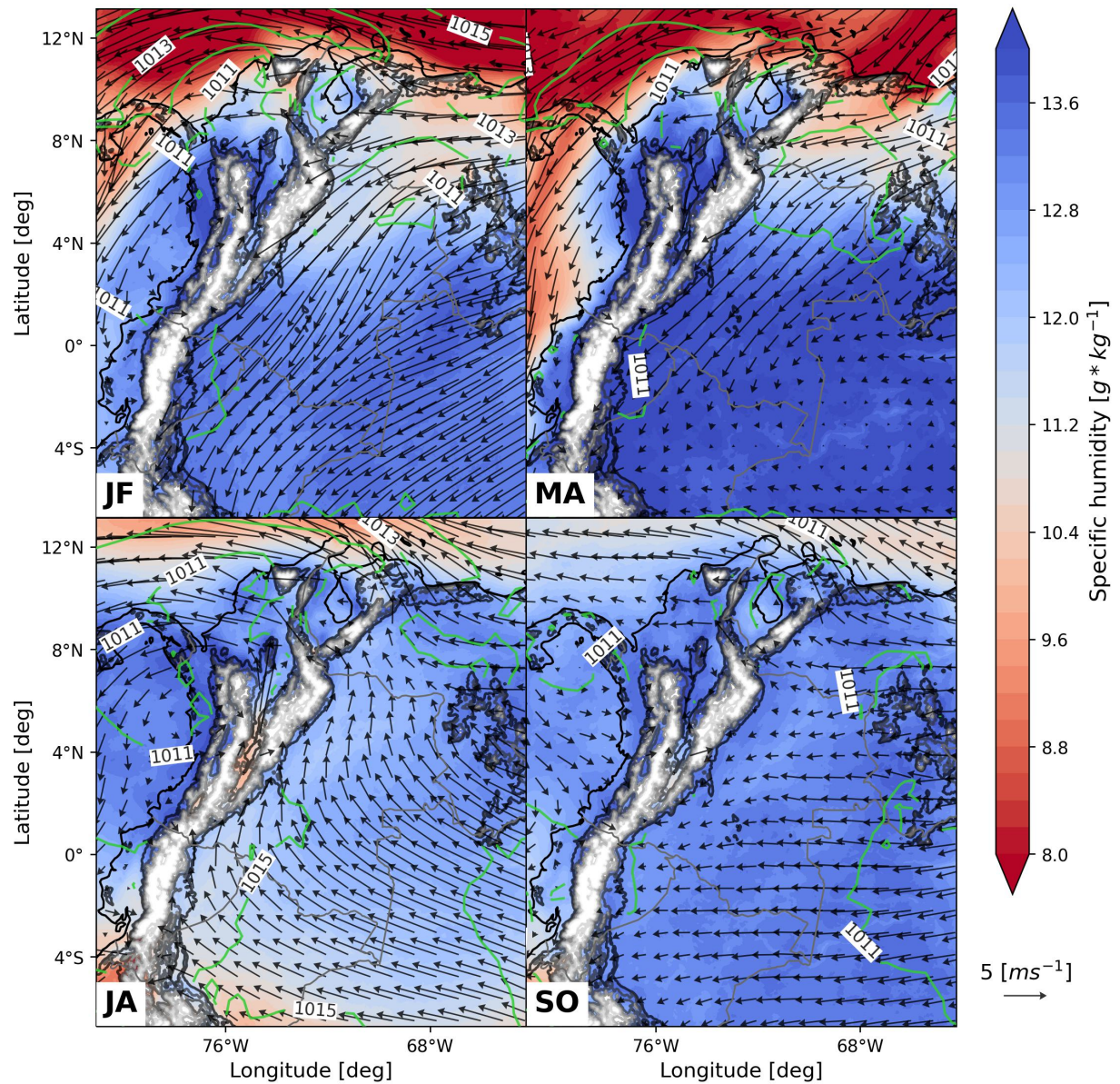
Figure 3.11: Average winds at 850 hPa (arrows), specific humidity at 850 hPa (colored contours),
and sea level pressure (green contours) for the four performed simulations through the year (from
left to right). Topography is represented by black-and-white contours.

Figure 3.12: Similar to Figure 3.11 but for 500 hPa and for geopotential height instead of sea level pressure.

3.4   Conclusions

In this chapter, the spatio-temporal representation of MCSs in NWSA was assessed at convection-permitting resolution. Four simulations with the WRF model were performed in order to represent the seasonal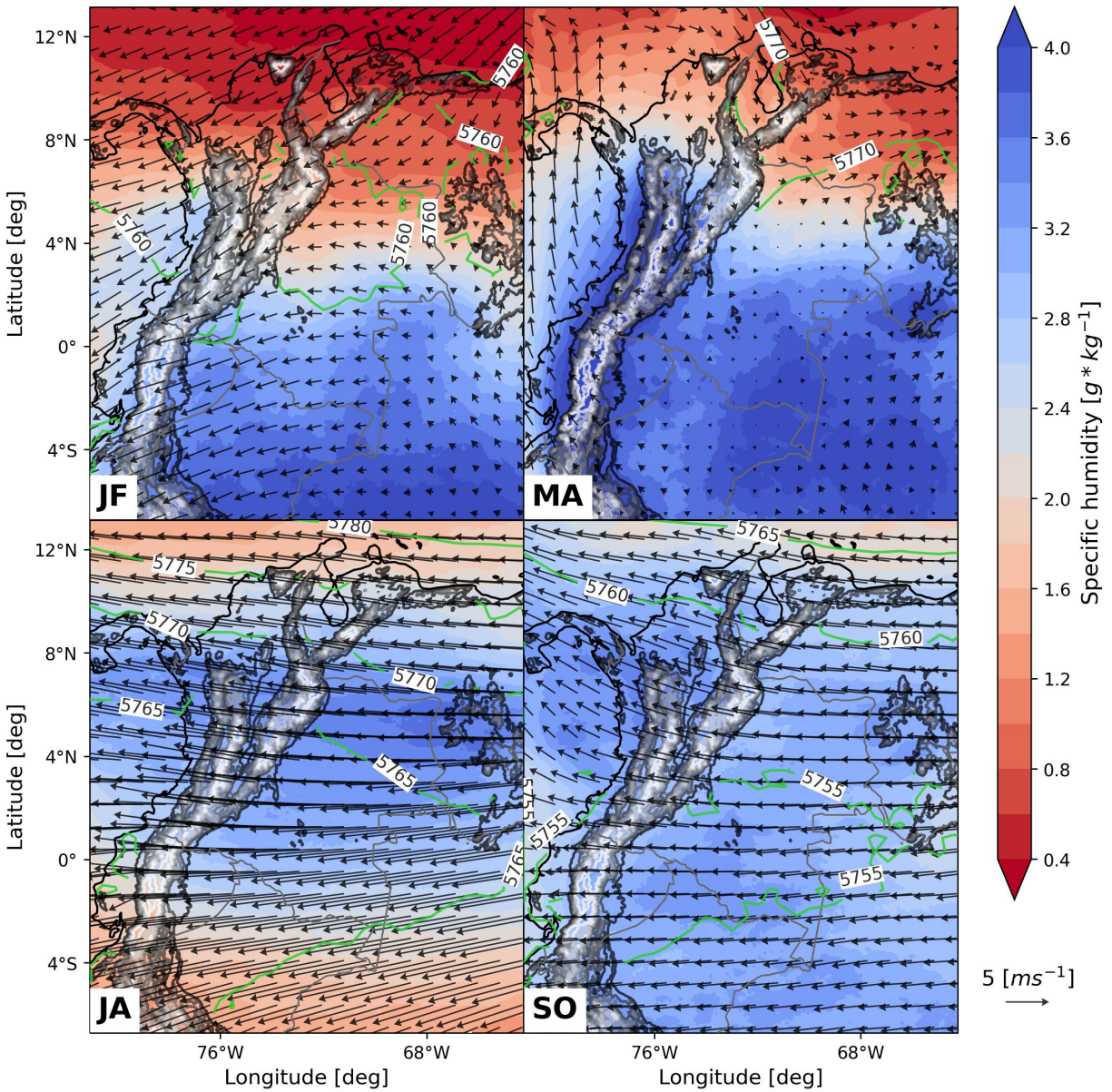ity of MCSs. An algorithm to identify and track MCSs was used to evaluate the ability of the model to reproduce the frequency, size, intensity, lifetime, and propagation of MCSs.

In general, the model underestimated the occurrence of MCSs during the four study periods. However, it could simulate differentiated periods with more and less convective activity in agreement with observations. Results showed that the model captured the seasonality of MCSs, with frequent systems in the south in JF and a pronounced occurrence in the northwest during JA, while in MA and SO, convective events occurred over the whole domain. In agreement with earlier research, modeled convective patterns throughout the year were consistent with the latitudinal migration of the ITCZ. This not only shows that deep convection in the NWSA is consistent with known seasonal variations but that convection-permitting WRF simulations are capable of simulating the mechanisms that trigger organized convection in NWSA under different large-scale conditions.

Diurnal patterns of convection were adequately simulated, with a marked nighttime occurrence in northwestern Colombia. Consistent with observations and previous studies, the model produced an offshore development of MCSs on the Pacific coast during the morning. Furthermore, WRF reproduced the diurnal cycle of precipitation and MCSs in different regions of interest, including the midnight convective activity in the Magdalena Valley and the early-morning rainfall peak in the Caribbean. Also, the diurnal occurrence of MCSs and the morning rainfall peak (06-07 LT) were correctly simulated in the Pacific region. However, in the Colombian Amazon, simulations exhibited a sharper afternoon peak, while in Maracaibo and Colombian Savannas, the amplitude and variation were well captured, but the modeled peaks occurred earlier. The successful reproduction of the diurnal cycle in the regions of interest motivates the development of investigations to comprehend local processes that trigger deep convection in NWSA.

Regarding the main features of the MCSs, WRF showed systems with smaller areas and higher intensity than the satellite observations. Despite the overestimation of precipitation, the spatial structure of rainfall in MCSs coincided with the satellite estimates. Also, the evolution of the MCSs was adequately captured by the model, with systems reaching a greater extent and intensity at about half of the lifetime and then beginning to decay. On the other hand, simulated MCSs had shorter lifetimes than those observed. Preferred initiation hours of short-lived MCSs were correctly simulated, while the model exhibited less agreement regarding initiation times of longer-lived systems. Finally, the model represented the general eastward propagation of MCSs in the region, with faster systems in the flatlands and a reduction in the velocity over and westward of the Andes.

The simulated MCSs during the different periods are related to seasonal changes in the cir-

culation fields and low-level humidity. In turn, the convective patterns in the NWSA are consistent with variations in the activity of the Choco and Orinoco low-level jets. Mid-level dynamics also change considerably throughout the year, which likely play a role in the organization of the storms, for example, via a more or less sheared environment. The implementation of convection-permitting simulations and the analysis performed to study MCSs are scarce in NWSA and need to be improved and deepened. These results motivate the use of convection-permitting models to study the environments and formation mechanisms of MCSs in NWSA.

Chapter 4. Mechanisms behind convective rainfall in northwestern South America

Abstract

A convection-permitting simulation is used to identify mechanisms behind the diurnal cycle of rainfall and convection organization in different regions of Northwestern South America (NWSA). Wet and dry days were separated to study the diurnal cycle of rainfall in the Pacific, the Magdalena Valley, and the Colombian Amazon, as well as the organization of convection in the Colombian Pacific. The results showed an increase in low-level moisture fluxes on days with a marked diurnal rainfall cycle (wet days) in the three regions of interest. Particularly, in the Pacific region, greater activity of the Choco low-level jet was evidenced along with a more unstable and sheared environment during humid days. In the Magdalena Valley, an intensification of down-valley and up-valley fluxes was observed during wet days, as well as weaker easterlies than during dry days. More marked wind shear and enhanced moisture transport from the Amazon rainforest and Venezuelan plains were present during wet days in the Colombian Amazon. While studying convection organization in the Pacific, anomalies in moisture fluxes toward the continent and equivalent potential temperature were present before the initiation of the events. Mesoscale Convective Systems (MCSs) during the mature stage exhibited a mid-level vortex apparently caused by latent heat released during ice-phase hydrometeor formation. As a crucial mechanism, the vortex enhanced mid-level convergence producing a top-heavy mass flux profile. Furthermore, the development of the storms seems to be favored under a weak mid-level shear in the rear, with cold pools in the convective-stratiform transition region. In the front of the MCSs, a low-level current and downdrafts within the cloud promote the development of convective cells, contributing to the organization of convection in the Pacific. This chapter demonstrates the potential of convection-permitting simulations to study mechanisms behind convection in NWSA.

Keywords: Mechanisms, Mesoscale convective systems, Rainfall diurnal cycle, Northwestern South America, WRF, Object-based analysis.

4.1 Introduction

Deep convection in the atmosphere is favored by the confluence of certain ingredients, including a temperature profile suitable for rising air masses (instability), high amounts of water vapor in the atmosphere, convergence at low levels, and orographic barriers causing lifting (Lohmann et al., 2016; Schumacher and Rasmussen, 2020). Understanding atmospheric processes that influence the occurrence of precipitation is useful for improving the predictability of rainfall events and projecting future changes in water availability.

The confluence of mechanisms that trigger convection depends on multiple factors, including the study region, season, and hour of the day, causing spatio-temporal complexity of convective patterns. From a global point of view, the high availability of energy and moisture in the tropics favors the development of deep convection, rising strong thunderstorms that produce large amounts of rain (Zuluaga and Houze, 2015; Lohmann et al., 2016). Land-atmosphere interactions modify energy, momentum, and moisture fluxes through the atmosphere, influencing the formation of convective precipitation events in specific regions (Santanello Jr et al., 2018; Karki et al., 2018; Gentine et al., 2019). Diurnally, solar radiation activates heat fluxes from the surface, controlling convection development and rainfall occurrence (Poveda et al., 2005; Schumacher and Rasmussen, 2020), whereas, the passage of synoptic-scale phenomena such as the Madden-Julian oscillation and easterly waves cause intra-seasonal variability of convection and rainfall (Grimm, 2019; Giraldo-Cardenas et al., 2022).

Deep convection can give rise to the formation of organized storm systems. These systems (here referred to as Mesoscale Convective Systems -MCSs-) groups on a scale larger than individual storms, have great vertical development and cause extreme weather events (Houze, 2004, 2018; Schumacher and Rasmussen, 2020). MCSs are more frequent in tropical regions (Houze et al., 2015; Zuluaga and Houze, 2015; Feng et al., 2021), where they affect vertical profiles of energy and humidity, and influence large-scale circulation (Moncrieff, 2010; Holloway et al., 2017; Houze, 2018). Organized convection poses a characteristic lifecycle (Houze, 2018; Feng et al., 2021). During the genesis (or initial) stage convective cells of deep convection are observed. In their mature stage, MCSs grow and develop a stratiform rainfall region along with new convective cells. Afterward, both convective and stratiform regions decline in the decaying stage.

Different mechanisms influence the development and organization of MCSs. As MCSs develop, a top-heavy heating profile forms, which is characteristic of stratiform regions (Houze, 2018). This mid to upper-level heating can influence circulation fields and cause the formation of a mesoscale vortex, contributing to the development of longer-lived MCSs (Yang et al., 2017; Feng et al., 2018). Downdrafts caused by the evaporation of rainwater (evaporative cooling) are essential for the development of new convective cells and the movement of MCSs (Houze, 2004; Schumacher and Rasmussen, 2020). Upon reaching the surface, these cold air masses spread horizontally, causing the rise of more humid and warmer air. Vertical wind shear has also been reported to be relevant for convection organization, although the role is much more complex. A more sheared environment can tilt the convective tower separating

zones of updrafts and downdrafts, which contribute to a longer duration of convection (Chen et al., 2015; Schumacher and Rasmussen, 2020). However, the formation of the mesoscale vortex has been reported to be more favored in low-sheared conditions (see Houze, 2004, and cited).

Under this framework, the main objective of this chapter is to identify mechanisms behind the diurnal cycle of rainfall and the organization of convection in distinct regions of the NWSA. Differences between dry and wet days are compared, and a one-month WRF simulation at CP resolution is used to take advantage of the physical consistency of the model. The remainder of the chapter is divided as follows: Section 4.2 presents the methodology for separating dry and wet days, and for computing composites of different fields; Section 4.3 shows the mechanisms evidenced and compares findings with other studies; Section 4.4 concludes.

4.2   Methods

4.2.1   Behind the diurnal cycle of rainfall

Three regions of interest studied in previous chapters were chosen to study the mechanisms behind the diurnal cycle of rainfall in the NWSA: the Colombian Pacific, the Inter-Andean Magdalena Valley, and the Colombian Amazon (See Figure 2.1). These regions have differences in spatial extension and topographic features, allowing the study of convection mechanisms in regions with distinct characteristics. To study the diurnal cycle of rainfall, a simulation with the WRF model between September 18th and October 18th, 2019, was selected for the analysis (see Chapter 3). The selection of a single simulation obeys the need to avoid seasonal variations among the patterns that influence convection, which, as shown in the previous chapter, is significant. In addition, in September-October convection is active over most of NWSA, causing precipitation in these three regions.

As previously reported, the selected regions have very marked diurnal cycles of rainfall, with a maximum in the morning (07 LT) in the Pacific, a peak around midnight in the Magdalena Valley (00 LT), and a maximum during the afternoon (14 LT) in the Amazon. The upper panels in Figure 4.1 show that diurnal cycles for September-October are consistent with rainfall diurnal cycles throughout the year and with satellite observations. In this sense, the one-month simulation between September-October can be used to understand the rainfall diurnal cycle in these regions.

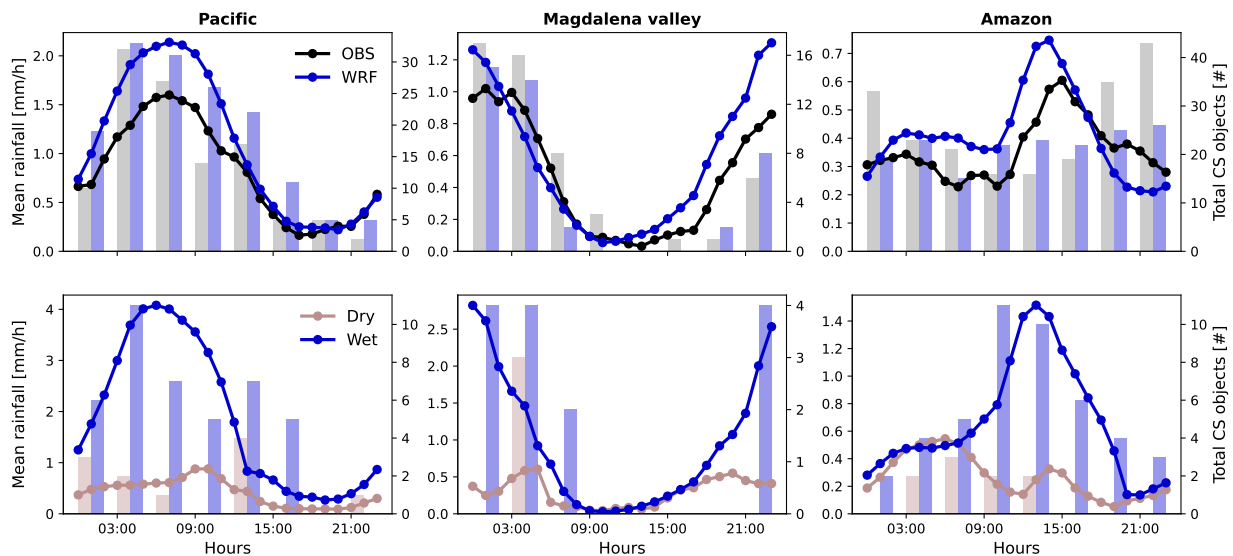**Figure 4.1:** Upper panels: Diurnal cycle rainfall (lines) and 3-hour MCSs objects (bars) during the period of the September-October simulation and for the three regions of interest. Results for the model are depicted in blue, while observations are represented by gray and black colors. Lower panels: Diurnal cycle rainfall (lines) and 3-hour MCSs objects (bars) for defined dry (blue) and wet (brown) days.

Dry and wet days were selected for each region based on simulated rainfall. First, we averaged precipitation around the hours of maximum amplitude of the diurnal cycle (here referred to as the maximum rainfall or rainfall peak) in each region. The 20_{th} and 80_{th} percentiles were used to separate values where averaged rainfall around the rainfall peak is lower and higher, respectively. This separation resulted in five weak and five strong rainfall peaks in each case. Then, dry days were defined as 18 hours before and 6 hours after (24 hours in total) rainfall peaks below the 20_{th} percentile, and wet days are similarly defined around the maximum rainfall values above the 80_{th} percentile. The selection of the days was done as a function of the rainfall peak in order to capture the atmospheric environment before, during, and after the occurrence of diurnal precipitation.

The lower panels in Figure 4.1 display the diurnal cycle of rainfall for wet (blue) and dry (brown) days. During dry days some rainfall was produced because the simulation period was very active in terms of convection and rainfall (as shown in the previous chapter). However, contrarily to dry days, wet days explain the amplitude of the diurnal cycle of rainfall and have a higher occurrence of convective systems in the regions of interest. As the use of percentiles is appropriate for comparability, composites of dynamic and thermodynamic variables for wet and dry days were constructed in each region of interest.

4.2.2   Mechanisms behind organized convection in the Pacific

As a region of great scientific relevance, the Colombian Pacific was selected to analyze mechanisms related to the organization of convection. The Colombian Pacific coast is widely known as a zone of cyclogenesis and high convective activity. Also, it is known as one of the rainiest regions on Earth. However, most advances in the study of convection over the Pacific have relied on observational approaches. As the model performed well in representing convective features in the Pacific (see Chapter 3), a unique opportunity is given to elucidate mechanisms behind Mesoscale Convective Systems in this region.

In accordance with the methodology used for the diurnal cycle, MCSs that occurred during wet days (see above for details) were selected for the analysis. As seen in Figure 4.1 MCSs during wet days are highly related to the rainfall peak and occur mainly during the early morning and morning hours. A preliminary analysis showed that some simulated MCSs initiate in the ocean during the afternoon. In order to ensure consistency, only systems that initiate near the continent were considered for the analysis. This allows capturing typical MCSs in the region, which form near the coast and propagate toward the ocean. After this, a total of seven MCSs were selected for the analysis.

Composites of different variables were computed before, during, and after the initiation of the MCSs, in order to analyze the environments of formation and evolution of MCSs in the region. Composites were obtained for both mean fields and anomalies. In order to remove diurnal and seasonal influence, anomalies were computed with respect to the average diurnal cycle of the September-October period at each pixel and vertical level. Additionally, composites of mean fields and anomalies were calculated in a 1° x 1° region centered on the MCS geometric centroid.

On the other hand, composites for the initiation and mature MCS stages were computed. Here, initiation refers to the first moment when a MCS object is identified, according to the identification and tracking algorithm ATRACKCS described in Chapter 3. The mature stage of MCS is simply taken as the moment when it reaches its maximum area during the entire track. For these two stages, differences in the dynamic and thermodynamic fields were described to infer possible mechanisms behind the evolution and growth of the systems. Furthermore, cross-section composites were computed following the movement of the MCS objects among the initiation and the mature stages to explore mechanisms associated with the movement and the growth of the systems.

4.3   Results and discussion

The results of this chapter are presented in two parts. First, the model is used to unveil physical processes under the diurnal rainfall cycle in three NWSA regions. Second, potential mechanisms associated with convection organization in the Pacific region are explored.

4.3.1   Diurnal cycle of rainfall

Figure 4.2 shows the distance (longitude) vs time (daytime) composites of lower tropospheric and upward moisture flux in the Pacific region for the wet and dry days. Notable differences can be observed between wet and dry days. Wet days showed a stronger moisture flux towards the Andes mountains, especially during the late afternoon and early evening, triggering moist convection on the western flank of the western Andes mountains. During the early morning, strong convection developed over the coastline, west of the Baudó mountain range (topographic bulge located between 77.5°W and 77°W), with a clear propagation pattern towards the ocean during the morning, when maximum rainfall occurs in this region (around 07 LT).

Previous studies have also reported a moisture flux increase toward the continent during wet days in the Pacific (Mejía et al., 2021; Riley Dellaripa et al., 2023), especially during the late night and early morning (Riley Dellaripa et al., 2023). This higher moisture flux is related to a stronger activity of the Choco low-level jet (Yepes et al., 2019). Furthermore, the early-morning propagation of convection into the ocean is widely recognized in the Pacific, especially in observational studies (Jaramillo et al., 2017; Yepes et al., 2020; Mejía et al., 2021). This ability to represent the westward propagation of moist convection encourages the development of modeling-based investigations to advance the understanding of convection in the region, in specific using convection-permitting simulations.

Figure 4.3 shows composites of dynamic and thermodynamic variables relative to the maximum rainfall in the Pacific. Wet days were characterized by stronger updrafts than dry days, even before midnight (more than 8 hours before 07 LT, when the maximum rain takes place). The environment preceding the rain maximum (up to 12 hours before) has a higher equivalent potential temperature during wet days, with average differences of 2K, followed by a temperature drop related to a more stable environment characteristic after strong convective events likely caused by cold pools. Zonal wind shear was also more pronounced during wet days, with noticeable differences more than 12 hours before the rainfall maximum. Regarding diabatic heating, more marked heating in mid-to-high levels was observed with maximum values around the maximum rainfall. To a lesser extent, more marked negative values were observed during wet days compared to dry days, which can be associated with stronger evaporative cooling.

The described mechanisms are in agreement with previous studies. Mejía et al. (2021) showed that wet days in the Pacific are related to enhanced moist static energy at 19LT, which agrees with the results for equivalent potential temperature. Also, a more sheared environment was found during precipitation days (Yepes et al., 2019; Mejía et al., 2021). Diabatic heating
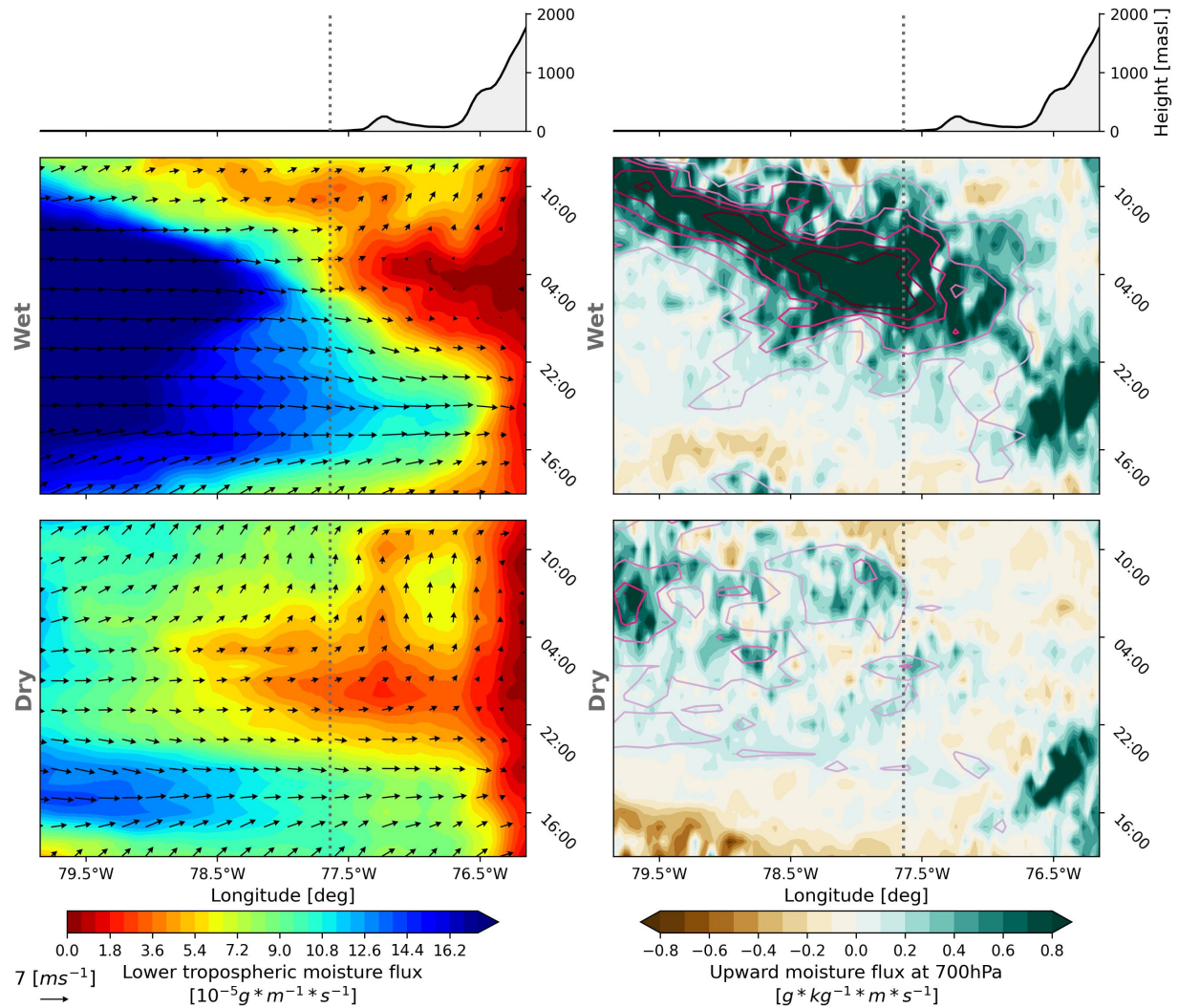
Figure 4.2: Mean distance (longitude) and time (diurnal cycle) plot of lower tropospheric (1000-800 hPa) horizontal moisture flux (left panels) and vertical moisture flux at 700 hPa (right panels) for wet (upper panels) and dry (lower panels) days in the Colombian Pacific. The convergence of lower tropospheric moisture flux is represented as purple contours in the right-side panels and arrows in the left-side panels show 925 hPa horizontal winds. Mean topography is indicated at the top of the figure. Values were averaged meridionally between 4°N and 6.7°N in the region shown in S.9.

could be related to the release of latent heat by condensation or the formation of solid-phase hydrometeors (e.g., see Chapter 2), which could induce feedback with the environment and enhance convection (Yang et al., 2017; Feng et al., 2018), whereas negative values could be related to evaporative cooling, inducing stronger downdrafts. However, further research is needed to understand the role of heat sources and sinks in developing and maintaining convection in the Pacific. Some insights about this role are reported in the next section.

Figure 4.4 shows meridional humidity fluxes along the inter-Andean Magdalena Valley for

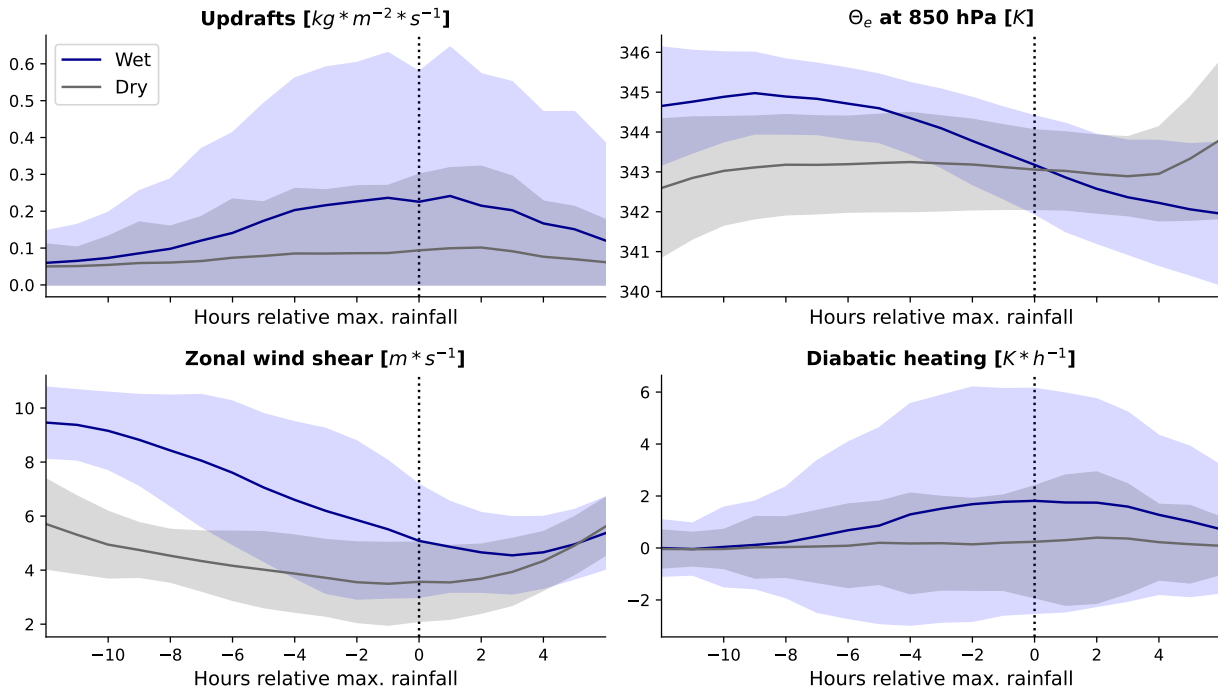**Figure 4.3:** Relative to the diurnal rainfall peak composites for vertically-averaged updrafts (upper left panel), equivalent potential temperature (upper right panel), 925hPa-700hPa zonal wind shear (lower left panel), and 500 to 300 hPa diabatic heating (lower right panel) in the Pacific region. Composites were computed for both dry (gray) and wet (blue) conditions. Shaded areas represent spatial one standard deviation uncertainties.

wet and dry days. In contrast to dry days, wet days presented an intensified along-valley flow, with a strong down-valley moisture flux during the afternoon that extends throughout the valley. Later around 19 LT, the along-valley flow reversed to northerly up-valley winds, associated with an entrance of humidity from the northwest. Up-valley fluxes, which were also stronger for wet rather than for dry days, contributed to the transport of moisture towards the middle Magdalena Valley. The evening shift in the along-valley winds produces a strong low-level convergence in the middle Magdalena (between 6°N and 6.5°N), where moist convection begins at 20 LT. Subsequently, generated convection propagates to the north, toward the low part of the valley, where convection is strongest around midnight, and the highest precipitation rates occur.

Composites relative to the rainfall peak are presented in Figure 4.5 for the Magdalena Valley. As evidenced in the Pacific, updrafts were more notable during wet days and around the peak of the rainfall. However, the difference between dry and wet days only begins to be evident about 3 hours before the maximum rainfall, in contrast to the Pacific, where differences were evident more than 8 hours before the maximum rainfall. Furthermore, in the Magdalena Valley, the equivalent potential temperature was similar between dry and wet days before the rain peak, which could indicate that rather than buoyancy-driven convection, the convergence of winds at low levels triggers moist convection in this region. On wet days
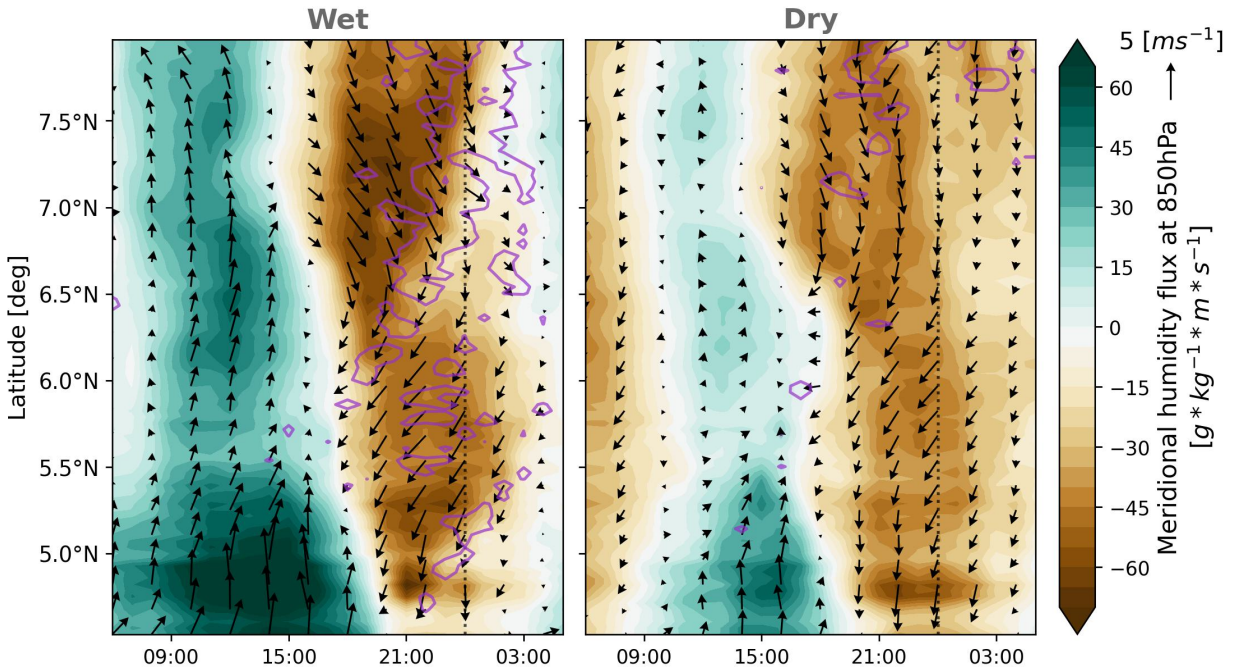
Figure 4.4: Mean latitudinal and diurnal behavior of 850 hPa humidity flux (contours) and winds (arrows) for wet (left panel) and dry (right panel) days in the Magdalena valley. Purple contours depict 0.5 $g*kg^{-1}*m*s^{-1}$ vertical humidity flux at 500 hPa. Values were zonally averaged between 74°W and 75.2°W in the region shown in S.9.

a decrease in the intensity of the mid-level easterly winds was observed. As in the Pacific, the diabatic heating behavior follows a similar behavior to the updrafts.

Consistent with findings of Gomez-Rios et al. (2023), winds along the valley determine low-level convergence and trigger convection in the Magdalena Valley at night. Days with rainfall occurrence also exhibited a reduction in mid-level winds, suggesting that synoptic-scale variations can impact convection in the region, nonetheless, more research is needed on the possible mechanism that explains this relationship.

Figure 4.6 shows the spatial distribution of moisture fluxes, low-level winds, and moist convection, for wet and dry days in the Colombian Amazon. An enhanced low-level moisture flux was observed during wet days. Low-level fluxes arrive mainly from the Amazon rainforest (from the southeast) and the Orinoco River basin (from the northeast), with fluxes more than twice as large as for dry days. A flow reduction occurred in the vicinity of the region of interest, resulting in a greater moisture flux convergence and more pronounced moist convection over the region of interest.

As well as for the Pacific and Magdalena Valley regions, the behavior of different variables before the rainfall peak in Amazon is illustrated in Figure 4.7. In agreement with previous regions, wet days in Amazon showed more pronounced updrafts, up to 5 hours before the maximum precipitation. Similarly to the Magdalena Valley, significant equivalent potential
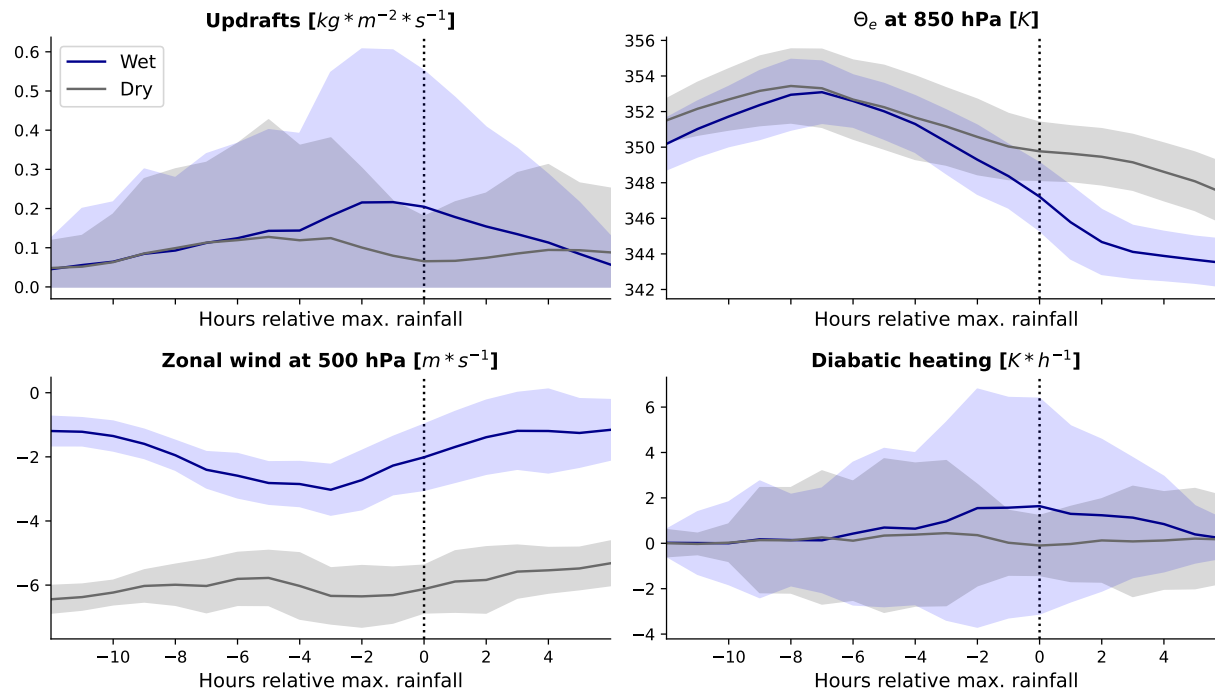
Figure 4.5: Relative to the diurnal rainfall peak composites for vertically-averaged updrafts (upper left panel), equivalent potential temperature (upper right panel), 500hPa zonal winds (lower left panel), and 500 to 300 hPa diabatic heating (lower right panel) in the Magdalena region. Composites were computed for both dry (gray) and wet (blue) conditions. Shaded areas represent spatial one standard deviation uncertainties.

temperature differences were not observed before the maximum rainfall between wet and dry days. However, the rainfall diurnal cycle in the Amazon seems to be favored by a sheared environment, with relatively high differences even 12 hours before the rainfall peak. Besides, diabatic heating in mid-to-high levels exhibited higher positive and negative values. As previously discussed, this could be associated with both latent heat release by condensation and evaporative cooling.

Convection and precipitation in the Colombian Amazon have been less studied than in other regions of NWSA. The Orinoco low-level jet, which is active from November to March (Jiménez-Sánchez et al., 2019), has been shown to be an important source of moisture for the NWSA. Particularly, Martinez et al. (2022) and Builes-Jaramillo et al. (2022) highlight the role of the jet to transport moisture toward the south and produce downwind rainfall. In addition, moisture transported from the southeast (from the Amazon rainforest) is crucial to determine convection in the Colombian flatlands (Builes-Jaramillo et al., 2022), which agrees with the results during wet days. However, the role of other mechanisms such as wind shear remains less explored. Convection-permitting simulations can serve as a tool to provide answers about convection and precipitation in the Colombian Amazon.

As a whole, the results of this section show that the model is consistent with previous studies
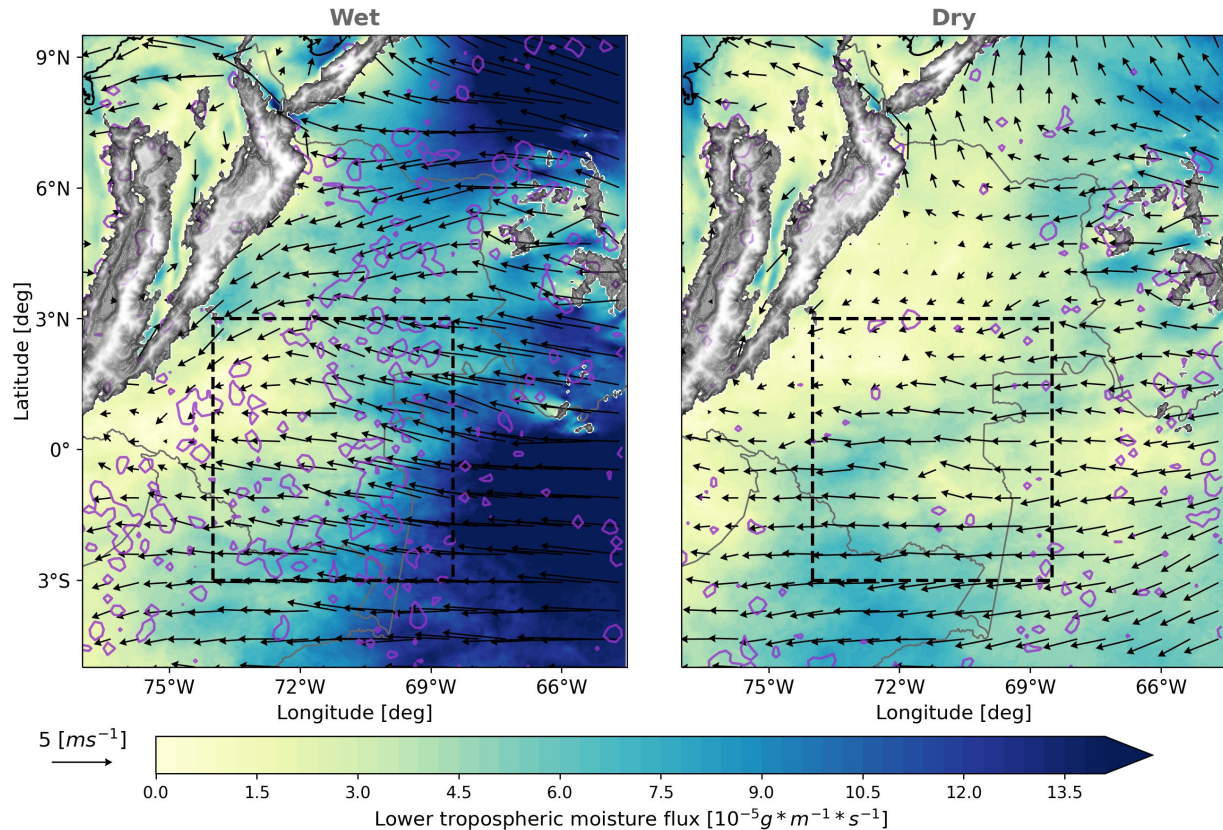
Figure 4.6: Magnitude of mean lower tropospheric (1000 to 800 hPa) moisture flux (colored contours) and horizontal winds at 850 hPa (arrows) in the Amazon. Values were averaged between 02 and 12 LT (12 to 2 hours prior to rainfall maxima). Composites for wet (dry) days are shown in the left (right) panel. Gray contours represent 0.3 $g * kg^{-1} * m * s^{-1}$ vertical moisture flux at 500 hPa during the hour of maximum rainfall. The enclosed region shows the location of the Colombian Amazon.

in different regions of the country, which provides confidence in using the model results to elucidate potential mechanisms triggering convection in the NWSA.

4.3.2   Mechanisms behind organized convection

Convection in the Colombian Pacific is of great scientific interest due to both the large precipitation rates in the region and the potential for cyclogenesis. In this section, we study the formation environments and mechanisms related to convection organization in the Pacific for the study period.

Figure 4.8 shows the environments prior to the initiation of MCSs during wet days in the Pacific. Between 12 and 08 hours before MCS initiation, moisture arrived from the southwest, and as the initiation approached, moisture fluxes shifted westward. It is noteworthy the marked zonal gradient in the equivalent potential temperature, with higher values in the continental zone in contrast to oceanic regions (especially between 12 and 04 hours before
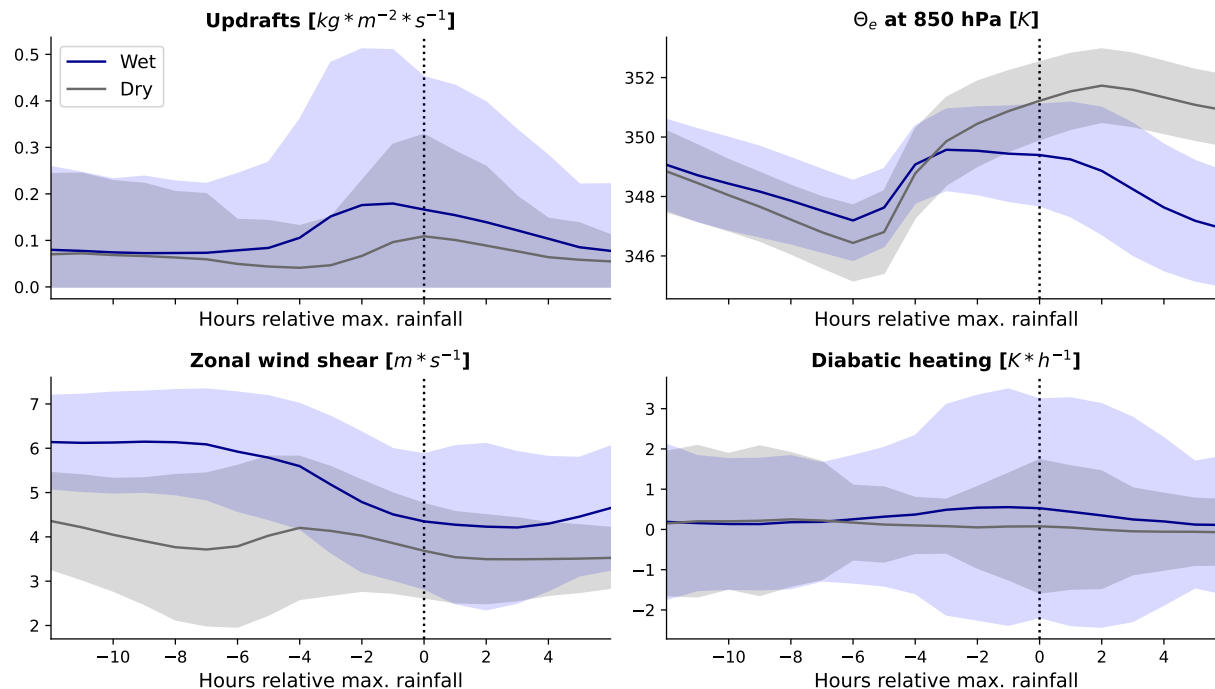
Figure 4.7: Relative to the diurnal rainfall peak composites for vertically-averaged updrafts (upper left panel), equivalent potential temperature (upper right panel), 925hPa-700hPa zonal wind shear (lower left panel), and 500 to 300 hPa diabatic heating (lower right panel) in the Amazon region. Composites were computed for both dry (gray) and wet (blue) conditions. Shaded areas represent spatial one standard deviation uncertainties.

initiation). This gradient is probably caused by diurnal heating, inducing a sea-land breeze and favoring the westward moisture flux. Anomalies presented in lower panels of Figure 4.8 revealed a greater flux across the Pacific before thunderstorm formation. Southwesterly moisture fluxes slightly recurved toward the Andes Mountains (to the west) prior to the initiation of convection. The interaction with the Andean mountains provokes orographic lifting and initiates convection. Additionally, positive equivalent potential temperature anomalies were observed prior to the MCS initiation, which is characteristic of a more unstable environment and more prone to deep convection. Also, this is consistent with results shown in Figure 4.3.

Figure 4.9 depicts the MCS-centered composites of winds and equivalent potential temperature anomalies for the initiation and mature stages. Strong convergence was observed at low levels (850 hPa) during MCS initiation, with a highly unstable environment (positive equivalent potential temperature anomalies), especially near the center of the system. In contrast, the mature stage was characterized by a relatively more stable environment at 850 hPa and a less marked low-level convergence. As discussed below, the relatively more stable signal is apparently caused by cold pools, which favor the development of new convective cells and support the system. At high levels (200 hPa) clear divergence patterns were observed at both stages indicating deep convection. For initiation, the divergence patterns
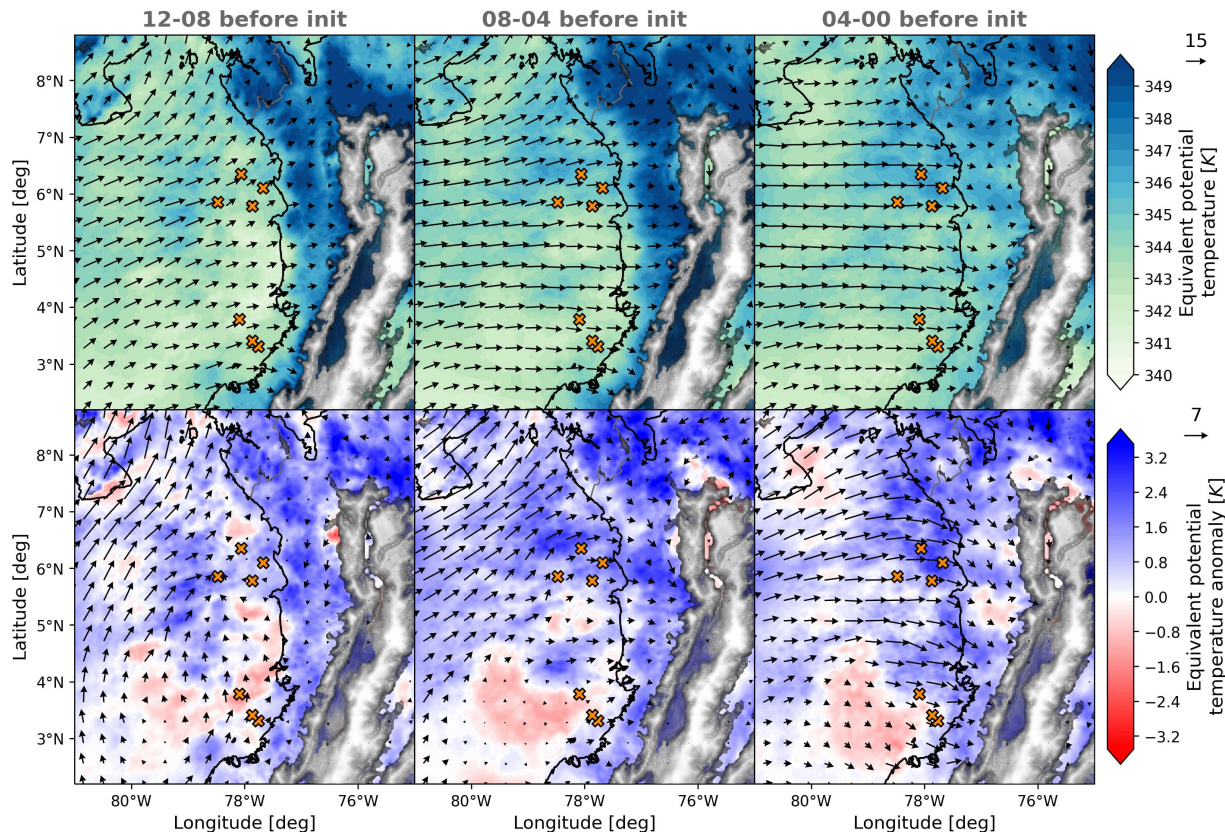
Figure 4.8: Atmospheric environment before the initiation of MCSs in wet days for the Pacific. Upper panels: composites of lower tropospheric integrated moisture flux (arrows) and equivalent potential temperature (colored contours) for different hours before the initiation of MCSs. Lower panels: similar to upper panels but for anomalies. Orange markers in each panel show the location of the initiation of the MCSs. Units for the reference arrows are $10^{-5} g * m^{-1} * s^{-1}$.

were more localized, while in the mature stage, the divergent flow was observed over a larger extent, which may be associated with a larger system size. On the other hand, mid-level (450 hPa) fields exhibited notable differences between the initiation and the mature stages. Specifically, a strong wind convergence was evidenced at mid-levels during the mature stage (orange square), which is consistent with a cyclonic circulation of around 40 km wide (see Figure S.10).

A mid-level vortex generates convergence and favors convection aloft (Houze, 2004). During the OTREC field campaign, Mejía et al. (2021) reported a Mesoscale Convective Vortex (MCV) during the occurrence of a thunderstorm in the Pacific, suggesting that these vortices play a role in convection organization in the region. WRF simulations at CP resolution have shown the capacity to represent MCVs (Yang et al., 2017; Feng et al., 2018), especially for long-lived MCSs. The scale of the simulated vortex is not enough to be considered strictly as a MCV (diameter less than 50 km). However, the simulated mid-level cyclonic circulation highlights the capacity of the model to represent these structures, which are essential for the organization of convection. Besides, these structures are usually weaker in the tropics
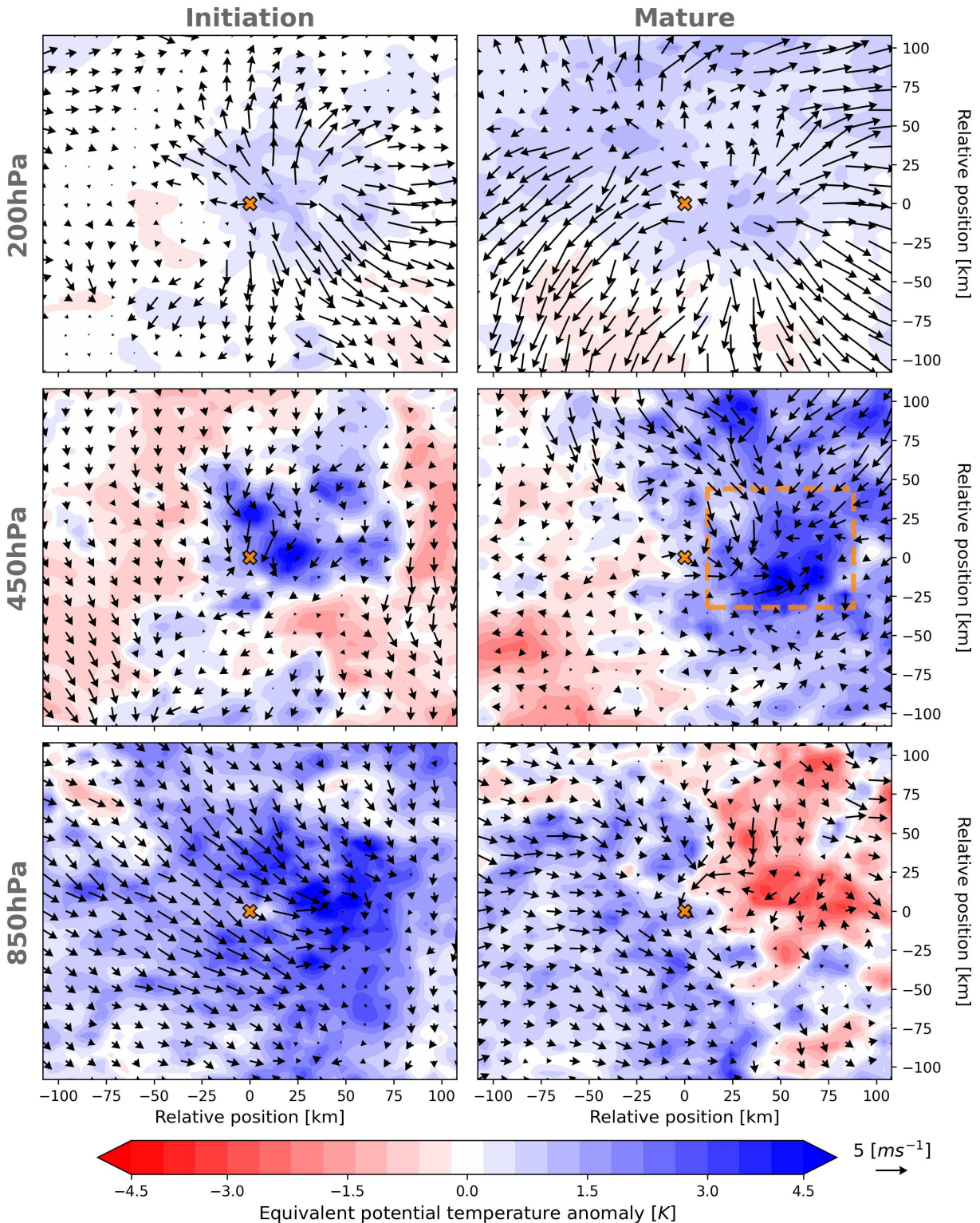
Figure 4.9: MCS-centered composites of anomalies for winds and equivalent potential temperature at 200 hPa (upper panels), 450 hPa (mid panels), and 850 hPa (lower panels) for the initiation (left-hand panels) and mature (right-hand panels) MCS stages during wet days. Values were centered using the geometric centroid of the MCS objects. Orange square in the mature stage shows the location of strong convergence and cyclonic circulation.

than in mid-latitudes (Houze, 2004) due to the weaker effect of Coriolis force, so they reach smaller dimensions.

Vertical profiles presented in Figure 4.10 permit to elucidate possible processes behind observed patterns in different levels and stages of the systems. Initiation and mature stages exhibited considerable differences in heating and mass flux, especially at mid and high levels. In comparison to the initiation, a top-heavier heating profile was evidenced during the mature stage with mean differences of around 1.5 Kh^{-1} in mid-levels (500 to 350 hPa). Increased heating during the mature phase could generate a stronger mid-level convergence and activate the previously highlighted cyclonic circulation. Mass flux profiles exhibited a top-heavy behavior for the mature stage of the MCSs, which is characteristic of a system with a developed stratiform region. This stronger mid- to upper-level convection for the mature stage could be explained by the enhanced mid-level convergence, generating deep convection. Similar to these results, Yang et al. (2017) and Feng et al. (2018) highlighted the role of diabatic heating to enhance mid-level cyclonic circulation contributing to forming longer-lived MCSs. These findings highlight the leading role of diabatic heating in the development of organized thunderstorms in the Pacific.

In order to understand the described differences in diabatic heating profiles, Figure 4.11 shows the profiles of hydrometeor species during MCSs initiation and mature stages. Consistent with the life cycle of MCSs, the mixing ratio for rain was higher during the mature stage.
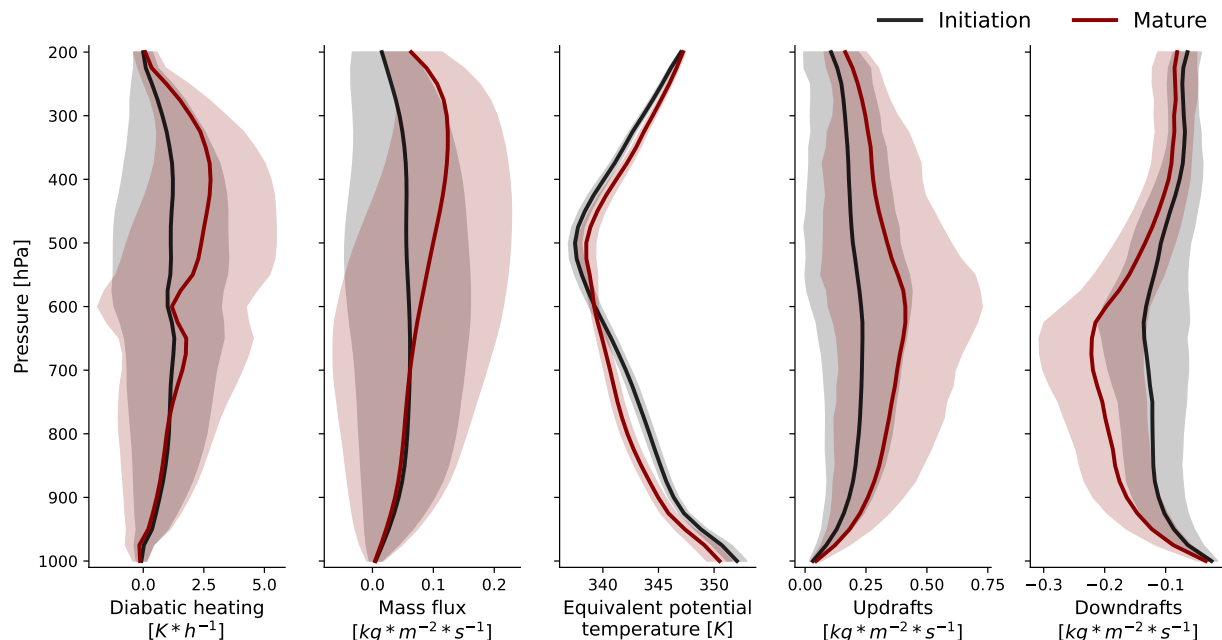

Figure 4.10: Vertical profiles of diabatic heating, mass flux, equivalent potential temperature, updrafts, and downdrafts for the initiation and mature stage of MCSs identified during wet days in the Pacific. Profiles were averaged over the region covering Figure 4.9. Shading represents spatial standard deviation.

Figure 4.11: Vertical profiles of hydrometeor species for the initiation and mature stage of MCSs identified during wet days in the Pacific. Profiles were averaged over the region covering Figure 4.9. Shading represents spatial standard deviation.
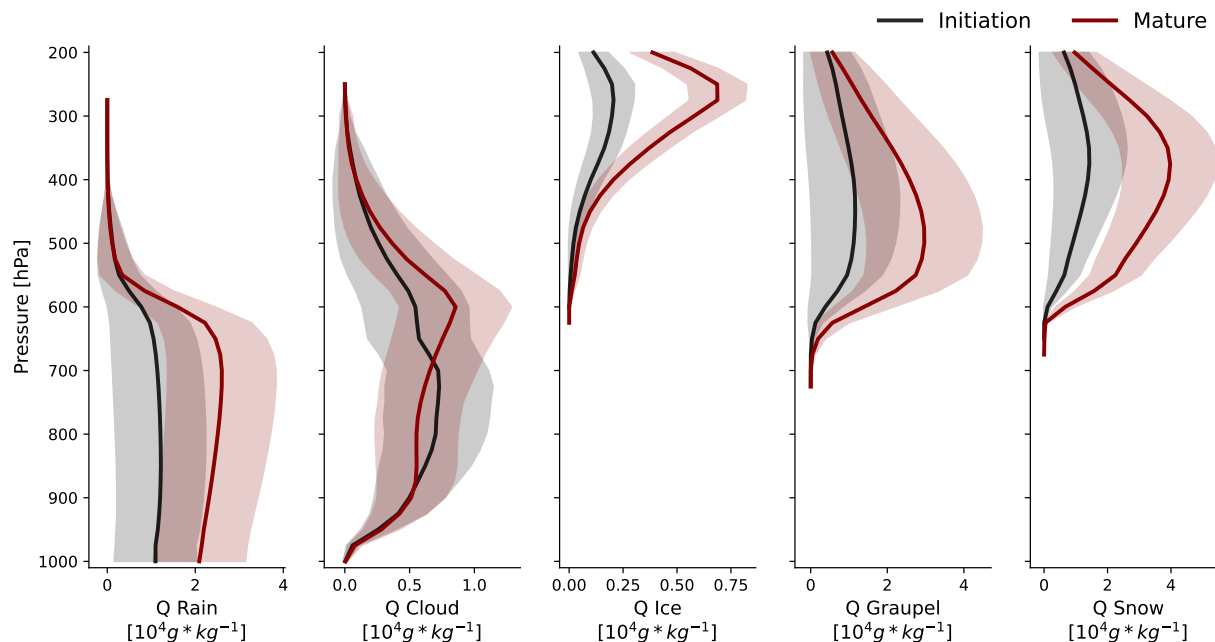
Compared to the initiation of MCSs, profiles for the mature stage showed a higher amount of solid-phase hydrometeors (ice, graupel, snow). Ice developed preferentially above 300 hPa, where homogeneous nucleation can occur (temperatures below -38°C). Snow hydrometeors formed mainly between 300 and 400 hPa, probably favored by water vapor deposition on ice crystals. Additionally, between 600 and 500 hPa the largest amounts of graupel were observed during the mature phase. Graupel production at mid-levels may be associated with riming, which may be favored by the presence of supercooled water droplets in the mixed phase region (the freezing point is around 600 hPa). These processes of solid-phase hydrometeor formation release large amounts of latent heat into the atmosphere, which helps to explain the differences between the mature phase and the initiation of the systems. These results are in agreement with the results presented in Chapter 2, where it was shown that high sensitivities between the microphysics schemes were related to higher latent heat release caused by the generation of solid-phase hydrometeors. In agreement with Yang et al. (2017) and Feng et al. (2018), the results of this chapter and those of Chapter 2 suggest that feedbacks between the system and the large-scale environment may be essential for the organization of convection in the Pacific, favoring the growth and enhancing the duration of the systems.

For the purpose of identifying mechanisms related to the evolution of the MCSs, Figure 4.12 shows cross-section composites of winds, mass flux, and rainfall following the movement of MCSs in the Pacific (to the left in the Figure). MCSs exhibit important features of organized thunderstorms, in agreement with earlier described mechanisms. In consistency with
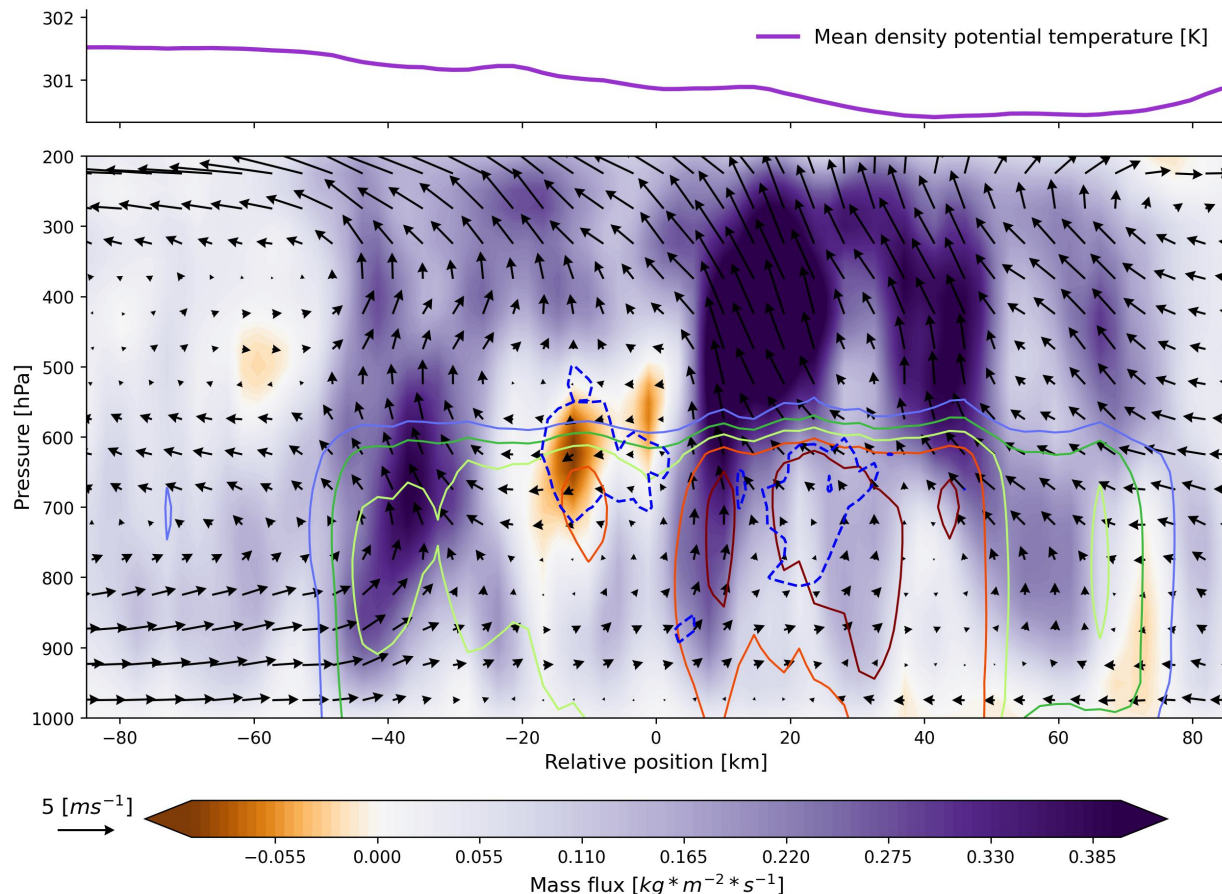
Figure 4.12: Cross section of winds, mass flux, and rain mixing ratio composites in the movement direction of MCSs objects (towards the left). Horizontal winds were projected to the movement plane and vertical winds were scaled using a factor of 5. Red contours mean a higher rain mixing ratio, while blue discontinuous contours represent 0.35 $kg*m^{-2}*s^{-1}$ downdrafts. Only MCS objects among the initiation and the mature stages were considered for the composites. The upper panel shows the averaged density potential temperature at the first model level, which was computed following Drager and van den Heever (2017).

Figures 4.9 and 4.10, divergence in high-levels is observed, as well as top-heavy mass fluxes, especially in the convective rain region (between 0 and 40 km relative to the centroid). Besides, in the rear (right side of the figure), low and mid-level winds are consistent with the direction of movement of the system. It is noteworthy that a weak-sheared environment is observed in mid-levels at the rear of the system, which could favor the development of the previously described vortex (Houze, 2004).

In the convective-stratiform transition zone (located between 40 and 60 km relative to the centroid) a region of lower potential density temperature is identified. Density potential temperature is used for the identification of cold pools at the surface (see Drager and van den Heever (2017) for more information). These cold pools are caused by the evaporative cooling produced by the evaporation of raindrops when falling. Cold pools in the rear expand hori-

zontally once reach the surface (Houze, 2004; Schumacher and Rasmussen, 2020), promoting the continued development of the main convective tower. The convective tower at the rear (located about 40 km from the centroid) is visibly tilted, consistently with observed shear at low levels in the convective-stratiform precipitation. Tilting allows the convective tower to continue to develop as downdrafts fall from the cloud (Schumacher and Rasmussen, 2020). Further research is required on the role of wind shear in the organization of convection in the Colombian Pacific.

Between low and mid-levels (between 800 and 600 hPa), strong downdrafts within the cloud are observed with a magnitude of 0.35 $kg*m^{-2}*s^{-1}$, which is comparable to the convective mass flux at mid-levels. These downdrafts occur just in the rear of the convective towers located around -30 and 10 km, where they could enhance the ascent of air in the convective towers at low to medium levels. The vertical profile of the downdrafts depicted in Figure 4.10 also highlights that in the mature stage, downdrafts are more marked than during the initiation, especially between low to mid-levels, indicating that downdrafts are relevant mechanisms for the development of the MCSs. As the system evolves, these downdrafts enhance the ascent of new convective cells contributing to the storm's development. Last but not least, in the front of the systems a low-level current extending up to 800 hPa moves in the direction of the MCS. The presence of this low-level current is characteristic of externally driven MCSs (Schumacher and Rasmussen, 2020), favoring conditions for convergence in the front of the system and enhancing the convective cell near -30 km in relation to the storm centroid. The interaction between this low-level flow and the downdrafts could cause the genesis of new convective cells in the front of the system, promoting its propagation and organization.

4.4 Conclusions

In this chapter, the main mechanisms behind the diurnal cycle of rainfall in different regions of the NWSA and the organization of convection in the Colombian Pacific were identified. For this purpose, a one-month WRF convection-permitting simulation was used, covering a period between September and October 2019. Results from previous chapters showed that the implemented configuration of the WRF model has a good capacity to capture the diurnal cycle of precipitation and the main features of MCSs. For each region, dry and wet days were defined using the 20_{th} and 80_{th} percentiles of the average rainfall around the maximum rainfall peak.

The results showed that low-level moisture fluxes contributed to explaining the diurnal rainfall cycle in the regions of interest. The well-known Choco low-level jet exhibited greater activity for the studied period in the Pacific. The associated low-level moisture flux favors convection once it interacts with the Andes mountain range. Wet days in the Magdalena Valley were characterized by an intensification of down-valley moisture flux during the afternoon and up-valley during the night, strengthening low-level convergence and enhancing nocturnal convection. In addition, for the Colombian Amazon, low-level moisture transported from the Amazon rainforest and the Venezuelan plains was notably greater during wet days.

In general, relative to the rainfall peak analysis showed higher convection on wet days and especially around the rainfall maximum. In the Pacific, the equivalent potential temperature and zonal wind shear displayed higher values on wet days, especially before the hour of maximum rainfall intensity. After the diurnal rainfall peak, the equivalent potential temperature decreased and a less sheared environment was observed. In the inter-Andean Magdalena Valley, the equivalent potential temperature before peak rainfall was relatively similar between dry and wet days. However, the zonal wind at mid-levels exhibited a significant reduction in intensity, with notable differences before and after the maximum rainfall, which suggests a synoptic influence on convection over the region. Finally, in the Amazon region, the equivalent potential temperature also showed no significant differences between wet and dry days, while a more sheared environment was identified on wet days. These results highlight some variables that could be useful for the predictability of rainfall in the different regions.

When studying the organization of storms in the Colombian Pacific, a higher activity of the Chocó jet and positive anomalies of the equivalent potential temperature were evident, showing this is a favorable environment for the initiation of MCSs. Once developed, MCSs exhibited important differences between the initiation and the mature stages, revealing possible mechanisms associated with the evolution of the systems. Specifically, the mature stage showed stronger divergence at high levels and convergence at mid-levels related to a mid-level vortex at 450hPa, which enhances mid to high-level convection. In agreement with previous studies, diabatic heating generated by water phase changes can influence mid-level circulation fields and enhance convergence into the system. The formation of solid-phase hydrometeors above 600 hPa during the mature stage is consistent with mid- to upper-level

heating patterns. These results along with the high sensitivities to the microphysics schemes reported in Chapter 2 suggest that feedbacks between the MCSs and the surroundings may contribute to the development and organization of convection in the region.

A cross-section analysis following the direction of displacement of MCSs provided insights into the mechanisms related to the motion and organization of the convection. At the rear of the event, winds showed relatively even patterns at different levels with a direction consistent with the displacement of the systems. Furthermore, the wind shear was weak, which could support a coherent structure of the convective towers. On the other hand, the influence of cold pools at the transition between the convective and stratiform rain regions can favor the continued development of the main convective tower. Similarly, strong downdrafts within the cloud appear to contribute to the development of convective cells, while in the front of the MCSs, a coherent towards-the-system flow at low levels was evidenced, favoring convergence at the front of the system and permitting the development of new convective cells. This ability of convection-permitting simulations to reproduce mechanisms related to organized MCSs in the Pacific has not been previously reported in other studies.

In general, the results presented in this chapter highlight the utility of convection-permitting simulations to elucidate possible mechanisms behind the occurrence of precipitation and organized convection in different regions. Future analyses could consider the study of convection and precipitation during this and other seasons. Besides, further research is required to study convection in different regions. The implementation of convection-permitting simulations can provide answers about mechanisms triggering convection in NWSA.

Chapter 5. General conclusions and future research

This research analyzed the representation of Convective Systems (CSs) and precipitation in northwestern South America (NWSA) using convection-permitting simulations. WRF simulations were performed at 4 km resolution covering the continental NWSA. A set of experiments were carried out with three Microphysics (MP) and two Planetary Boundary Layer (PBL) parameterization schemes to study the processes causing high sensitivity to the selection of parameterizations. Subsequently, four one-month-length simulations under different hydro-climatological conditions were developed to assess the spatio-temporal representation of CSs in the NWSA and to identify mechanisms behind the organization of convection and precipitation occurrence. Model evaluation was based on satellite-measured brightness temperature and precipitation. An object-based evaluation was also performed using a CSs identification and tracking algorithm. The main findings of this research are presented below.

Simulations with different parameterization schemes were able to represent the spatio-temporal behavior of precipitation, with better results for the less computationally expensive WSM6 (MP) and YSU (PBL) parameterization schemes. MP and PBL schemes exerted a high sensitivity to simulated rainfall, with large differences in the Colombian Amazon and Pacific regions. A more detailed study of sensitivity simulations revealed key processes behind the representation of precipitation in these regions. We observed that PBL schemes not only influenced low-level dynamics and turbulent fluxes but also vertical cloud distribution in the Amazon. On the other hand, in the Pacific region MP schemes influenced cloud development through latent heat release caused by solid-phase hydrometeor formation. These results suggest that modeling studies should carefully consider both the selection of MP and PBL schemes due to their sensitivity to represent rainfall in NWSA.

While assessing the spatio-temporal representation of Convective Systems, the model adequately represented the seasonal variations in the occurrence of CSs in NWSA, which is consistent with the latitudinal migration of the ITCZ. WRF also captured the diurnal cycle of CSs and precipitation in different regions of the country, with nocturnal convection in northwestern Colombia, a notable oceanic hotspot during the morning in the Colombian Pacific, and a diurnal maximum in the Savannas-Amazon flatlands. Regarding the features of the CSs, WRF underestimated the area and overestimated the intensity, although it captured the evolution of CSs from the initiation to the dissipation stages. Also, the model correctly captured the initiation hour, especially for systems lasting less than 10 hours. Consistent with observations, simulated CSs propagated westward and presented higher speeds on the Amazon-Savannas flatlands, whereas lower velocities were observed over and to the west of the Andes. In general, convective patterns are associated with the seasonality of low-level winds and moisture, which are highly modulated by the Choco and Orinoco low-level jets.

A more detailed study of a one-month simulation permitted the identification of mechanisms related to the diurnal cycle of precipitation in the Pacific, the Magdalena Valley, and the Colombian Amazon, as well as the mechanisms behind the organization of convection in the Pacific. The main findings of these results showed an increase in low-level moisture fluxes on days with a marked diurnal rainfall cycle (wet days) in the three regions of interest. Particularly, in the Pacific region, greater activity of the Choco low-level jet was evidenced along with a more unstable and sheared environment during wet days. In the Magdalena Valley, an intensification of down-valley and up-valley fluxes was observed during wet days, as well as weaker easterlies than during dry days. More marked wind shear and enhanced moisture transport from the Amazon rainforest and Venezuelan plains were present during wet days in the Colombian Amazon. Regarding convection organization in the Pacific, anomalies in moisture fluxes toward the continent and a more unstable atmosphere characterized the environment before the initiation of the events. CSs during the mature stage exhibited a mid-level vortex apparently caused by latent heat released during ice-phase hydrometeor formation. As a crucial mechanism, the vortex enhanced mid-level convergence producing a top-heavy mass flux profile. Furthermore, the development of the storms seems to be favored under a less-sheared environment in the rear, with cold pools in the convective-stratiform transition region. In the front of the CSs, a low-level current and downdrafts within the cloud promoted the development of convective cells, contributing to the organization of convection in the Pacific.

According to a literature review, this is the first effort to assess the representation of CSs in the region using subcontinental convection-permitting simulations, providing insights into the strengths and weaknesses in the simulation of CSs in NWSA. The main results demonstrate the usefulness of convection-permitting simulations to study mechanisms behind convection and encourage the development of future modeling studies in NWSA. Due to the importance of parameterization schemes, further research is required to study the sensitivity for convection representation in NWSA, including longer periods and sensitivity to more schemes. A detailed object-based evaluation, involving the segregation of convective features into isolated deep convection and organized MCSs, can improve the understanding of the model's capacity to represent convection in the region. Finally, more investigations into the understanding of the wide spatio-temporal variability of convection in NWSA are required, especially using convection-permitting simulations.

Bibliography

Arias, P., Bellouin, N., Coppola, E., Jones, R., Krinner, G., Marotzke, J., Naik, V., Palmer, M., Plattner, G.-K., Rogelj, J., et al. (2021). Climate change 2021: The physical science basis. contribution of working group i to the sixth assessment report of the intergovernmental panel on climate change; technical summary.

Builes-Jaramillo, A., Yepes, J., and Salas, H. D. (2022). The orinoco low-level jet and its association with the hydroclimatology of northern south america. *Journal of Hydrometeorology*, 23(2):209–223.

Ceballos B, L., Zapata Henao, M., Hernandez, J., Guzmán, G., and Hoyos Ortiz, C. (2017). Aburrá valley's weather forecast system: Implementation and improvements using radar and radiometer data assimilation. In *AGU Fall Meeting Abstracts*, volume 2017, pages A21P–02.

Chawla, I., Osuri, K. K., Mujumdar, P. P., and Niyogi, D. (2018). Assessment of the weather research and forecasting (wrf) model for simulation of extreme rainfall events in the upper ganga basin. *Hydrology and Earth System Sciences*, 22(2):1095–1117.

Chen, Q., Fan, J., Hagos, S., Gustafson Jr, W. I., and Berg, L. K. (2015). Roles of wind shear at different vertical levels: Cloud system organization and properties. *Journal of Geophysical Research: Atmospheres*, 120(13):6551–6574.

Chen, T., Rossow, W. B., and Zhang, Y. (2000). Radiative effects of cloud-type variations. *Journal of climate*, 13(1):264–286.

Comin, A. N., Justino, F., Pezzi, L., de Sousa Gurjão, C. D., Shumacher, V., Fernández, A., and Sutil, U. A. (2021). Extreme rainfall event in the northeast coast of brazil: a numerical sensitivity study. *Meteorology and Atmospheric Physics*, 133:141–162.

Crook, J., Klein, C., Folwell, S., Taylor, C. M., Parker, D. J., Stratton, R., and Stein, T. (2019). Assessment of the representation of west african storm lifecycles in convection-permitting simulations. *Earth and Space Science*, 6(5):818–835.

Das, S. K., Hazra, A., Deshpande, S. M., Krishna, U. M., and Kolte, Y. K. (2021). Investigation of cloud microphysical features during the passage of a tropical mesoscale convective system: Numerical simulations and x-band radar observations. *Pure and Applied Geophysics*, 178:185–204.

Davis, C. A., Brown, B. G., Bullock, R., and Halley-Gotway, J. (2009). The method for object-based diagnostic evaluation (mode) applied to numerical forecasts from the 2005 nssl/spc spring program. *Weather and Forecasting*, 24(5):1252–1267.

Drager, A. J. and van den Heever, S. C. (2017). Characterizing convective cold pools. *Journal of Advances in Modeling Earth Systems*, 9(2):1091–1115.

Dudhia, J. (1989). Numerical study of convection observed during the winter monsoon experiment using a mesoscale two-dimensional model. *Journal of Atmospheric Sciences*, 46(20):3077–3107.

Efstathiou, G., Zoumakis, N., Melas, D., Lolis, C., and Kassomenos, P. (2013). Sensitivity of wrf to boundary layer parameterizations in simulating a heavy rainfall event using different microphysical schemes. effect on large-scale processes. *Atmospheric research*, 132:125–143.

Escobar, M., Hoyos, I., Nieto, R., and Villegas, J. C. (2022). The importance of continental evaporation for precipitation in colombia: A baseline combining observations from stable isotopes and modelling moisture trajectories. *Hydrological Processes*, 36(6):e14595.

Fan, J., Liu, Y.-C., Xu, K.-M., North, K., Collis, S., Dong, X., Zhang, G. J., Chen, Q., Kollias, P., and Ghan, S. J. (2015). Improving representation of convective transport for scale-aware parameterization: 1. convection and cloud properties simulated with spectral bin and bulk microphysics. *Journal of Geophysical Research: Atmospheres*, 120(8):3485–3509.

Feng, Z., Leung, L. R., Hagos, S., Houze, R. A., Burleyson, C. D., and Balaguru, K. (2016). More frequent intense and long-lived storms dominate the springtime trend in central us rainfall. *Nature communications*, 7(1):13429.

Feng, Z., Leung, L. R., Hardin, J., Terai, C. R., Song, F., and Caldwell, P. (2023). Mesoscale convective systems in dyamond global convection-permitting simulations. *Geophysical Research Letters*, 50(4):e2022GL102603.

Feng, Z., Leung, L. R., Houze Jr, R. A., Hagos, S., Hardin, J., Yang, Q., Han, B., and Fan, J. (2018). Structure and evolution of mesoscale convective systems: Sensitivity to cloud microphysics in convection-permitting simulations over the united states. *Journal of Advances in Modeling Earth Systems*, 10(7):1470–1494.

Feng, Z., Leung, L. R., Liu, N., Wang, J., Houze Jr, R. A., Li, J., Hardin, J. C., Chen, D., and Guo, J. (2021). A global high-resolution mesoscale convective system database using satellite-derived cloud tops, surface precipitation, and tracking. *Journal of Geophysical Research: Atmospheres*, 126(8):e2020JD034202.

Flores Rojas, J. L., Moya-Alvarez, A. S., Kumar, S., Martínez-Castro, D., Villalobos-Puma, E., and Silva-Vidal, Y. (2019). Analysis of possible triggering mechanisms of severe thunderstorms in the tropical central andes of peru, mantaro valley. *Atmosphere*, 10(6):301.

Fuchs-Stone, Ž., Raymond, D. J., and Sentić, S. (2020). Otrec2019: Convection over the east pacific and southwest caribbean. *Geophysical Research Letters*, 47(11):e2020GL087564.

Gbode, I. E., Dudhia, J., Ogunjobi, K. O., and Ajayi, V. O. (2019). Sensitivity of different physics schemes in the wrf model during a west african monsoon regime. *Theoretical and Applied Climatology*, 136:733–751.

Gentine, P., Massmann, A., Lintner, B. R., Hamed Alemohammad, S., Fu, R., Green, J. K., Kennedy, D., and Vilà-Guerau de Arellano, J. (2019). Land–atmosphere interactions in the tropics–a review. *Hydrology and Earth System Sciences*, 23(10):4171–4197.

Giraldo-Cardenas, S., Arias, P. A., Vieira, S. C., and Zuluaga, M. D. (2022). Easterly waves and precipitation over northern south america and the caribbean. *International Journal of Climatology*, 42(3):1483–1499.

Gomez-Rios, S., Zuluaga, M. D., and Hoyos, C. D. (2023). Orographic controls over convection in an inter-andean valley in northern south america. *Monthly Weather Review*, 151(1):145–162.

Grimm, A. M. (2019). Madden–julian oscillation impacts on south american summer monsoon season: precipitation anomalies, extreme events, teleconnections, and role in the mjo cycle. *Climate Dynamics*, 53(1-2):907–932.

Gutowski, W. J., Ullrich, P. A., Hall, A., Leung, L. R., O'Brien, T. A., Patricola, C. M., Arritt, R., Bukovsky, M., Calvin, K. V., Feng, Z., et al. (2020). The ongoing need for high-resolution regional climate models: Process understanding and stakeholder information. *Bulletin of the American Meteorological Society*, 101(5):E664–E683.

Halder, M., Hazra, A., Mukhopadhyay, P., and Siingh, D. (2015). Effect of the better representation of the cloud ice-nucleation in wrf microphysics schemes: A case study of a severe storm in india. *Atmospheric Research*, 154:155–174.

Hartmann, D. L., Ockert-Bell, M. E., and Michelsen, M. L. (1992). The effect of cloud type on earth's energy balance: Global analysis. *Journal of Climate*, 5(11):1281–1304.

Hernandez-Deckers, D. (2022). Features of atmospheric deep convection in northwestern south america obtained from infrared satellite data. *Quarterly Journal of the Royal Meteorological Society*, 148(742):338–350.

Holle, R. L. and Murphy, M. J. (2017). Lightning over three large tropical lakes and the strait of malacca: Exploratory analyses. *Monthly Weather Review*, 145(11):4559–4573.

Holloway, C. E., Wing, A. A., Bony, S., Muller, C., Masunaga, H., L'Ecuyer, T. S., Turner, D. D., and Zuidema, P. (2017). Observing convective aggregation. *Surveys in Geophysics*, 38:1199–1236.

Hong, S.-Y. and Lim, J.-O. J. (2006). The wrf single-moment 6-class microphysics scheme (wsm6). *Asia-Pacific Journal of Atmospheric Sciences*, 42(2):129–151.

Hong, S.-Y., Noh, Y., and Dudhia, J. (2006). A new vertical diffusion package with an explicit treatment of entrainment processes. *Monthly weather review*, 134(9):2318–2341.

Houze, R. A. (2004). Mesoscale convective systems. *Reviews of Geophysics*, 42(4).

Houze, R. A. (2018). 100 years of research on mesoscale convective systems. *Meteorological Monographs*, 59:17–1.

Houze, R. A., Rasmussen, K. L., Zuluaga, M. D., and Brodzik, S. R. (2015). The variable nature of convection in the tropics and subtropics: A legacy of 16 years of the tropical rainfall measuring mission satellite. *Reviews of Geophysics*, 53(3):994–1021.

Hoyos, C. D., Ceballos, L. I., Pérez-Carrasquilla, J. S., Sepúlveda, J., López-Zapata, S. M., Zuluaga, M. D., Velásquez, N., Herrera-Mejía, L., Hernández, O., Guzmán-Echavarría, G., et al. (2019). Meteorological conditions leading to the 2015 salgar flash flood: lessons for vulnerable regions in tropical complex terrain. *Natural Hazards and Earth System Sciences*, 19(11):2635–2665.

Hoyos, I., Dominguez, F., Cañón-Barriga, J., Martínez, J., Nieto, R., Gimeno, L., and Dirmeyer, P. (2018). Moisture origin and transport processes in colombia, northern south america. *Climate Dynamics*, 50:971–990.

Huang, Y., Wang, Y., Xue, L., Wei, X., Zhang, L., and Li, H. (2020). Comparison of three microphysics parameterization schemes in the wrf model for an extreme rainfall event in the coastal metropolitan city of guangzhou, china. *Atmospheric Research*, 240:104939.

Huffman, G., Stocker, E., Bolvin, D., Nelkin, E., and Tan, J. (2019). Gpm imerg final precipitation l3 1 day 0.1 degree x 0.1 degree v06, edited by andrey savtchenko, greenbelt, md, goddard earth sciences data and information services center (ges disc). https://doi.org/10.5067/GPM/IMERGDF/DAY/06.

Huffman, G. J., Bolvin, D. T., Braithwaite, D., Hsu, K.-L., Joyce, R. J., Kidd, C., Nelkin, E. J., Sorooshian, S., Stocker, E. F., Tan, J., et al. (2020). Integrated multi-satellite retrievals for the global precipitation measurement (gpm) mission (imerg). *Satellite Precipitation Measurement: Volume 1*, pages 343–353.

Janowiak, J., Joyce, B., and Xie, P. (2017). Ncep cpc l3 half hourly 4km global (60 s–60 n) merged ir v1, goddard earth sciences data and information services center (ges disc). https://doi.org/10.5067/P4HZB9N27EKU.

Jaramillo, L., Poveda, G., and Mejía, J. F. (2017). Mesoscale convective systems and other precipitation features over the tropical americas and surrounding seas as seen by trmm. *International Journal of Climatology*, 37:380–397.

Jiménez, P. A., Dudhia, J., González-Rouco, J. F., Navarro, J., Montávez, J. P., and García-Bustamante, E. (2012). A revised scheme for the wrf surface layer formulation. *Monthly weather review*, 140(3):898–918.

Jiménez-Sánchez, G., Markowski, P. M., Jewtoukoff, V., Young, G. S., and Stensrud, D. J. (2019). The orinoco low-level jet: An investigation of its characteristics and evolution using the wrf model. *Journal of Geophysical Research: Atmospheres*, 124(20):10696–10711.

Junquas, C., Heredia, M., Condom, T., Ruiz-Hernández, J., Campozano, L., Dudhia, J., Espinoza, J., Menegoz, M., Rabatel, A., and Sicart, J.-E. (2022). Regional climate modeling of the diurnal cycle of precipitation and associated atmospheric circulation patterns over an andean glacier region (antisana, ecuador). *Climate Dynamics*, 58(11-12):3075–3104.

Karki, R., ul Hasson, S., Gerlitz, L., Talchabhadel, R., Schenk, E., Schickhoff, U., Scholten, T., and Böhner, J. (2018). Wrf-based simulation of an extreme precipitation event over the central himalayas: Atmospheric mechanisms and their representation by microphysics parameterization schemes. *Atmospheric Research*, 214:21–35.

Klein, C., Heinzeller, D., Bliefernicht, J., and Kunstmann, H. (2015). Variability of west african monsoon patterns generated by a wrf multi-physics ensemble. *Climate Dynamics*, 45:2733–2755.

Klein, C., Nkrumah, F., Taylor, C. M., and Adefisan, E. A. (2021). Seasonality and trends of drivers of mesoscale convective systems in southern west africa. *Journal of Climate*, 34(1):71–87.

Lehner, M. and Rotach, M. W. (2018). Current challenges in understanding and predicting transport and exchange in the atmosphere over mountainous terrain. *Atmosphere*, 9(7):276.

Li, J., Feng, Z., Qian, Y., and Leung, L. R. (2021). A high-resolution unified observational data product of mesoscale convective systems and isolated deep convection in the united states for 2004–2017. *Earth System Science Data*, 13(2):827–856.

Liu, D., Yang, B., Zhang, Y., Qian, Y., Huang, A., Zhou, Y., and Zhang, L. (2018). Combined impacts of convection and microphysics parameterizations on the simulations of precipitation and cloud properties over asia. *Atmospheric research*, 212:172–185.

Liu, N., Liu, C., Chen, B., and Zipser, E. (2020a). What are the favorable large-scale environments for the highest-flash-rate thunderstorms on earth? *Journal of the Atmospheric Sciences*, 77(5):1583–1612.

Liu, Y., Chen, X., Li, Q., Yang, J., Li, L., and Wang, T. (2020b). Impact of different microphysics and cumulus parameterizations in wrf for heavy rainfall simulations in the central segment of the tianshan mountains, china. *Atmospheric research*, 244:105052.

Lohmann, U., Lüönd, F., and Mahrt, F. (2016). *An introduction to clouds: From the microscale to climate.* Cambridge University Press.

Mace, G. G., Benson, S., Sonntag, K. L., Kato, S., Min, Q., Minnis, P., Twohy, C. H., Poellot, M., Dong, X., Long, C., et al. (2006). Cloud radiative forcing at the atmospheric radiation measurement program climate research facility: 1. technique, validation, and comparison to satellite-derived diagnostic quantities. *Journal of Geophysical Research: Atmospheres*, 111(D11).

Mapes, B. E., Warner, T. T., Xu, M., and Negri, A. J. (2003). Diurnal patterns of rainfall in northwestern south america. part i: Observations and context. *Monthly Weather Review*, 131(5):799–812.

Martinez, J. A., Arias, P. A., Junquas, C., Espinoza, J. C., Condom, T., Dominguez, F., and Morales, J. S. (2022). The orinoco low-level jet and the cross-equatorial moisture

transport over tropical south america: Lessons from seasonal wrf simulations. *Journal of Geophysical Research: Atmospheres*, 127(3):e2021JD035603.

Martinez, J. A., Camacho, J. C., Vasquez, D., Espinosa, D., and Arias, P. A. (2021). Simulation of mesoscale convective systems near the tropical andes: Insights from convection-permitting simulations of two events. In *EGU General Assembly Conference Abstracts*, pages EGU21–10264.

Martínez-Castro, D., Kumar, S., Flores Rojas, J. L., Moya-Álvarez, A., Valdivia-Prado, J. M., Villalobos-Puma, E., Castillo-Velarde, C. D., and Silva-Vidal, Y. (2019). The impact of microphysics parameterization in the simulation of two convective rainfall events over the central andes of peru using wrf-arw. *Atmosphere*, 10(8):442.

Mejía, J. F. and Poveda, G. (2020). Upper-air measurements at nuquí, colombia. https://doi.org/10.26023/M951-SXZK-NF0N.

Mejía, J. F., Yepes, J., Henao, J. J., Poveda, G., Zuluaga, M. D., Raymond, D. J., and Fuchs-Stone, Ž. (2021). Towards a mechanistic understanding of precipitation over the far eastern tropical pacific and western colombia, one of the rainiest spots on earth. *Journal of Geophysical Research: Atmospheres*, 126(5):e2020JD033415.

Mlawer, E. J., Taubman, S. J., Brown, P. D., Iacono, M. J., and Clough, S. A. (1997). Radiative transfer for inhomogeneous atmospheres: Rrtm, a validated correlated-k model for the longwave. *Journal of Geophysical Research: Atmospheres*, 102(D14):16663–16682.

Mohan, P. R., Srinivas, C., Yesubabu, V., Baskaran, R., and Venkatraman, B. (2018). Simulation of a heavy rainfall event over chennai in southeast india using wrf: Sensitivity to microphysics parameterization. *Atmospheric Research*, 210:83–99.

Moncrieff, M. W. (2010). The multiscale organization of moist convection and the intersection of weather and climate. *Climate dynamics: why does climate vary*, 189:3–26.

Morrison, H., Thompson, G., and Tatarskii, V. (2009). Impact of cloud microphysics on the development of trailing stratiform precipitation in a simulated squall line: Comparison of one-and two-moment schemes. *Monthly weather review*, 137(3):991–1007.

Morrison, H., van Lier-Walqui, M., Fridlind, A. M., Grabowski, W. W., Harrington, J. Y., Hoose, C., Korolev, A., Kumjian, M. R., Milbrandt, J. A., Pawlowska, H., et al. (2020). Confronting the challenge of modeling cloud and precipitation microphysics. *Journal of advances in modeling earth systems*, 12(8):e2019MS001689.

Moya-Álvarez, A. S., Estevan, R., Kumar, S., Rojas, J. L. F., Ticse, J. J., Martínez-Castro, D., and Silva, Y. (2020). Influence of pbl parameterization schemes in wrf_arw model on short-range precipitation's forecasts in the complex orography of peruvian central andes. *Atmospheric Research*, 233:104708.

Moya-Alvarez, A. S., Martínez-Castro, D., Flores, J. L., and Silva, Y. (2018). Sensitivity study on the influence of parameterization schemes in wrf_arw model on short-and medium-range precipitation forecasts in the central andes of peru. *Advances in Meteorology*, 2018.

Nakanishi, M. and Niino, H. (2006). An improved mellor–yamada level-3 model: Its numerical stability and application to a regional prediction of advection fog. *Boundary-Layer Meteorology*, 119:397–407.

Nesbitt, S. W., Zipser, E. J., and Cecil, D. J. (2000). A census of precipitation features in the tropics using trmm: Radar, ice scattering, and lightning observations. *Journal of climate*, 13(23):4087–4106.

Niu, G.-Y., Yang, Z.-L., Mitchell, K. E., Chen, F., Ek, M. B., Barlage, M., Kumar, A., Manning, K., Niyogi, D., Rosero, E., et al. (2011). The community noah land surface model with multiparameterization options (noah-mp): 1. model description and evaluation with local-scale measurements. *Journal of Geophysical Research: Atmospheres*, 116(D12).

Posada-Marín, J. A., Rendón, A. M., Salazar, J. F., Mejía, J. F., and Villegas, J. C. (2019). Wrf downscaling improves era-interim representation of precipitation around a tropical andean valley during el niño: implications for gcm-scale simulation of precipitation over complex terrain. *Climate Dynamics*, 52:3609–3629.

Poveda, G., Jaramillo, L., and Vallejo, L. F. (2014). Seasonal precipitation patterns along pathways of south american low-level jets and aerial rivers. *Water Resources Research*, 50(1):98–118.

Poveda, G., Mesa, O. J., Salazar, L. F., Arias, P. A., Moreno, H. A., Vieira, S. C., Agudelo, P. A., Toro, V. G., and Alvarez, J. F. (2005). The diurnal cycle of precipitation in the tropical andes of colombia. *Monthly Weather Review*, 133(1):228–240.

Poveda, G., Waylen, P. R., and Pulwarty, R. S. (2006). Annual and inter-annual variability of the present climate in northern south america and southern mesoamerica. *Palaeogeography, Palaeoclimatology, Palaeoecology*, 234(1):3–27.

Prein, A., Gobiet, A., Suklitsch, M., Truhetz, H., Awan, N., Keuler, K., and Georgievski, G. (2013). Added value of convection permitting seasonal simulations. *Climate Dynamics*, 41:2655–2677.

Prein, A. F., Liu, C., Ikeda, K., Bullock, R., Rasmussen, R. M., Holland, G. J., and Clark, M. (2020). Simulating north american mesoscale convective systems with a convection-permitting climate model. *Climate Dynamics*, 55:95–110.

Prein, A. F., Liu, C., Ikeda, K., Trier, S. B., Rasmussen, R. M., Holland, G. J., and Clark, M. P. (2017a). Increased rainfall volume from future convective storms in the us. *Nature Climate Change*, 7(12):880–884.

Prein, A. F., Rasmussen, R. M., Ikeda, K., Liu, C., Clark, M. P., and Holland, G. J. (2017b). The future intensification of hourly precipitation extremes. *Nature climate change*, 7(1):48–52.

Qian, Y., Yan, H., Berg, L. K., Hagos, S., Feng, Z., Yang, B., and Huang, M. (2016). Assessing impacts of pbl and surface layer schemes in simulating the surface–atmosphere interactions and precipitation over the tropical ocean using observations from amie/dynamo. *Journal of Climate*, 29(22):8191–8210.

Que, L.-J., Que, W.-L., and Feng, J.-M. (2016). Intercomparison of different physics schemes in the wrf model over the asian summer monsoon region. *Atmospheric and Oceanic Science Letters*, 9(3):169–177.

Ramírez-Cardona, Á., Robledo, V., Rendón, A. M., Henao, J. J., Hernández, K. S., Gómez-Ríos, S., and Mejía, J. F. (2022). Algorithm for tracking convective systems (atrackcs) (v1.0). https://doi.org/10.5281/zenodo.7025990.

Rasmussen, K. L., Prein, A. F., Rasmussen, R. M., Ikeda, K., and Liu, C. (2020). Changes in the convective population and thermodynamic environments in convection-permitting regional climate simulations over the united states. *Climate Dynamics*, 55:383–408.

Riley Dellaripa, E. M., Maloney, E. D., and DeMott, C. A. (2023). The diurnal cycle of east pacific convection, moisture, and cygnss wind speed and fluxes. *Journal of Geophysical Research: Atmospheres*, page e2022JD038133.

Roberts, N. M. and Lean, H. W. (2008). Scale-selective verification of rainfall accumulations from high-resolution forecasts of convective events. *Monthly Weather Review*, 136(1):78–97.

Rogelis, M. C. and Werner, M. (2018). Streamflow forecasts from wrf precipitation for flood early warning in mountain tropical areas. *Hydrology and Earth System Sciences*, 22(1):853–870.

Ruiz-Vásquez, M., Arias, P. A., Martínez, J. A., and Espinoza, J. C. (2020). Effects of amazon basin deforestation on regional atmospheric circulation and water vapor transport towards tropical south america. *Climate Dynamics*, 54:4169–4189.

Sakamoto, M. S., Ambrizzi, T., and Poveda, G. (2011). Moisture sources and life cycle of convective systems over western colombia. *Advances in Meteorology*, 2011.

Santanello Jr, J. A., Dirmeyer, P. A., Ferguson, C. R., Findell, K. L., Tawfik, A. B., Berg, A., Ek, M., Gentine, P., Guillod, B. P., Van Heerwaarden, C., et al. (2018). Land–atmosphere interactions: The loco perspective. *Bulletin of the American Meteorological Society*, 99(6):1253–1272.

Schumacher, R. S. and Rasmussen, K. L. (2020). The formation, character and changing nature of mesoscale convective systems. *Nature Reviews Earth & Environment*, 1(6):300–314.

Skamarock, W. C., Klemp, J. B., Dudhia, J., Gill, D. O., Liu, Z., Berner, J., Wang, W., Powers, J. G., Duda, M. G., Barker, D. M., et al. (2019). A description of the advanced research wrf model version 4. *National Center for Atmospheric Research: Boulder, CO, USA*, 145(145):550.

Srinivas, C., Yesubabu, V., Prasad, D. H., Prasad, K. H., Greeshma, M., Baskaran, R., and Venkatraman, B. (2018). Simulation of an extreme heavy rainfall event over chennai, india using wrf: Sensitivity to grid resolution and boundary layer physics. *Atmospheric Research*, 210:66–82.

Stensrud, D. J. (2009). *Parameterization schemes: keys to understanding numerical weather prediction models.* Cambridge University Press.

Taraphdar, S. and Pauluis, O. M. (2021). Impact of planetary boundary layer and cloud microphysics on the sensitivity of monsoon precipitation using a gray-zone regional model. *Earth and Space Science*, 8(5):e2020EA001535.

Thomas, B., Viswanadhapalli, Y., Srinivas, C., Dasari, H. P., Attada, R., and Langodan, S. (2021). Cloud resolving simulation of extremely heavy rainfall event over kerala in august 2018–sensitivity to microphysics and aerosol feedback. *Atmospheric Research*, 258:105613.

Thompson, G., Field, P. R., Rasmussen, R. M., and Hall, W. D. (2008). Explicit forecasts of winter precipitation using an improved bulk microphysics scheme. part ii: Implementation of a new snow parameterization. *Monthly Weather Review*, 136(12):5095–5115.

Tian, J., Liu, J., Wang, J., Li, C., Yu, F., and Chu, Z. (2017). A spatio-temporal evaluation of the wrf physical parameterisations for numerical rainfall simulation in semi-humid and semi-arid catchments of northern china. *Atmospheric Research*, 191:141–155.

Torrealba, E. R. and Amador, J. A. (2010). La corriente en chorro de bajo nivel sobre los llanos venezolanos de sur américa. *Revista de climatología*, 10.

Urrea, V., Ochoa, A., and Mesa, O. (2019). Seasonality of rainfall in colombia. *Water Resources Research*, 55(5):4149–4162.

Vizy, E. K. and Cook, K. H. (2018). Mesoscale convective systems and nocturnal rainfall over the west african sahel: role of the inter-tropical front. *Climate dynamics*, 50(1-2):587–614.

Wilks, D. S. (2011). *Statistical methods in the atmospheric sciences*, volume 100. Academic press.

Woodhams, B. J., Birch, C. E., Marsham, J. H., Bain, C. L., Roberts, N. M., and Boyd, D. F. (2018). What is the added value of a convection-permitting model for forecasting extreme rainfall over tropical east africa? *Monthly Weather Review*, 146(9):2757–2780.

Yáñez-Morroni, G., Gironás, J., Caneo, M., Delgado, R., and Garreaud, R. (2018). Using the weather research and forecasting (wrf) model for precipitation forecasting in an andean region with complex topography. *Atmosphere*, 9(8):304.

Yang, Q., Houze Jr, R. A., Leung, L. R., and Feng, Z. (2017). Environments of long-lived mesoscale convective systems over the central united states in convection permitting climate simulations. *Journal of Geophysical Research: Atmospheres*, 122(24):13–288.

Yepes, J., Mejía, J. F., Mapes, B., and Poveda, G. (2020). Gravity waves and other mechanisms modulating the diurnal precipitation over one of the rainiest spots on earth: Observations and simulations in 2016. *Monthly weather review*, 148(9):3933–3950.

Yepes, J., Poveda, G., Mejía, J. F., Moreno, L., and Rueda, C. (2019). Choco-jex: A research experiment focused on the chocó low-level jet over the far eastern pacific and western colombia. *Bulletin of the American Meteorological Society*, 100(5):779–796.

Zhang, C. and Wang, Y. (2017). Projected future changes of tropical cyclone activity over the western north and south pacific in a 20-km-mesh regional climate model. *Journal of Climate*, 30(15):5923–5941.

Zhu, Y., Qiao, F., Liu, Y., Liang, X.-Z., Liu, Q., Wang, R., and Zhang, H. (2022). The impacts of multi-physics parameterization on forecasting heavy rainfall induced by weak landfalling typhoon rumbia (2018). *Atmospheric Research*, 265:105883.

Zuluaga, M. D. and Houze, R. A. (2015). Extreme convection of the near-equatorial americas, africa, and adjoining oceans as seen by trmm. *Monthly Weather Review*, 143(1):298–316.

Supplementary material
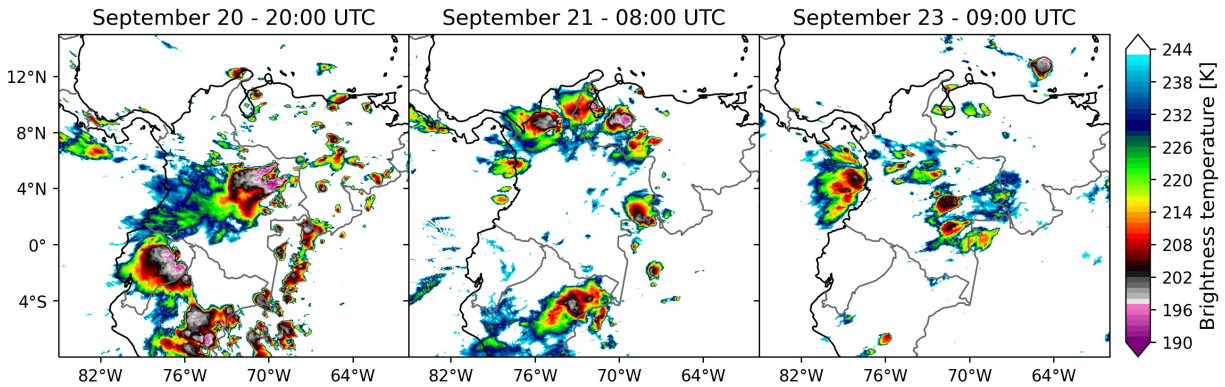
Figure S.1: Convective events that occurred in different regions of the country during the study period.
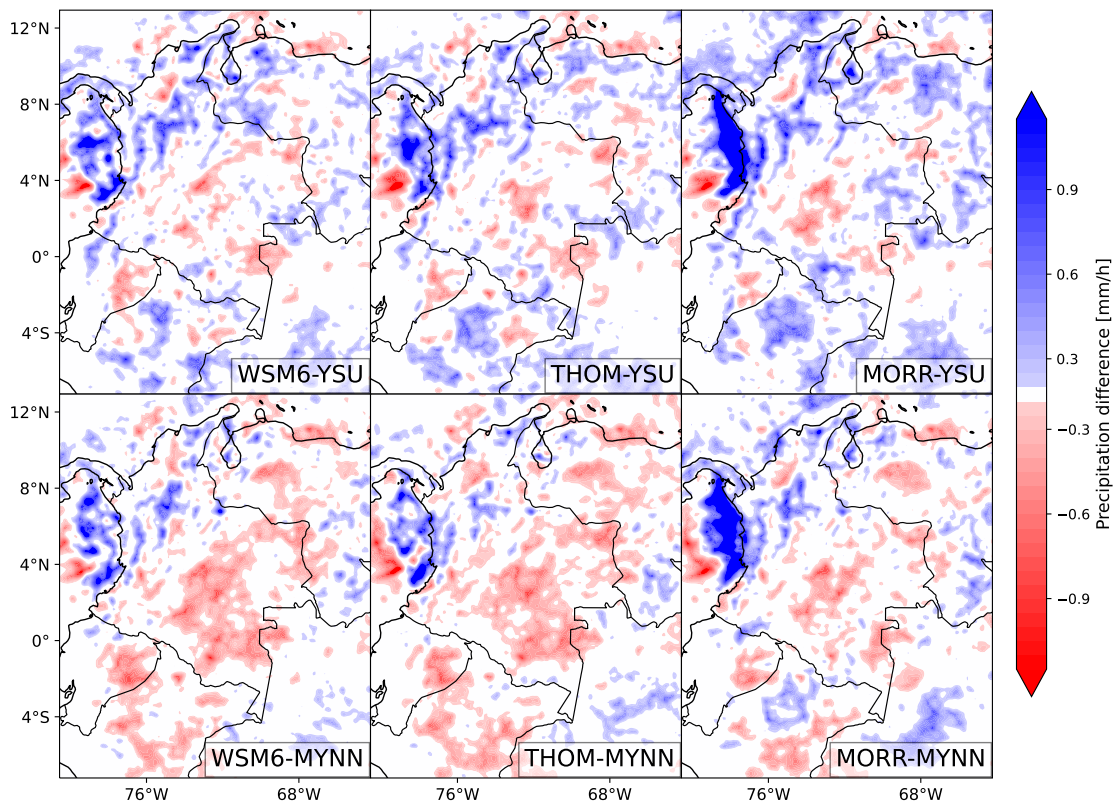

Figure S.2: Differences between satellite-derived (GPM) precipitation and model-derived precipitation (WRF) using the different parameterization schemes. WRF data were linearly interpolated to the GPM grid in order to do the subtraction.
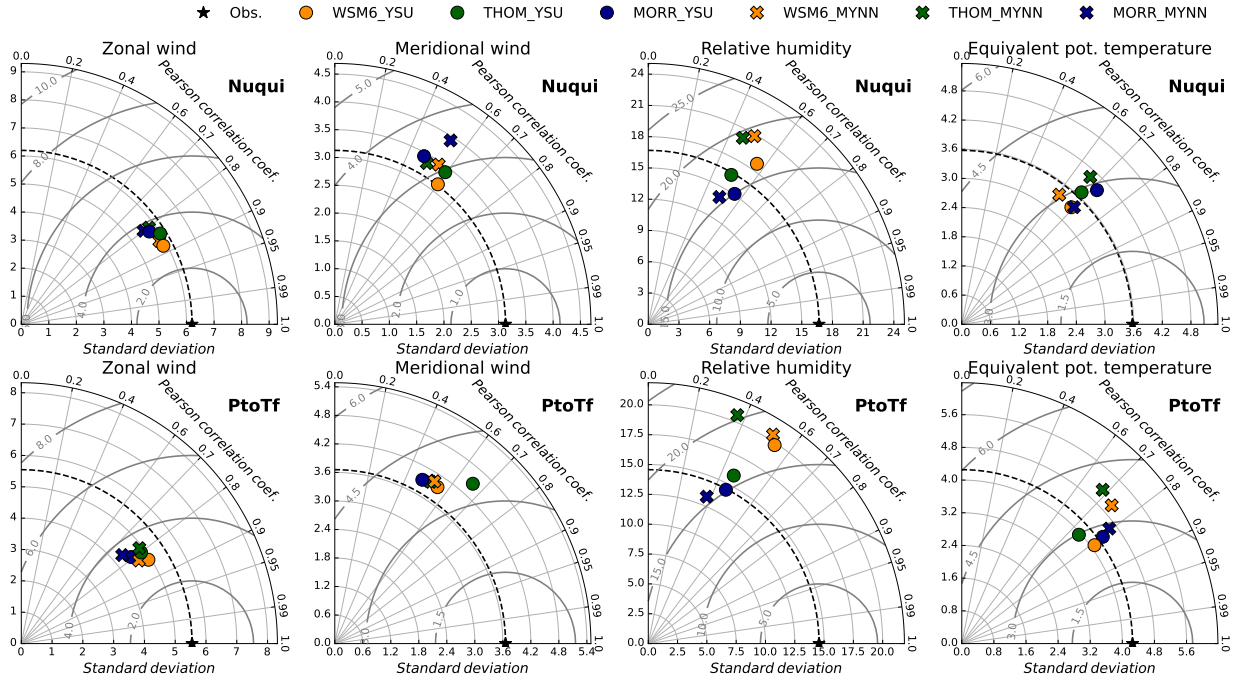
Figure S.3: Taylor diagrams for different dynamic and thermodynamic variables measured by the OTREC soundings. Error metrics were calculated for the vertical and temporal behavior of the variables.
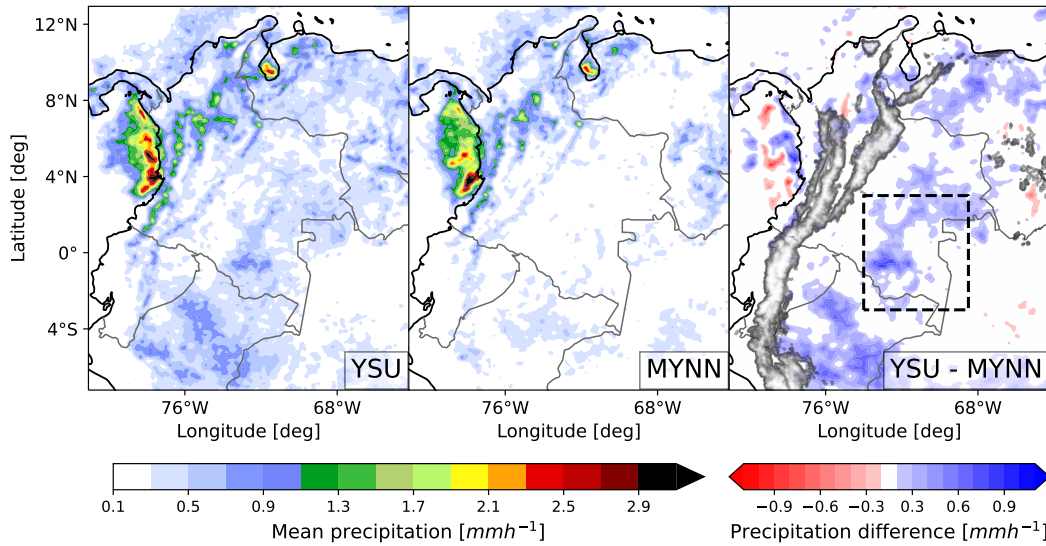
Figure S.4: Mean rainfall simulated by YSU (left) and MYNN (mid), and differences (right). Simulations of each PBL scheme are an average computed with the three PBL schemes. The Amazon region is delimited by black discontinuous lines.
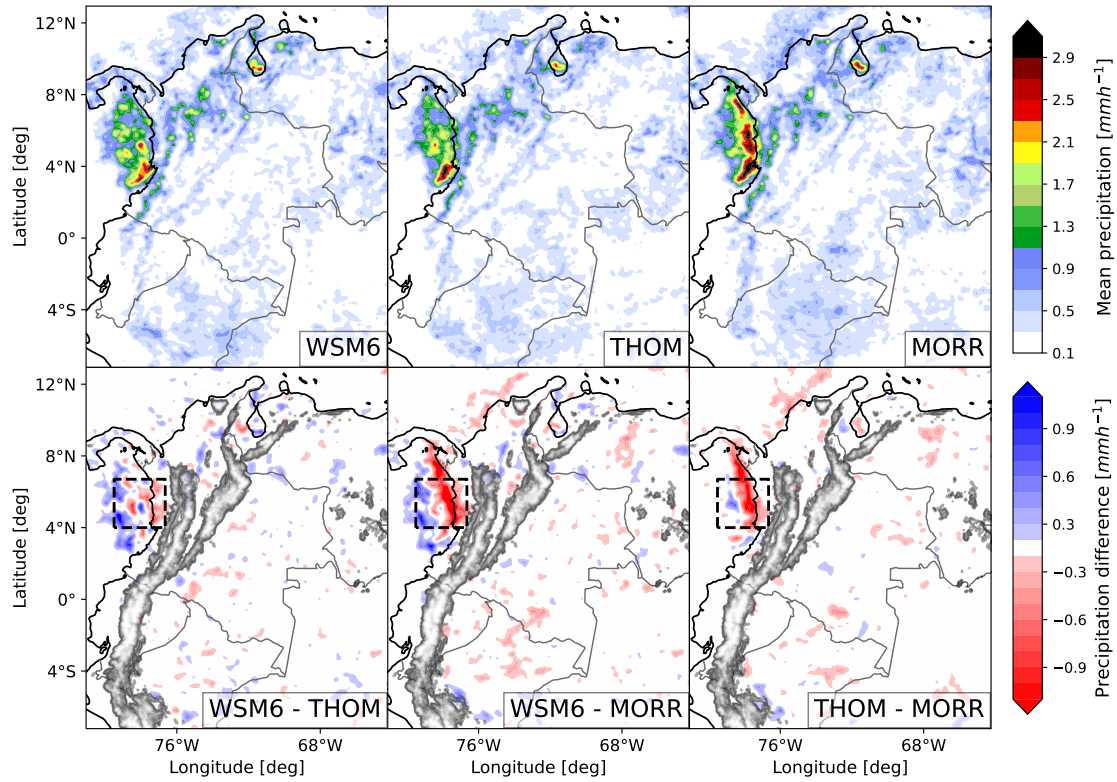
Figure S.5: Mean rainfall simulated by WSM6 (upper left), THOM (upper center), and MORR (upper right) MP parameterization schemes. The lower panels show differences between schemes: WSM6-THOM (lower left), THOM-WSM6 (lower center), and MORR-WSM6 (lower right). Simulations of each MP scheme are an average computed with the two PBL schemes. The Pacific region is delimited by black discontinuous lines.
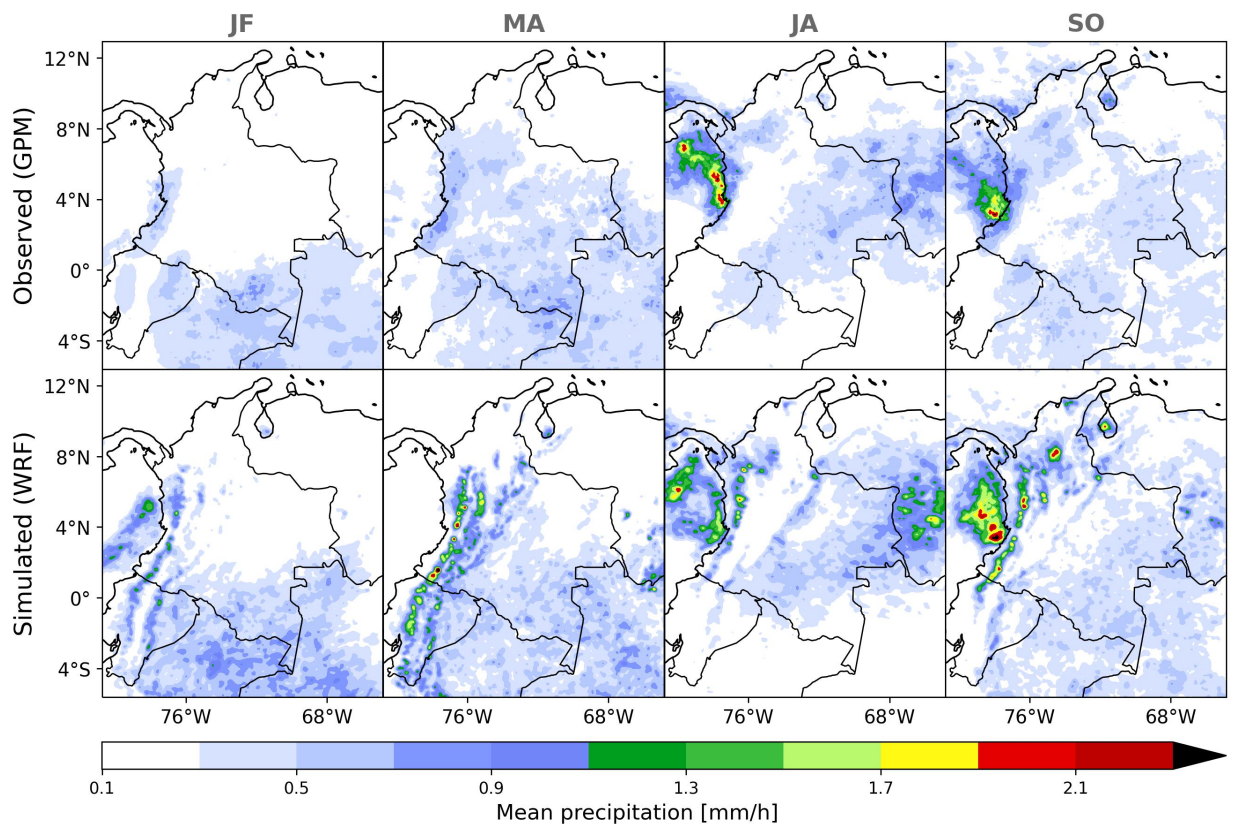
Figure S.6: Mean observed (upper panels) and simulated (lower panels) hourly precipitation for the different study periods.
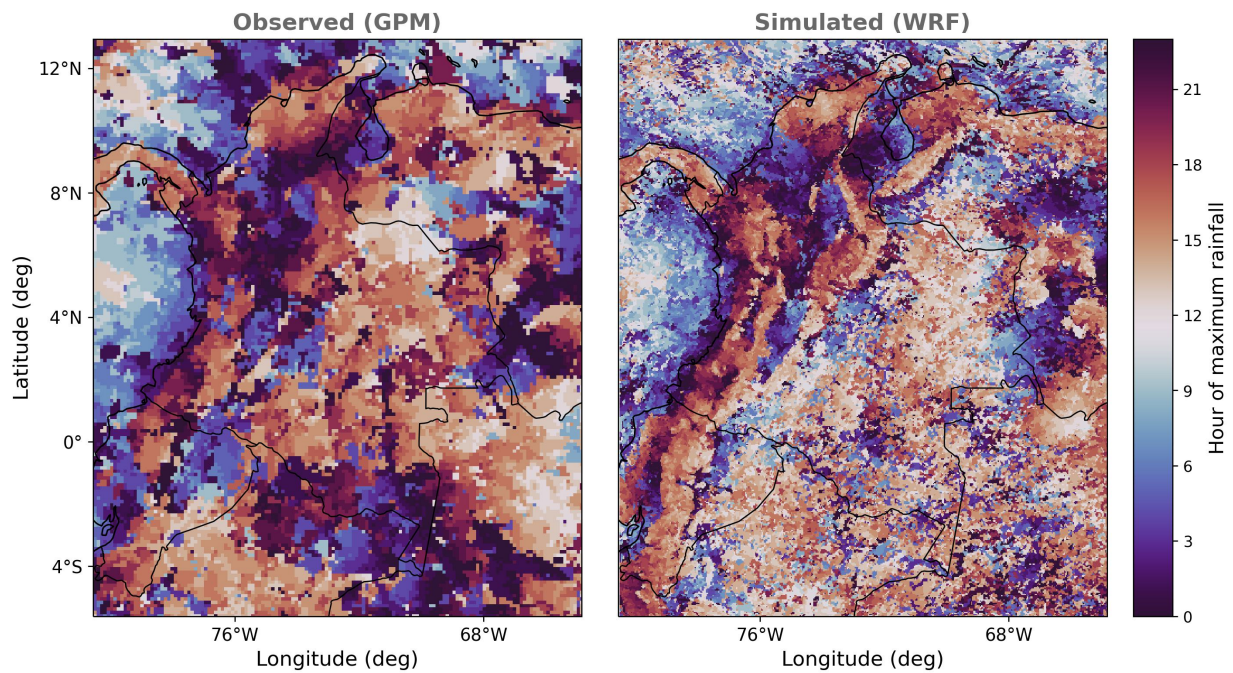
Figure S.7: Observed (left panel) and simulated (right panel) hours of maximum precipitation in NWSA for the whole study period. Red colors represent maximum rainfall during the afternoon and night, while blues indicate an early morning and morning maximum.
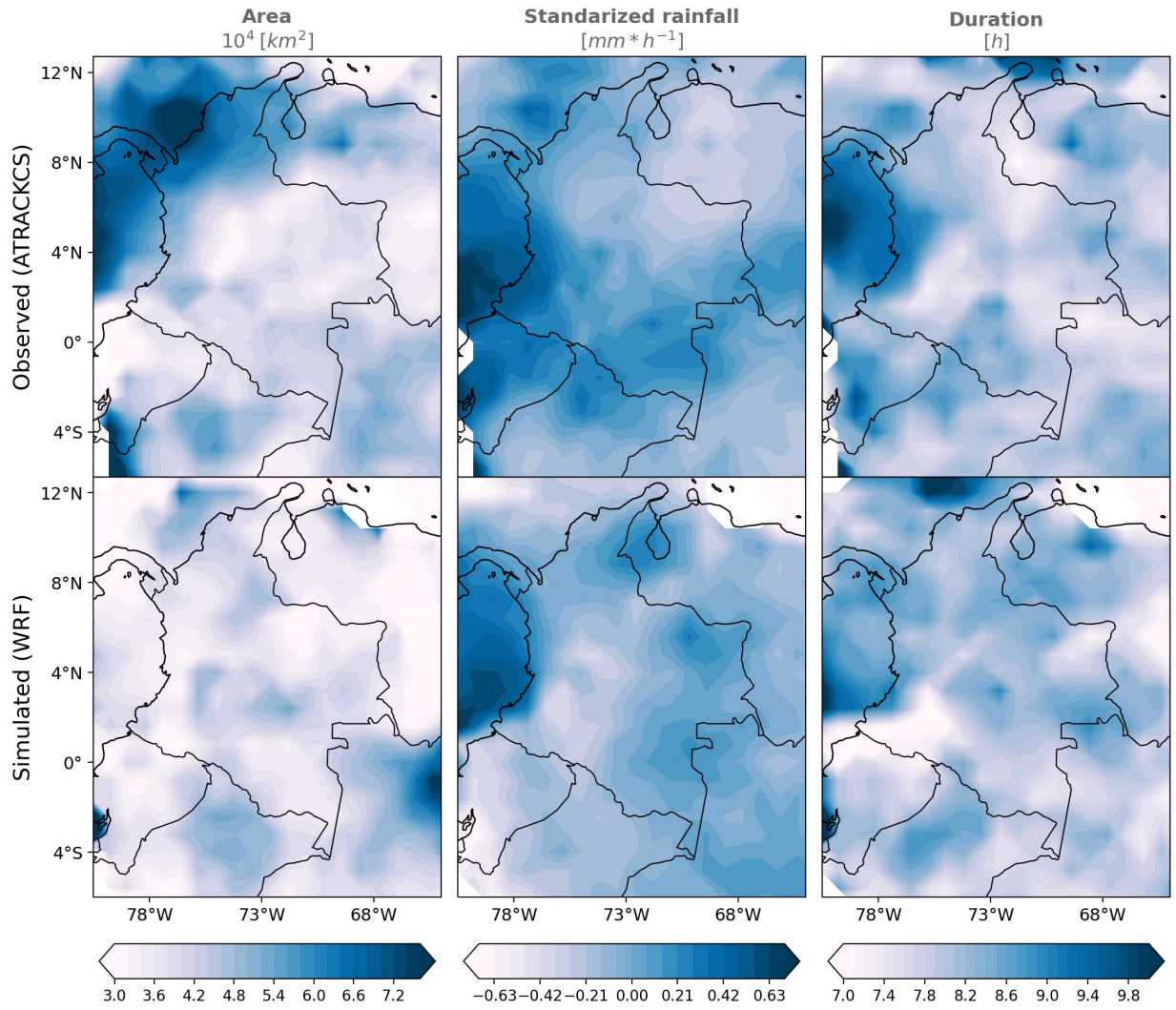
Figure S.8: Spatial distribution of observed (upper panels) and simulated (bottom panels) mean area, standardized rainfall, and duration of CSs.
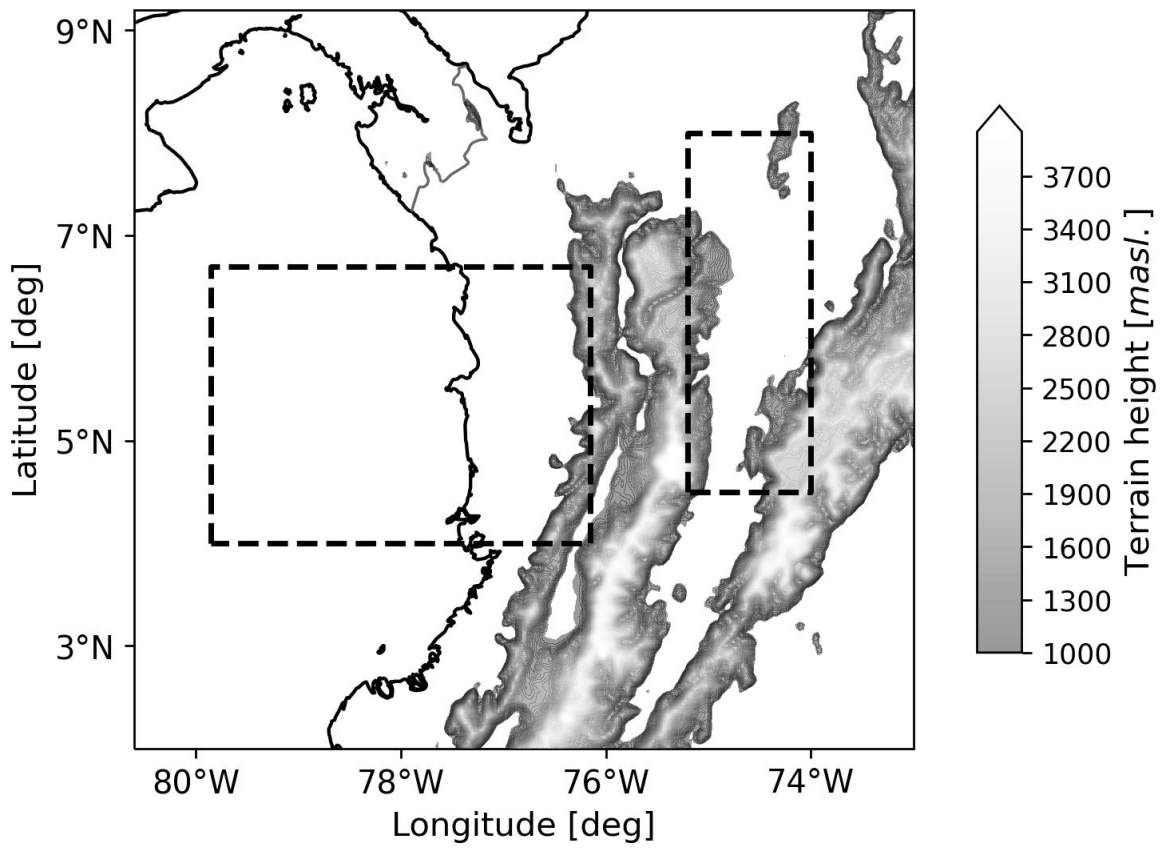
Figure S.9: Regions for zonal and meridional composites in the Pacific (left rectangle) and Magdalena Valley (right rectangle).
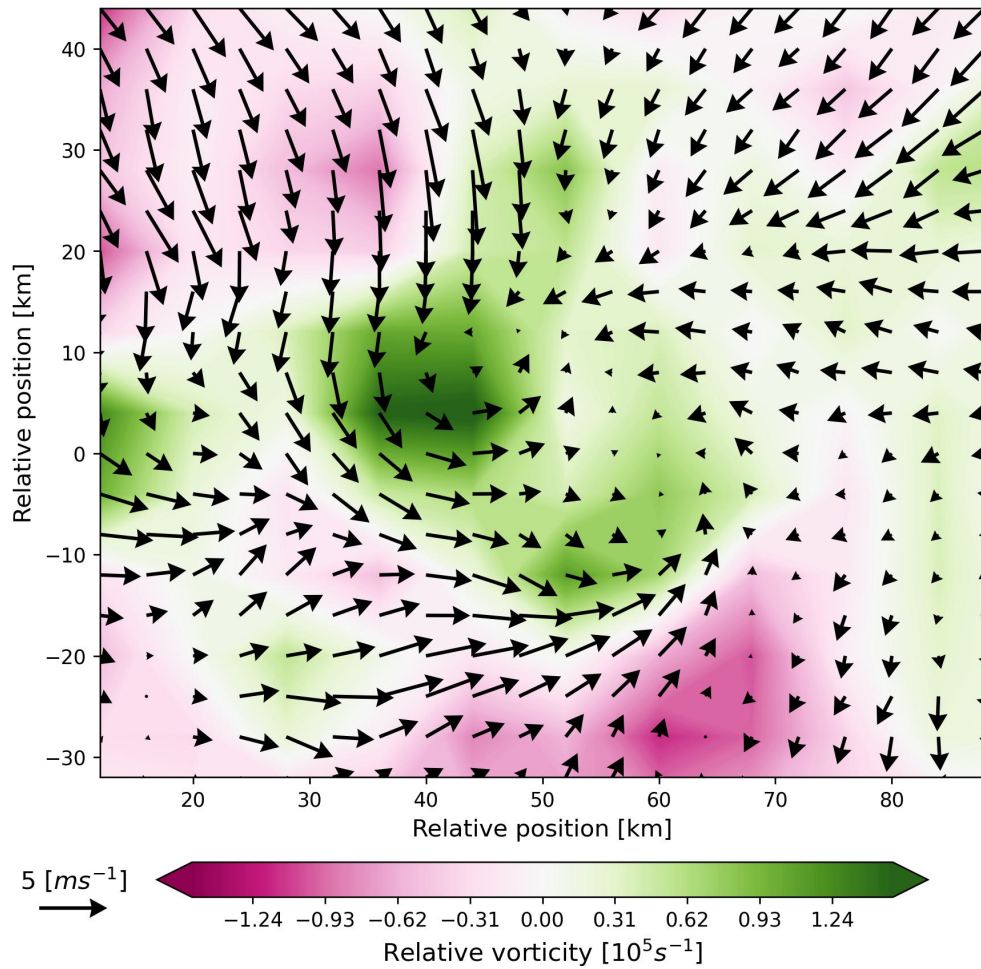
Figure S.10: Composites of anomalies for winds and relative vorticity at 450 hPa during the mature stages. Composites were performed for the region delimited by the orange square of Figure 4.9.